AD NUMBER

AD095113

NEW LIMITATION CHANGE

TO

Approved for public release, distribution unlimited

FROM

Distribution authorized to U.S. Gov't. agencies and their contractors; Administrative/Operational Use; NOV 1955. Other requests shall be referred to Bureau of Aeronautics, Department of the Navy, Washington, DC 20350.

AUTHORITY

NAVAIR ltr dtd 20 Oct 1972

AD 95113

Martin Model 270

WATER LOADS INVESTIGATION

STRUCTURAL AND IMPACT LOADS CONSIDERING AIRPLANE FLEXIBILITY

FC

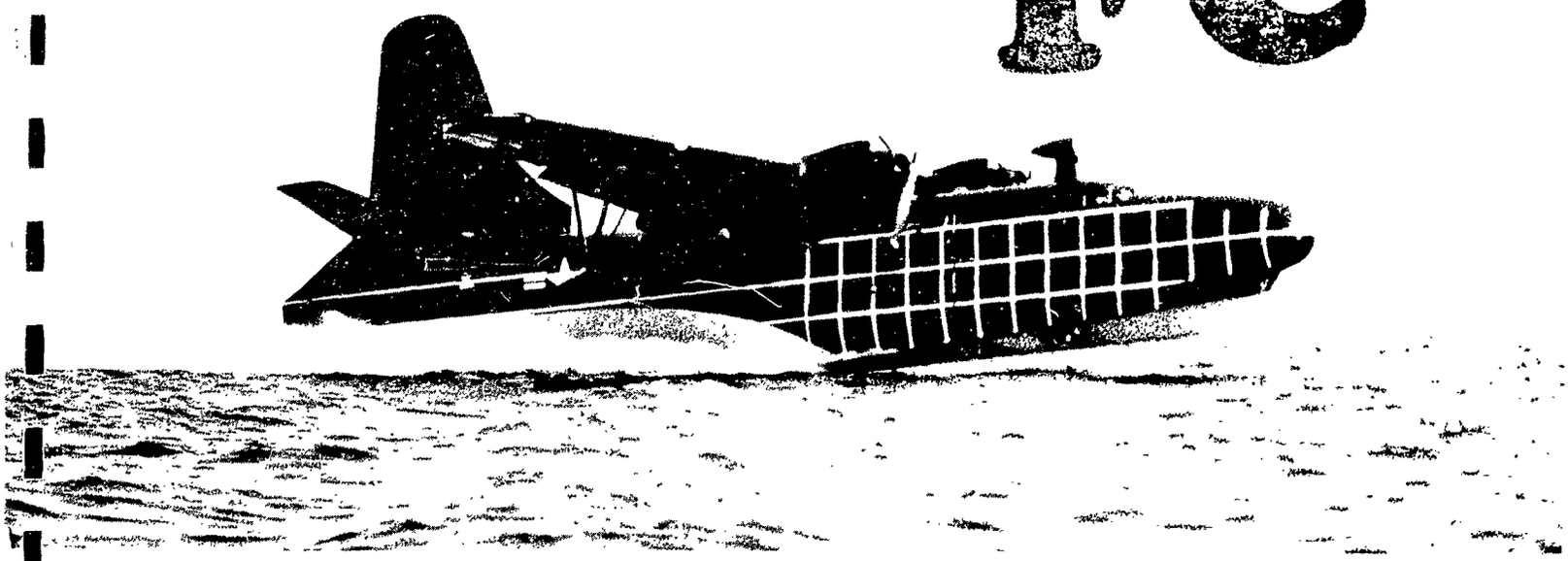

ER 7515
NOVEMBER 1955

MARTIN

Martin Model 270

WATER LOADS INVESTIGATION

STRUCTURAL AND IMPACT LOADS CONSIDERING AIRPLANE FLEXIBILITY

Prepared By	Approved By
Robert H. Schwab	John J. Saunders
E Widmayer, Jr.	H. C. Johnson

ER 7515

NOVEMBER 1955

MARTIN

FOREWORD

The water loads and structural reactions of the Glenn L. Martin Model 270 seaplane were investigated under Contract NOa(s) 11064, Amendments 14 and 15. This report, together with ER 7516, is submitted in fulfillment of the contractural requirements.

CONTENTS

CONTENTS (CONTINUED)

TABLES

ILLUSTRATIONS

ILLUSTRATIONS (CONTINUED)

ILLUSTRATIONS (CONTINUED)

SUMMARY

A theory for calculating structural loads due to water landing impact has been developed. This theory has, for the most part, been substantiated by the results of an experimental program in which both the input function (hull bottom loads) and response (accelerations) of the M-270 airplane were measured.

The theoretical and experimental studies show that the airplane impact loads are dependent on rate-of-descent, trim angle, landing speed, hull shape, and degree of flexibility of the entire airplane. It is emphasized that the forcing function itself (hull bottom pressure) is influenced by the airplane flexual characteristics. The M-270, a relatively rigid airplane for its size and weight, showed a 7 per cent reduction in applied load due to consideration of airplane flexibility. More alleviation may be expected in larger, more flexible airplanes. The method of calculating impact landing loads by means of a Reeves Electronic Analog Computer proved to be capable of conveniently handling more variables (changing trim angle, pitching acceleration and moments, load input at several stations) than conventional methods.

I. INTRODUCTION

A research program was initiated by the Bureau of Aeronautics to study loads developed during impact of water landings. The M-270 airplane, a flying boat with a low beam-to-length ratio, flared chine, and rounded keel, was used as the research vehicle. The scope of this research is divided into three catagories:

1) Development of a theory for calculating structural loads due to water landing impact and the calculation of these loads over a wide range of landing conditions.

2) An experimental program to measure structural loads (accelerations and strains) resulting from landings of the M-270 airplane. Hull bottom pressures, also measured during these tests, are presented. However correlation of these pressure results with the theoretical results is included in the hydrodynamic presentation of ER 7516.

3) Comparison and correlation of experimental and theoretical loads due to impact landings on smooth seas.

Historically, the water landing impact problem has been separated into two distinct parts; the determination of the maximum water loads, and the determination of the transient structural loads arising from the structural response to these water loads. This separation of the generation of water loads from the structural response has been long recognized as an artificial device, and a method of including the influence of wing structural flexibility on the water loads has been given in Ref. 1.

For relatively rigid seaplanes, the transient structural loads determined from the maximum water loads generally have been sufficient for engineering purposes. However, for more flexible seaplanes a formulation of the impact problem which allows the full interaction of the hydrodynamic forces and the dynamic response of the elastic seaplane is desired. Since the dynamic response of an elastic seaplane is a function of rate-of-load application as well as the peak value of the load, the formulation of the impact problem should permit rapid solution for a wide range of initial landing conditions.

In Chapter III an analytical method of treating the step landing impact problem in smooth water is developed. It gives in closed form the simultaneous determination of both the water loads and the transient structural loads. In solving the resulting equations of motion, a procedure using an electronic analog computer has been developed which permits the rapid solution of the landing problem for a large range of initial landing conditions. Solutions of the

impact problem obtained for the M-270 seaplane, considered as being completely rigid and as being completely flexible, for a range of landing conditions are presented and discussed.

In Chapter IV, the experimental program for the M-270 is discussed. This program had a two-fold purpose: (1) to determine hull bottom pressures and loads during landing for comparison to the theoretical pressures presented in hydrodynamic theory discussed in ER 7516, and (2) to determine experimentally the accelerations throughout the airplane during impact of landing to substantiate the analytical results.

In Chapter V, the results of the experimental program are compared with the results of the theoretical analysis. These comparisons are discussed with respect to both the time variation and the maximum values of the various parameters.

II. SYMBOLS

The following is a list of the symbols which are used throughout the report.

A = acceleration

a_n = coefficient of n^{th} vibratory mode

b_x = distance in x direction from mass center of airplane to mass station, positive aft

C = wetted width of hull

C_p = pressure coefficient

D = viscous damping coefficient

e = base of Naperian logarithm

F_s = hydrodynamic force acting through step of airplane normal to keel, positive down

G = structural damping coefficient

g = acceleration due to gravity

Z_l = draft of hull after chine immersion

Z_c = draft of hull at chine immersion

ℓ_k = wetted length of hull measured from step

m = mass considered to act at a given airplane station

M_s = hydrodynamic moment about step, positive nose up

M_w = virtual mass of water

P_{ave}, P_{max} = hydrodynamic pressures

t = time

V_h = forward speed

V_n = speed normal to keel

$t_{F_{max}}$ = time at which force reaches a maximum value

x = coordinate in fore and aft direction of airplane

y = coordinate in span direction

z = coordinate in direction normal to keel

Δ = hydrodynamic force associated with dynamic pressure positive down

μ = Wagner's function for spray thickness

ρ = density of water

φ = slope of deformed structure

ω_n = circular frequency of n^{th} mode

τ = trim angle, positive nose up

SUPERSCRIPTS

^{oo,o} = time derivations

SUBSCRIPTS

$_c$ = at chine or chine immersion

$_{ave}$ = average

$_{max}$ = maximum

$_s$ = at step

$_o$ = initial condition

$_{n,r,s}$ = model designation

$_n$ = normal

$_h$ = horizontal

III. THEORETICAL LANDING LOADS ANALYSIS

In this chapter consideration is given to the development of a theory for calculating structural loads due to water impact. This includes elastic and hydrodynamic effects and allows for a closed solution of the problem. The conditions existing at any instant during impact are considered to be given in terms of the instantaneous hydrodynamic force and moment acting on the seaplane and the corresponding internal structural forces due to acceleration, structural damping, and deformation. The flexible structure has been approximated by the first four symmetric airplane modes of vibration in addition to the rigid body translation and rotation. The hydrodynamic forces and moments have been expressed in terms of the hull geometry and the instantaneous values of the acceleration, velocity, and displacement of the hull bottom step.

The equations of motion for the dynamic impact of the seaplane have been derived. The solution to these equations has been obtained using an electronic analogue computor. An approximation of the effect of trim on the hydrodynamic forces has been developed which permits the removal of any restraint on the airplane pitch degree of freedom. The results of the anlysis are presented for a range of initial conditions and are discussed.

A. AIRPLANE REPRESENTATION

The airplane coordinate system is shown in Fig. 1. The displacement of any point in the elastic structure is considered to be represented by the sum of the displacements of that point in each mode of vibration including the zero frequency modes. This may be expressed as follows:

$$Z(x,y) = b(x) + \sum_{o}^{\infty} a_n Z_n(x,y) \qquad (1)$$

The selection of the modal shapes necessary to approximate accurately the structure during impact is governed largely by the vibratory characteristics of the structure and by the time variation of the applied forces. Bases for the inclusion of a sufficient number of modes have been discussed in previous literature on dynamic response (Chapter VIII of Ref. 2), and therefore will not be discussed here. For the purposes of this report, the displacement of an airplane element in the elastic case is represented by the contributions of the first four flexural airplane modes in conjunction with rigid body translation and rotation. The displacement of an airplane element in the rigid body case is represented by rigid body translation and rotation. The method of calculation and the vibratory modes obtained for the airplane are given in Appendix A.

B. HYDRODYNAMIC FORCES AND MOMENTS

The hydrodynamic forces and moments generated during a step landing are given by equations (2) and (3).

$$F_s = -\Delta - M_w \left(\ddot{Z}_s - 0.65\, \ell_k\, \ddot{\tau}\right) \tag{2}$$

$$M_s = -F_s\, (0.65\, \ell_k) \tag{3}$$

The theoretical development of equations (2) and (3) is discussed in detail in Ref. 3 and will not be treated here. However, the results of the theory necessary for a solution to the equations of motion are discussed below.

The term Δ is associated with effects of the dynamic pressure and is given in equation (4).

$$\Delta = \rho\, V_n |V_n| \int_0^{\ell_k} (C_p C d(\ell_k) \tag{4}$$

where: $V_n = Z_s + V_n \sin\tau - 0.65\, \ell_k\, \dot{\tau}$

The functions C_p and C have discontinuities at the point of chine immersion. The wetted width, C, varies with draft until the chines are immersed, and for further increase in draft, C is assumed to be constant. Prior to chine immersion, C_p is given by the following equation:

$$C_p = \frac{P_{ave}}{P_{max}} \times \frac{1}{\sin^2\tau + \mu^2 \cos^2\tau + \left(\frac{Z_c}{C}\right)} \cdot \frac{}{\sin^2\tau}$$

After chine immersion, C_p, is given by

$$C_p = \frac{P_{ave}}{P_{max}} \times \frac{1}{\sin^2\tau \left[1 + \left(\frac{Z_c}{C}\right)^2 + \left(\frac{Z_l}{C}\right)^2\right]}$$

In these expressions for C_p the quantity $\frac{P_{ave}}{P_{max}}$ is a function of the draft. Knowing the variation C_p, C, and ℓ_k as a function

of Z_s for a given value of τ, the integral $\int_o^{\ell_k} C_p(\ell_k)$ could be evaluated.

The second term in equation (2) is associated with the forces given by:

$$M_w = \pi \rho \int_o^{\ell k} C^2 d\,(\ell k)$$

With the variation of C with Z_s known, $\int_o^{\ell k} C^2 d\,(\ell k)$ may be evaluated for a given τ.

In the actual evaluation of the above integrals, it was convenient to utilize digital machine computational methods. The integrals were evaluated for τ equal to 3°, 6°, and 9° for the range of Z_s expected to be encountered by the airplane, and the results were shown in graphical form. It was then found to be possible to approximate the curves for constant τ with analytic expressions in which Z_s and τ appeared as simple functions. Further, it was found that the family of curves was adequately given when the value of τ was permitted to vary. Consequently, when the simple analytic expressions for the integrals are substituted into the equation for the hydrodynamic force, the restriction of the landing conditions to constant values of trim is no longer necessary to the solution of the landing impact problem.

The expressions for the $\int_o^{\ell k} C_p\, Cd\,(\ell_k)$ and $\int_o^{\ell k} C^2 d\,(\ell_k)$ were found to be as follows:

$$0 < Z_s < .2\, Z_c \qquad \int_o^{\ell k} C_p Cd\,(\ell_k) = \frac{4.59 - 12.0\,\tau}{\tau} Z$$

$$0.2 < Z_s < Z_c \qquad \int_o^{\ell k} C_p Cd\,(\ell_k) = \frac{1.31 - 2.2\,\tau}{\tau}\,(e^{2Z} - .82) \qquad (5)$$

$$Z_c < Z \qquad \int_o^{\ell k} C_p Cd\,(\ell_k) = \frac{-87.1 + 94.5\, e^{-3.3\,(Z-1)} + 40.1 - 34.2\, e^{-1.88\,(Z-1)}}{\tau}$$

and

$$0 < Z_s < Z_c \qquad \pi\rho \int_o^{\ell k} C^2 d\,(\ell_k) = \frac{17.8}{\tau} Z\,(Z^2 + .1435)$$

$$Z_c < Z \qquad \pi\rho \int_o^{\ell k} C^2 d\,(\ell_k) = \frac{76.8}{\tau}\,(Z - .735) \qquad (5a)$$

In the present problem, these expressions gave excellent approximations of the integrals for values of Z_s up to 36 inches and gave reasonable agreement for values of Z_s in excess of 36 inches. It should be noted that for that portion of the landing most important to the airplane response, i.e., during the build-up to maximum force, these analytical expressions are most valid.

The forces arising from the explicit variation of trim in equation (2) include a component due to the dynamic pressure and a component due to the virtual mass. In the force due to dynamic pressure, V_n has components of velocity arising from both the trim and the rate of pitch of the airplane. During the early portions of impact the contribution due to the instantaenous trim does not vary appreciably. However, the contribution due to the rate of change in trim, $\overset{o}{\tau}$, in those cases where there is large wetted length, may become important. The component of force due to the acceleration of the "virtual" mass of water is affected by the angular acceleration. In those cases where the wetted length is long and the pitching acceleration is large, the affect of this acceleration on the forces is appreciable.

In permitting trim variation, it was necessary to determine the centroid of the pressure distribution acting on the bottom. For the high-beam loaded hull where chine immersion occurs early in impact, the center of pressure is taken at 65 per cent of the instantaneous value of the wetted length. The factors on which the selection of $0.65\ l_k$ is based are discussed in Ref. 3. The location of the pressure centroid is of importance for landings at low initial values of trim where the wetted length may be expected to exceed 4 times the beam of the hull.

C. STRUCTURAL DAMPING

The presentation of the energy dissipated by the structure has been included in the equations of motion. The importance of the role of structural damping in the aircraft landing problem has been emphasized in Ref. 2, where it was shown that for some structure the inclusion of damping in the analysis gave substantial reductions in the calculated "g" loadings. In Ref. 2, the damping coefficient was taken to include the effects of both aerodynamic and structural damping. In this analysis, only the effects of structural damping are included. The omission of aerodynamic damping is felt to be conservative (would tend to give larger accelerations) and may be considered as a simplification of the problem.

In the analog solution of the equations of motion, it was found convenient to represent the structural damping force as $-D_n \overset{o}{Z}_n$; where: $D_n = \sum_m a_n G_n \omega_n d_m$.
The damping term as used herein gives an acceptable representation of the damping force when $\overset{o}{Z}_n$ is not approximately $\omega_n Z_n$. Some discrepancy in the damping representation is present. However, for the purpose of this report the representation is adequate.

D. EQUATIONS OF MOTION

The equations of motion relating the behavior of the airplane to the hydrodynamic forces encountered during impact may be derived using the principle of virtual work. Assuming that the aerodynamic lift equals the weight of the airplane throughout the landing, the acceleration force on an element of mass in the airplane is given by $-m\overset{oo}{Z}$ and the work done moving through a differential displacement δZ is $-m\overset{oo}{Z}\,\delta Z$. Similarly, the work due to structural damping is given by $-D\,\overset{o}{Z}\,\delta Z$ and the spring work is $-\omega^2 Z\,\delta Z$. The work done moving the hydrodynamic force and moment through a distance is given by
$F_s \delta Z_s + M_s\,(\delta\tau + \delta\phi_n)$.
Summing the elements over the airplane,

$$\delta W = -\Sigma\, m\overset{oo}{Z}\,\delta Z \;-\Sigma\, D_n \overset{o}{Z}\,\delta Z \;-\omega_n^2\, \Sigma\, mZ\delta Z \qquad (6)$$

$$+ F_s \delta Z_s + M_s\,(\tau_s + \phi)(\delta\tau + \delta\phi_n)$$

If $Z(x\ y)$ is replaced by the right hand side of equation 1 and δZ is taken as,

$$\delta Z = \sum_{o}^{\infty} a_n\ \delta Z_n + b_x \delta\tau$$

then equation 6 becomes,

$$\delta W = \left[-\sum_{m} m \sum_{1}^{n} a_n Z_n + b_x \tau^{oo} + a_o Z_o^{oo} \right] \left[A_n \delta Z_n + b_x \delta\tau + a_o \delta Z_o \right]$$

$$-i \sum mG \sum \left[\omega_n a_n {}^{o}Z_n \right] \left[a_n \delta Z_n \right]$$

$$-\sum \omega_n^2\, m \sum \left[a_n Z_n \right] \left[a_n \delta Z_n \right]$$

$$+\sum \left[F_s \sum (a_n \delta Z_n + b_x \delta\tau + a_o \delta Z_o) + M_s\ (\Sigma\delta\tau + \delta\phi_n) \right]$$

$$\frac{\partial W}{\partial \delta Z_n} = 0 \text{ is to be satisfied} \qquad (7)$$

From equation 4 and the orthogonality condition

$$\Sigma\ m Z_r\ \delta Z_\lambda = 0 \qquad r \neq \lambda$$

$$\Sigma\ m Z_r\ \delta Z_\lambda \neq 0 \qquad r = \lambda$$

the following equations are obtained

$$-Z_o^{\infty} + \frac{F_s}{\Sigma m} = 0 \qquad (8)$$

$$n = 1, 2, 3, 4$$

$$-\tau^{\infty} + \frac{F_s\, b_s + M_s}{\Sigma m\, b_{(x)}^2} = 0$$

$$-Z_o^{\infty} - g\, \omega_n\, {}^{o}Z_n - \omega_n^2\, Z_n + \frac{a_{sn} F_s + \phi_{sn} M_s}{\Sigma a^2 n\, m} = 0$$

When the initial values of Z_S, τ and V_n are given, equations (8) may then be solved for the $Z_S\ (t)$, $\tau(t)$, and $M_S\ (t)$.
In addition, the acceleration at any mass station may be obtained by use of the following relation:

$$Z_{(x\ y)}^{\infty} = a_o\, Z_o^{oo} + b_{(x)}\, \tau^{\infty} + \sum_{1}^{n} a\ (x_1 y)_n\, Z_n^{\infty}$$

With these quantities known, the impact forces and the structural response are determined, and the distribution of load over the structure may be studied.

E. SOLUTION TO EQUATIONS OF MOTION

From an examination of equation (8), it can be seen that the equations are non-linear functions of Z, $\dot{Z}$, $\ddot{Z}$, and τ. Previously, when it was sufficient to treat the landing problem as the rigid body, the translatory response to the hydrodynamic forcing function solutions was obtained either by a step-by-step integration or by use of an analog computer. The inclusion of additional degrees of freedom has increased the complexity of the problem and has made the analog solution attractive.

The solution to equation (8) has been obtained readily using a Reeves Electronic Analog Computer. The left-hand side of equations (8), giving the forces arising within the structure, presents no difficulty in machine programming. The use of a simple analytical expression for the hydrodynamic force and moments, while requiring additional machines, may also be readily programmed. Continuous records of hydrodynamic forces and moments, displacement and structural accelerations, shears, and bending moments may then be obtained.

F. RESULTS AND DISCUSSION

Solutions of the equations of motion for hydrodynamic impact have been obtained and are presented in Tables 1 and 2 and Figs. 2a to 2e. The solutions, as obtained from the analog computer, are in the form of the time variation of the quantities being studied. These data have been reduced to the form of peak values and are reported in terms of the conditions existing at the time of peak values. Oscillograms of landings are also presented, which representatively illustrate variations of hydrodynamic force and moment, motions of the aircraft, and the acceleration response of the aircraft having significance in the structural dynamics problem.

The primary purpose of this portion of the report is to examine the influence of structural response to the dynamic loading on the hydrodynamic loading and on the distributed loading experienced by the structure. No detailed effort is made here to correlate the variation of the hydrodynamic force and moments with those which might be expected from previous hydrodynamic experience. However, it may be noted that the trends exhibited by the hydrodynamic data behave in general as would be expected. The validity of the hydrodynamic input data has been substantiated by experimental landing data presented and discussed in another section of this report.

It is a well known result that the response of a simple mechanical system to suddenly applied forces is a function of the time rate of force application and the indicial admittance of the system, thus:

$$x(t) = F_{(o)} A_{(t)} + \int_o^t \frac{dF}{dt_1} A\,(t-t_1)\, dt_1$$

The response of a mechanical system also may be expressed in terms of the response of each normal vibratory mode to the harmonics of the force. In either approach to the problem, the rate of force application or the harmonic content of the force, in conjunction with the frequency spectrum of the system has an important bearing on the response of the system. For aircraft of high rigidity, that is, having a fundamental frequency well above $\frac{1}{4t_{F_{max}}}$ cycles per second (This is the frequency of a harmonic function which will peak at $t_{F_{max}}$.) of the impact forcing function, the most severe distributed structural loads are generally obtained in the hardest impact condition. For the flexible aircraft having a frequency close to or within the frequency of $\frac{1}{4t_{F_{max}}}$, it is possible for maximum local loads to be obtained for impacts other than that having the greatest hydrodynamic force. This condition requires that a range or envelope of impact conditions be examined in order to insure that the most severe loads are utilized in the design of the aircraft structure.

Table 1 shows that a variation of $t_{F_{max}}$ was obtained with variations in the rate of descent. The range of $t_{F_{max}}$ was from approximately 0.10 seconds for the high rates of descent to approximately 0.40 seconds for the low rates of descent. Figures 2a to 2e present the shape of the force and moment generated in representative landings. The spikes appearing in these curves resulted from switching equations in the REAC and may be disregarded. It may be noted that the general shape of the forces and of the moments are similar for different impact conditions with only $t_{F_{max}}$ changing. Also, it may be seen that some delay in the generation of the moment with respect to the generation of the force was experienced. This delay is caused by the hydrodynamic center of pressure being close to the airplane center of gravity for short wetted lengths. As the wetted lengths become greater, the moment increases at a greater rate and reaches a maximum at approximately the same instant as the force. Consequently, the loads induced by both the force and the moment must be considered in the landing analysis.

Figures 2a to 2c show that the frequencies excited in the structure are a function of $t_{F_{max}}$ and hence the rate of loading. In case 2a, the hull may be seen to respond to both 140 cpm and at 390 cpm, the first and third modes of vibration. In case 2b it may be noted for the shorter $t_{F_{max}}$ that the hull responds principally in the second vibratory mode at 354 cpm. In case 2c having $t_{F_{max}}$ of 0.1 seconds the hull response was at 510 cpm which is between the third and fourth modal frequencies.

The maximum accelerations at various locations on the airplane are given in Table 1 for each landing condition. While actual shears and moments were not obtained in this analysis (the shear and moment distributions as a function of time could have been obtained with the equipment available, but the data obtained illustrates the point) it may be seen that the maximum positive or negative accelerations were not necessarily obtained at the impact having the maximum force. For instance, the maximum positive bow and wing tip acceleration were obtained for landing 2, while the maximum positive stern and stabilizer tip accelerations and the maximum negative bow acceleration were obtained for landing 10. In landing 18, having the maximum force only, maximum negative accelerations were obtained at the wing tip, the stern, and the center of gravity. These results indicate that even for the rather rigid M-270 airplane an envelope of landing impacts would be necessary for accurate estimation of the landing loads.

A second, and equally important point is illustrated by these data. Comparing the acceleration loading obtained for the airplane center of gravity with the acceleration loading at the other stations, it may be seen that the maximum CG acceleration differed considerably in magnitude from those maximum accelerations experienced at the other stations. In this case the extremity loadings are greater than the center of gravity loadings. This dynamic modulation of the loadings is expected from theoretical considerations and is well known. While for this case the loadings were amplified, it is also possible to obtain load alleviation due to the dynamic response of the structure. This alleviation would depend upon the relationship of the applied load to the frequency spectrum of the airplane.

A comparison of the maximum forces obtained for the flexible airplane analysis with the maximum forces obtained for the rigid airplane analysis afford an opportunity to study the influence of flexibility on the hydrodynamic loads. Comparing column 4 of Table 1 with column 4 of Table 2, it may be seen that in most instances the maximum forces for the flexible airplane were less than the maximum force for the rigid airplane for the same initial conditions. For the amount of flexibility present in the M-270 airplane, the maximum reduction in force was approximately 7 per cent. For more flexible airplanes, particularly if considerable weight is carried in the wings,

it is conceivable that larger reductions in applied force might be obtained. This interaction between the response of the airplane and the hydrodynamic force, and the resulting reduction in applied load may have an important effect on the distributed loading experienced by the aircraft.

In regards to the influence of flexibility on the hydrodynamic moment, no definite trend is exhibited by the data. Since the moment depends among other things on the force and wetted length, there is the possibility of compensating variations in both factors for the rigid airplane case. For more flexible airplanes, appreciable changes in pitching moment may be obtained. When such information becomes available more definite conclusions may be made on the influence of flexibility on the pitching moment.

At this point some comment on the assumptions and neglected quantities is in order. First, consider the assumption that the distributed hydrodynamic forces are given entirely in terms of the kinematics of the step. For the M-270 airplane this assumption appears valid, since the rigidity of the hull and vibratory modal shapes was such that adequate average values of coefficients could be used. However, for the more flexible hull, it may be necessary to describe the forces in terms of the kinematics of more than one hull station. The use of many hull stations, analogous to aerodynamic strip theory, would permit more accurate application of shape factors and of local kinematics. However, the increase in number of hull stations is accompanied by an increase in computational difficulty and for analog methods may exceed the available machine capacities.

Second, in the formulation of the hydrodynamic forces and moments two quantities have been considered as negligible. These quantities are buoyant force and moment and pitching moment due to water resistance to forward motion of the airplane. In addition, it has been assumed that the weight of the airplane is equal to the lift for the duration of impact. Some consideration of the effect of loss of lift in landing impact has been given in Refs. 4 and 5. The work of these references, while treating the problem only approximately indicates that some account for the effects of lift variation may be required. For impacts of long duration or for flexible highly coupled lifting surfaces, the lift variation might enter appreciably into the dynamics of the landing.

As landing impact becomes more critical in determing the design loads for aircraft structure(in addition to the hull bottom) and as more powerful computational methods are used, these forces may be included in the analysis.

G. CONCLUDING REMARKS

A procedure for analyzing step landing impacts in smooth water, which includes the flexibility of the airframe and continuous trim variation, has been presented. The procedure has been applied to an analysis of the M-270 research airplane and a range of landing conditions has been studied. From the results of these analyses, it was seen that the maximum load in a flexible structure is not given necessarily by the impact having the largest external force. Depending on the structural dynamic characteristics of the airplane, a range of impact conditions should be examined to determine the maximum distributed loads for design purposes. The influence of flexible structure on the hydrodynamic force also was seen. In general, this influence appeared as a reduction in total load, for this airplane not more than 7 per cent. The results in regard to the pitching moment in this respect were not conclusive but may be of consequence in more flexible airplanes. From this study it is believed that rigid airplane landing analysis is no longer adequate for design purposes.

IV. INSTRUMENTATION AND EXPERIMENTAL PROGRAM

A test program was initiated to obtain experimental data for correlation with theoretical hull bottom water loads and airplane accelerations during landing impact of the M-270 airplane. Previous to the landing tests, a drop test program was conducted with a specimen section of the M-270 hull and results of these tests are presented in Ref. 3. Results of the landing tests are discussed and presented in this chapter.

A. INSTRUMENTATION

Instrumentation for the water loads investigation of the Model M-270 consisted of the installation of a total of 49 transducers, which included 13 Statham accelerometers, 20 Statham flush-type pressure transducers, and 16 strain gages. Accelerometers were located at several points along the left hand wing and at several points in the hull from the bow to the stern. Strain gages were mounted on structural components of the hull bottom and crown (See Fig. 3). Pressure transducers were installed at points along the hull bottom forward of the step and flush with the hull bottom skin as shown in Figs. 4, 5, and 6.

Ouput from all pickups was recorded on three synchronized Consolidated 18-channel oscillographs and one Sanborn visual recorder in conjunction with five direct current bridge-balancing units all powered by 3 twelve-volt batteries and the ship's auxiliary power unit (Figs. 7 and 8). Use of the Sanborn visual recorder made possible the immediate evaluation of the left hand engine mount load factor to insure that testing would not take place beyond its limit. Calibration of the entire system was conducted prior to take-off and then again after flight to insure accurate calibration factors.

Rate of descent for each landing was measured at first by means of the Radar (Doppler) Rate of Descent equipment by which the antenna mounted on the port side of the hull transmitted and received the signal reflected from the water. Output was fed to the pilot's panel and photo-panel indicators and also to the Sanborn recorder and one oscillograph.

Because of the questionable reliability of the radar equipment over anything but an extremely smooth sea, a photo-theodolite system was installed at the point where the landings took place. By means of a motion picture camera which followed the ship to the water, the rate of descent could be measured along with the hull trim angle as a check on the radar equipment. On the basis of resulting data, it was evident that the photo-theodolite was the more reliable

instrument to measure rate of descent. Since the load factor at the center of gravity varies not only according to gross weight, landing speed, and sea state, but also with the trim angle and rate of descent, it was imperative that these two quantities be measured in the most reliable manner available.

B. TEST PROGRAM

The program to be followed in the testing of this ship was divided into three phases, each with a different condition prevailing. Phase I was conducted at a gross weight of 64,000 pounds CG at 26 per cent MAC, sea state smooth (approximately six inches), and wind velocity not more than six knots. A series of take-offs and landings was made and data were recorded for each of the landings at various rates of descent and hull trim angle. Symmetric landings (both tip floats touching simultaneously) were executed throughout thetest program.

Procedure for Phase II was identical as that followed in Phase I with the exception of the gross weight which was increased to 71,000 pounds.

Phase III was set up to record data from landings with the gross weight of 55,000 pounds made at various rates of descent on a rough sea of about $3\frac{1}{2}$-foot waves. Weather conditions adverse to the execution of this phase were encountered and as a consequence this portion of the program was cancelled.

Strength (limit load factor of 4.5) of the engine mount structure placed a limitation upon the maximum rate of descent which the airplane could safely approach while performing the test. A continual check of the load experienced by the left hand engine mount was kept by means of the Sanborn recorder following each landing so that this factor would not be exceeded. Inspection of the structure of the ship was also carried out after each flight.

General handling characteristics of the aircraft place limitations on acquiring the desired rates of descent and hull trim angles as originally planned. It was found difficult to obtain a high trim angle at high rates of descent and low trim angles at low rates of descent. However, the flights were performed within these limits and all possibilities were exploited (see Fig. 9).

C. TEST RESULTS

Maximum load factors, pressures, and stresses occurring during the series of landings are recorded in tabular form (Tables 3 thru 7). These values are peak loads and are not constant loads for any length of time. With the exception of the strain gages data, all loads recorded were those maxima occurring during the first impact of landing.

During the landings on smooth water at a gross weight of 64,000 pounds, a maximum vertical load factor of 3.85 was obtained at the center of gravity on landing 4 of flight 29 at a rate of descent of 13.3 feet per second. At a gross weight of 71,000 pounds, the maximum center of gravity load factor obtained was 2.56 at a rate of descent of 8.0 feet per second on landing 8 of flight 31.

Time histories of all active pickups from the touchdown of each landing are included for landings 1, 4, 5, and 8 of flights 28, 29, 27, and 31 respectively, since the greatest vertical load factors at the center of gravity occurred during these four particular landings (see Fig. 10 thru 13). Figure 14 shows plots of maximum load factor at the center of gravity and the corresponding rates of descent for the various hull trim angles and gross weight conditions. A plot of maximum stress at the center of the longeron, walkway stringer and top of the keel former for each landing vs the corresponding rate of descent is shown in Fig. 15. The apparent trend of both graphs illustrates the effect of the degree of rate of descent and hull angle on these stresses. In Fig. 15, no distinction is made in regards to hull trim angle, thus partially causing a deviation of strain values from the curve at lower rates. However, in the case of the keel former, the inherent characteristics of the structure itself apparently cause the loads to fluctuate more or less independently of the rate of descent.

Landings were performed within the specified limits of the test program in regard to hull trim angle and rate of descent. These were largely determined by the manner in which the ship responded during the landings, since it was difficult to obtain a high trim angle at high rates of descent and low trim angles at low rates of descent. However, all possibilities were exploited and the resulting range of conditions is shown in Fig. 9. The program was originally set up to obtain trim angles of 3, 5, 7, and 9 degrees at rates of descent of 3, 6, and 10 feet per second. These quantities are indicated by solid and broken lines in Fig. 9.

With the data obtained from accelerometers at specified locations along the hull and wing, it was possible to derive the forcing function resulting from the aerodynamic and water loads during the first impact of landings. In this analysis, the aerodynamic lift was assumed to equal the gross weight of the ship. Accelerations were read at certain time intervals and the values

thus obtained were multiplied by the corresponding mass for the certain pick-up location according to the weight distribution curve of the ship. The results were plotted against the time intervals, thus producing a time history of the applied force (see Figs. 16, 17, and 18).

By taking a summation of the moments of each mass increment about a point (such as the CG or the nose of the airplane) and dividing the resulting values by the forces as determined previously, the travel of the point of application (center of pressure) can be determined. For the purpose of comparison with theoretical data, moments of each mass increment were taken about the step of the ship and the summations of these moments were plotted against the corresponding time intervals (Figs. 16, 17, and 18).

D. DISCUSSION

Use of Statham accelerometers and flush-type pressure transducers made it possible to measure accurately the loads experienced by the airplane. According to data supplied by Statham in regard to pressure transducers, accuracy and linearity of the pickup itself is 1% of full scale or better. Accelerometers are equally accurate; however, other factors involved, such as the type of system used, calibration, and data reduction, bring the per cent of error to about 2 - 5%.

Hull bottom pressure values measured were the result of peak loads occurring locally for short periods of time and not necessarily simultaneously over the wetted hull bottom area at touch-down. High frequency loads, though large in magnitude, are therefore of less significance since they would be absorbed locally in the structure rather than over large areas of the hull bottom, as would be the case for low frequency loads.

Hull bottom instrumentation using the flush-type pickup was complicated by the need to consider the effect of response to acceleration within the pickup, which was found to be 2% of full scale per g. Further complicating the problem was the necessity of completely waterproofing the pickup contacts and protecting the pickup and receptacle from corrosion caused by salt water. This problem was solved to meet the requirements of the test.

Significant in the evaluation of data measured during the landings was the factor of rate of descent, which was one of the most important variables upon which the loads depended. Measuring this quantity and hull trim angle was accomplished by use of the phototheodolite camera. Use of this equipment created a need for a specific flight path and favorable wind direction, which made it impossible to perform the rough water landings during the allotted time. However, since this was the more reliable of the two methods,

its data is used exclusively in the report. It is evident that in a test of this type where such information is required, a more dependable radar-type rate of descent equipment is necessary. It would be of great value to improve the radar-type rate of descent indicator used at the beginning of this program or to develop an entirely new system, which could be carried on the ship itself thus allowing landings to be made at any convenient location.

V. COMPARISON OF EXPERIMENTAL AND THEORETICAL DATA

In this chapter a comparison of the analytical results is made with quantities measured during landing impacts on the M-270 airplane. These comparisons have been made with respect to both the time variation and the magnitude of the forces, moments, some accelerations and motions for some landing conditions. The results of these comparisons are presented and discussed.

Briefly reviewing, the landing impact analysis was performed for symmetric step landings in smooth water. Among the major assumptions of the analysis is that the only hydrodynamic forces acting on the airplane would be approximated by an analytical expression which is a function of the forebody shape and the kinematics of the step. Also, it was assumed that the dynamical response of of the airplane is given by the rigid body response and the superposition of the response of the first four flexible airplane modes of vibrations. Further discussion of the assumptions in analytical procedure is given in Chapter I. The vibratory analysis of the airplane was performed for a gross weight of 55,000 pounds and is described in Appendix A. It was found after completion of the vibratory analysis that certain changes in the experimental program required the landing tests to be performed at gross weights of 64,000 pounds and 71,000 pounds. As a consequence, some correction is to be made in interpreting the comparison of the analytical results with the experimental results. A suggested basis for this correction is in terms of the peak loads that might be expected for the rigid airplane as given on Page 38 of Ref. 6. The loads in accordance with this correction would vary as the ratio of the gross weights taken to the two-thirds power.

The experimental program was formulated for landings at discrete rates of descent, trim angle and landing speed. However, in actual practice it was found that only broad ranges of rate of descent and trim angle could be obtained. The analysis (REAC) is a result of discrete initial conditions; there is no direct correspondence between the analytical and nominal experimental initial conditions. One exception to this was landing No. 4 of flight 29 where all the initial conditions were duplicated in the REAC solution. Rate of descent ($\overset{o}{Z}_o$) was measured relative to the earth and not the water surface, so that even 1/2 to 1 foot waves or swells could increase or decrease effective $\overset{o}{Z}_o$. Analytical (REAC) data is compared to experimental trends rather than individual test points for this reason.

A. TIME-HISTORIES

The comparison of the time variation of the analytically determined quantities with the experimentally determined quantities for two landings may be made in Figs. 19 through 22. These figures show the hydrodynamic force, pitching moment, trim, pitching velocity, normal accelerations, and in one instance the pitching acceleration. In Fig. 19, the analysis was performed for the initial conditions of landing 4, flight 29. This landing represents a rather hard impact, with the variables being of sufficient magnitude that they could be determined with some precision. It is seen for the force that the analytical results are in excellent agreement with the experimental results. The two curves are almost coincident up to $t_{F_{max}}$ and are reasonably close after $t_{F_{max}}$. Excellent agreement was also obtained between analytical and experimental results for τ and $\overset{o}{\tau}$ over the greater portion of the impact; some divergence being observed after $t_{F_{max}}$ has occurred. In regards to the pitching moment, it may be seen that there is a considerable difference between the curves over the range of time from 0.06 seconds to 0.225 seconds. No apparent reason has been found for this discrepancy. The agreement for the pitching acceleration is considered to be good in light of the manner of measurement. The shape of the analytical curve is given reasonably by the experimental curve and the maximum values are of the same order. A comparison of the analytical acceleration response of the structure as depicted at three stations with the measured response at those stations is shown in Fig. 20. The experimental acceleration response is seen to be predicted quite well by the analytical response. The absence of the higher harmonic content in the analytical response may be attributed to using only four vibratory modes in the structural representation. As may be seen, this harmonic contribution while adding some distortion to the response does not materially affect the correlation between experiment and analysis.

Landing 8 of flight 31 for a gross weight of 72,000 pounds also offers an opportunity to compare analytical and experimental results. Referring to Fig. 21, again it may be seen that the shape of the experimental curves for both the force and moment is given by the analytical curves. Applying the previously suggested correction for gross weight, the comparable magnitude for the experimental force for the 72,000 pound airplane corrected to 55,000 pounds is given by 84 per cent of the magnitude. This reduction brings the experimental force magnitude into excellent agreement with the analytical force magnitude, particularly at the maximum values. The application of the correction to the moments also tends to bring the moment magnitudes into agreement with the analytical moment magnitude. The τ variation for the analytical impact is in agreement also with that of the experiment. Comparison of the pitching velocities showed little or no agreement and no comparison of pitching accelerations was attempted.

The structural acceleration response for the 72,000 pound airplane may be seen in Fig. 22. Recalling that the difference in gross weights of the airplane is achieved by the addition of concentrated weights in the hull about the airplane center of gravity, it is to be expected that the vibratory characteristics of the hull would be greatly incluenced, and the wing to a lesser degree, by the presence of the concentrated weights. Comparing the experimental acceleration response of the 72,000 pound airplane with the calculated response for the 55,000 pound airplane, it may be seen that this occurs. The shape and magnitude of the calculated center of gravity and wing tip accelerations are in reasonable agreement with the experimental accelerations. The experimental bow accelerations, apparently showing the influence of the added hull weight, are seen to behave somewhat differently from the calculated accelerations. In light of the above discussion, it is felt that where some basis for comparison with the heavy airplane existed, the analytical results are in agreement with the experimental results.

B. PEAK VALUES

Figures 23a to 23d present the maximum values of force and of structural acceleration from the analysis as a function of rate of descent for the different initial trim angles and forward speeds. For purposes of comparison, experimental values having approximately the same initial trim angles and forward speeds are also shown against rate of descent. The analytical results for the structural response of the structure are in good agreement with the experimental data. Reduction of experimental data for the hydrodynamic force was not done for all landings. However, at a forward speed of 160 feet per second, the agreement between the analytically predicted force and the experimentally determined force is good in trend and magnitude.

C. CONCLUDING REMARKS

The above comparisons of experimental data with analytical data have shown that the analytically determined results have described accurately the landing impact conditions. The correlation of hydrodynamic forces and moments has indicated that the representation of these forces and moments in the equations of motion has been substantiated. The structural response as given by the equation of motion agrees very well with the actual structural response of the airplane, and indicates that the flexibility of the airplane was adequately represented by the flexible modes of the analysis. The response of the rigid airplane in pitch given in the analysis was in agreement with the experimental observed response. In light of this, it is believed that the hydrodynamic step impact and the dynamic response for the flexible seaplane may be accurately given by the method of analysis presented in this report.

VI. CONCLUSIONS AND RECOMMENDATIONS

A. CONCLUSIONS

A theoretical method of computing the dynamical impact loading, including the effects of structural flexibility and continuous trim variation, has been developed in "closed" form. This method, utilizing an electronic analog computer, permits rapid study of a wide range of initial conditions for the impact problem.

The dynamic acceleration response of the M-270 airplane was obtained from experimental measurements over a range of impact conditions. From these measurements the hydrodynamic force and moment on the airplane were obtained. The most critical parameter in measuring the effects of landing impact was found to be the rate of vertical descent.

A comparison of the experimental impact data with the results of the analysis showed that the analytical results generally were in good agreement with the experimental results. This agreement includes both time variation and magnitude. It is concluded that the hydrodynamic step impact and the dynamic response of the flexible seaplane may be accurately given by the method of analysis presented in this report.

The response of the flexible airplane was found to be a function of both the magnitude and shape of the forcing function. The maximum inertial loading for some structure was not obtained for the conditions of maximum hydrodynamic loading. In order to obtain the maximum loads for the flexible airplane it was necessary to study a range of landing impacts.

The inclusion of airplane flexibility in the equations of motion tended to reduce the hydrodynamic force obtained for the rigid airplane. In this instance the maximum reduction was of the order of 7 per cent. However, for a more flexible airplane this reduction may be of a large magnitude.

B. RECOMMENDATIONS

1) In the design of flexible seaplanes a range of landing impact conditions should be studied to obtain the maximum dynamic loads experienced by the structure.

2) Further experimental and analytical studies should be made using an airplane in which flexibility plays a more important role.

3) The methods of this analysis should be extended to include the effects of waves and impact locations other than the step.

4) It is recommended that further study be made to develop a method of measuring rate of descent in smooth and rough seas. It would be desirable to have such an instrument airborn so that landings would not be restricted to fixed points where required sea conditions may be difficult to obtain.

VII. REFERENCES

1. Mayo, W. L., "Hydrodynamic Impact of a System with a Single Elastic Mode-I Theory and Generalized Solution with an Application to an Elastic Airframe", NACA Report 1074, 1952.

2. Goland, M., Luke, Y. and Kahn, E.A., "Prediction of Dynamic Landing Loads", AF TR 5815, AMC 1949.

3. "Model 270 Water Loads Investigation and Impact Loads", Martin Company Engineering Report 7516, July 1955.

4. Benscoter, Stanley V., "Effect of Partial Wing Lift in Seaplane Landing Impact", NACA TN 1563, 1948.

5. O'Brien, T.F., and Pian, T.H.H., "Effect of Structural Flexibility on Aircraft Loading Part 1 Ground Loads", AF TR 6358, Pt I, July 1951.

6. MIL-A-8629, "Airplane Strength and Rigidity"

7. Targoff, W.P., "Associated Matrices of Bending and Coupled-Bending-Torsion Vibration", JAS, Vol. 14, No. 10, October 1947.

APPENDIX A

VIBRATORY ANALYSIS OF M-270 AIRPLANE

The M-270 dynamic landing load analysis is based on the use of airplane modes. An airplane mode is the case where the wing, hull and stabilizer are considered as flexible beams.

The following assumptions were made:

1) The weight of the fuselage was concentrated at 8 mass sta. along the center line of the ship;

2) The weight of the wing was concentrated at 6 mass sta. along the elastic axis of the wing;

3) The weight of the stabilizer was concentrated at 4 mass sta. along the elastic axis of the stabilizer;

4) The second hull mass contains the weight of the vertical tail;

5) The first hull mass was transferred to the elastic axis of the stabilizer;

6) The bending mode shapes were computed on the basis of unit deflection of the stabilizer tip;

7) For symmetric modes, the shear, slope, and torque are zero at the wing and stabilizer tips. At the fuselage, the end conditions are that the shear, moment, and torque are zero;

8) Stabilizer shear, moment, slope, deflection, torsion and torque at the root mass equals hull shear, torque, torsion deflection, slope and moment respectively times the proper sign and multiplying factor. The same set of conditions applies to the wing root.

1. Basic Data

The wing was divided into bays as shown in wing plan form, Fig. 24a. The stabilizer planform may be found in Fig. 24b, and the hull planform in Fig. 24c. The hull plan form further shows the relative location of the wing and stabilizer.

Weights and stiffness data were obtained from the M-270 project group (the M-270 is a hybrid consisting of the PBM-5 wings mounted on the rebuilt XP5M-1 hull). A breakdown of the weight and stiffness data is given in Table 9. Stiffness curves for bending and torsion per bay may be found in Figs. 25 and 26 respectively.

2. Coupled Airplane Modes of Vibration

The associated matrices method of Ref. 7 was used to obtain the symmetric modes. The deflection shapes are shown in Figs. 27 to 30.

The frequencies obtained were:

Mode	Frequency (CPM)
I	140.25
II	352.40
III	383.91
IV	459.23

TABLE 1

Analytical Data for the Flexible Airplane

1 V_x	2 τ_o	3 Z_o	4 $F_{(lb)}$	5 $M_{(in-lb)}$	6 $Z_{(in)}$	7 $\tau_{(rad)}$	8 $\dot{\tau}$	9 $\ddot{\tau}$	10 $A_{1H(g)}$	11 A_{5H}	12 A_{8H}	13 A_{1W}	14 A_{1T}	15 Z at F_{Max}	16 $T_{F_{Max}}$	17 Landing No.	
185	3	4	- 25,000	+ 3.83×10^6	+12.67	+.12	+ .10	+ .32	+ .31	- .40	- .95	- .775	- .37	+12.0	+.34	1	
		8	- 64,000	$+13.0 \times 10^6$	+19.67	+.20	+ .32	+1.28	- .875	-1.2	+2.75	+3.15	- .95	+12.0	+.20	2	
		12	-110,000	$+23.33 \times 10^6$	+28.33	+.20	+ .55	+2.4	-1.00	-1.78	-5.38	-5.00	-1.50	+13.33	+.125	3	
	6	4	- 31,000	+ 2.13×10^6	+10.16	+.09	-.031	- .06	- .68	- .55	- .70	-1.07	- .76	+10.0	+.325	4	
		8	- 90,000	+ 9.33×10^6	+15.33	+.14	+.06	+ .48	-1.38	-1.6	-2.40	-4.0	-1.63	+15.33	+.225	5	
		12	-150,000	$+18.0 \times 10^6$	+19.66	+.198	+.18	+1.16	-2.60	-2.45	-5.0	-6.88	-2.95	+16.67	+.15	6	
160	3	4	- 23,500	+ 3.83×10^6	+13.73	+.138	+.115	+ .36	- .28	- .42	- .90	- .688	- .33	+13.33	+.45	7	
		8	- 60,000	$+12.0 \times 10^6$	+21.73	+.198	+.346	+1.24	- .875	-1.10	-2.56	-2.90	-1.00	+15.33	+.20	8	
		12	-104,000	$+21.33 \times 10^6$	+32.0	+.215	+.565	+2.26	-1.05	-1.70	-5.20	-4.50	-1.00	+16.67	+.125	9	
		16	-153,000	$+33.33 \times 10^6$	+44.33	+.20	+.665	+3.50	+3.46	-2.40	+8.50	-6.50	+4.85	+16.67	+.10	10	
	6	4	- 28,500	$+53.33 \times 10^6$	+11.33	+.09	-.017	- .048	- .575	- .49	- .635	- .95	- .65	+11.00	+.325	11	
		8	- 83,000	+ 9.13×10^6	+17.07	+.148	+.084	+ .52	-1.32	-1.48	-2.40	-3.66	-1.60	+15.33	+.20	12	
		12	-130,000	$+16.33 \times 10^6$	+21.73	+.21	+.22	+1.16	-2.08	-2.30	-4.15	-6.0	-2.60	+18.0	+.15	13	
		16	-180,000	$+25.07 \times 10^6$	+27.5	+.21	+.374	+2.0	-9.5	-3.2	-7.65	-7.5	-5.10	+20.83	+.125	14	
	9	4	- 31,000	+ 1.47×10^6	+10.27	+.12	+.25	- .11	- .80	- .55	- .56	-1.05	- .85	+10.0	+.325	15	
		8	- 83,000	+ 5.93×10^6	+16.27	+.135	-.038	- .16	-1.70	-1.50	-1.75	-3.55	-1.87	+16.0	+.225	16	
		12	-135,000	$+11.83 \times 10^6$	+20.67	+.173	+.04	+ .43	-2.94	-2.35	-3.60	-6.20	-3.20	+17.33	+.16	17	
		16	-185,000	$+18.53 \times 10^6$	+26.67	+.20	+.14	+ .94	-4.88	-3.04	-6.5	-7.0	-6.0	+24.0	+.15	18	
135	3	4	- 23,400	+ 4.1×10^6	+14.67	+.15	+.133	+ .36	- .24	- .39	- .85	- .69	- .28	+14.0	+.40	19	
		8	- 55,000	$+11.13 \times 10^6$	+25.33	+.21	+.36	+1.12	- .80	- .90	-2.25	-2.80	- .90	+16.0	+.20	20	
		12	- 95,000	$+20.33 \times 10^6$	+39.17	+.20	+.525	+2.05	- .55	-1.45	-4.6	-4.15	- .75	+14.17	+.125	21	
		16	-140,000	$+31.67 \times 10^6$	+53.33	+.21	+.60	+3.25	+3.5	-2.20	-7.88	-6.0	+4.5	+16.67	+.10	22	
	6	4	- 26,000	+ 2.13×10^6	+12.27	+.105	-.009	+ .072	- .50	- .45	- .75	- .83	- .57	+12.00	+.35	23	
		8	- 72,000	+ 8.53×10^6	+18.67	+.17	+.11	+ .52	-1.15	-1.30	-2.2	-3.33	-1.35	+17.33	+.25	24	
		12	-120,000	$+16.4 \times 10^6$	+23.33	+.20	+.25	+1.12	-2.30	-1.96	-4.15	-5.25	-2.90	+20.00	+.175	25	
		16	-160,000	$+23.67 \times 10^6$	+33.33	+.20	+.40	+1.90	-3.06	-2.70	-6.9	-6.65	-4.25	+23.33	+.15	26	
	9	4	- 29,200	+ 1.60×10^6	+11.87	+.13	-.051	- .086	- .65	- .51	- .525	- .95	- .69	+11.8	+.375	27	
		8	- 80,000	+ 6.13×10^6	+17.60	+.15	-.019	+ .124	-1.72	-1.30	-1.76	-3.2	-1.96	+16.67	+.225	28	
		12	-120,000	$+11.2 \times 10^6$	+23.33	+.194	+.075	+.472	-2.8	-1.92	-3.4	-5.25	-3.10	+20.00	+.15	29	
		16	-162,000	$+17.33 \times 10^6$	+30.0	+.20	+.188	+.96	-3.8	-2.64	-5.75	-6.5	+4.70	+23.33	+.15	30	

TABLE 2

Analytical Data for the Rigid Airplane

1 V_x	2 τ_o	3 Z_o	4 $F_{(lb)}$	5 $M_{(in-lb)}$	6 $Z_{(in)}$	7 $\tau_{(rad)}$	8 $\dot{\tau}$	9 $\ddot{\tau}$	10 $A_{1H(g)}$	11 A_{5H}	12 A_{8H}	13 A_{1W}	14 A_{1T}	15 Z at F_{Max}	16 $T_{F_{Max}}$	17 Landing No.	
185	3	4	- 25,600	+ 3.93x10^6	+12.93	+.12	+.099	+ .32	- .20	- .45	- .85	- .45	- .20	+12.0	+.35	31	
		8	- 68,000	+13.67x10^6	+20.0	+.205	+.33	+1.304	- .74	-1.225	-2.74	-1.25	- .75	+16.33	+.20	32	
		12	-115,000	+23.6x10^6	+30.0	+.205	+.575	+2.40	- .52	-1.97	-4.75	-1.97	- .52	+18.33	+.14	33	
	6	4	- 32,600	+ 2.27x10^6	+10.33	+.09	-.028	- .06	- .595	- .58	- .60	- .575	- .60	+10.00	+.30	34	
		8	- 98,000	+10.0x10^6	+16.0	+.14	+.063	+ .504	-1.21	-1.70	- .565	-1.70	-1.25	+15.33	+.20	35	
		12	-157,000	+18.67x10^6	+21.0	+.18	+.188	+1.184	-1.65	-2.76	-4.00	-2.8	-1.60	+18.33	+.15	36	
160	3	4	- 23,800	+ 4.08x10^6	+14.33	+.13	+.115	+ .376	- .166	- .45	- .87	- .46	- .18	+13.87	+.42	37	
		8	- 61,200	+12.33x10^6	+22.67	+.205	+.34	+1.20	- .720	-1.10	-2.46	- .112	- .72	+16.00	+.20	38	
		12	-102,000	+21.33x10^6	+33.33	+.195	+.55	+2.20	- .45	-1.8	-4.2	-1.82	- .45	+18.33	+.15	39	
		16	-148,000	+32.67x10^6	+46.67	+.20	+.665	+3.36	- .63	-2.6	-6.4	-2.76	- .63	+18.33	+.10	40	
	6	4	- 29,800	+ 2.27x10^6	+11.33	+.20	-.012	- .048	- .50	- .53	- .59	- .55	- .51	+11.33	+.35	41	
		8	- 88,000	+ 9.33x10^6	+17.60	+.15	+.083	+ .524	-1.03	-1.54	-2.18	-1.52	-1.05	+17.00	+.225	42	
		12	-138,000	+17.07x10^6	+22.67	+.21	+.218	+1.15	-1.48	-2.4	-3.66	-2.46	-1.48	+18.66	+.15	43	
		16	-190,000	+25.07x10^6	+29.0	+.222	+.36	+1.9	-1.90	-3.36	-5.50	-3.36	-1.90	+17.66	+.10	44	
	9	4	- 33,000	+ 1.53x10^6	+10.4	+.124	-.061	- .11	- .73	- .60	- .495	- .60	- .74	+10.33	+.30	45	
		8	- 91,000	+ 6.53x10^6	+16.4	+.14	-.033	- .16	-1.60	-1.59	-1.64	-1.63	-1.62	+16.0	+.225	46	
		12	-143,000	+12.67x10^6	+21.2	+.177	+.046	+ .452	-2.30	-2.56	-2.94	-2.60	-2.32	+19.73	+.175	47	
		16	-190,000	+18.67x10^6	+26.67	+.196	+.147	+ .912	-3.00	-3.44	-4.35	-3.48	-2.96	+21.67	+.125	48	
135	3	4	- 24,000	+ 4.23x10^6	+15.73	+.122	+.13	+ .384	- .16	- .40	- .84	- .45	- .16	+14.67	+.40	49	
		8	- 56,000	+11.33x10^6	+26.67	+.20	+.354	+1.12	- .675	- .95	-2.22	-1.03	- .70	+16.67	+.20	50	
		12	- 92,000	+19.73x10^6	+41.0	+.20	+.52	+2.0	- .41	-1.60	-3.84	-1.72	- .44	+18.33	+.125	51	
		16	-138,000	+30.00x10^6	+56.0	+.195	+.60	+3.06	- .60	-2.34	-5.85	-2.46	- .60	+16.67	+.10	52	
	6	4	- 27,400	+ 2.33x10^6	+12.67	+.11	-.009	+ .072	- .425	- .485	- .57	- .50	- .425	+12.33	+.35	53	
		8	- 74,000	+ 8.67x10^6	+19.07	+.155	+.11	+ .54	- .85	-1.35	-1.94	-1.38	- .85	+18.0	+.225	54	
		12	-120,000	+14.93x10^6	+25.33	+.195	+.246	+1.088	-1.26	-2.10	-3.2	-2.20	-1.25	+ 8.33	+.125	55	
		16	-165,000	+22.4x10^6	+33.33	+.21	+.40	+1.76	-1.66	-2.96	-4.75	-3.04	-1.74	+18.33	+.10	56	
	9	4	- 30,600	+ 1.57x10^6	+11.60	+.13	-.05	- .084	- .64	- .54	- .475	- .55	- .65	+11.67	+.35	57	
		8	- 80,000	+8.067x10^6	+18.27	+.15	-.018	+ .126	-1.33	-1.42	-1.52	-1.42	-1.36	+17.73	+.25	58	
		12	-120,000	+ 11.2x10^6	+23.73	+.185	+.078	+ .496	-1.90	-2.20	-2.60	-2.26	-1.90	+19.33	+.15	59	
		16	-164,000	+16.67x10^6	+30.00	+.197	+.19	+ .936	-2.44	-2.96	-3.75	-3.00	-2.42	+22.67	+.125	60	

Table 3 a.

Maximum Load Factors G.W. = 71,000

Flight No. 31 - 5 Nov. '54

Pickup No.	Ldg 1		Ldg 2		Ldg 3		Ldg 4		Ldg 5		Ldg 6		Ldg 7		Ldg 8
21			2.0		2.16		1.50		1.83		2.0		2.58		2.91
22	1.09		1.53		2.11		1.58		1.98		1.93		2.29		2.56
23			2.04		2.09		1.80		1.40		1.70		2.19		2.39
24			1.53		2.26		1.37		1.53		2.10		2.21		2.52
25			1.51		2.15		1.60		1.77		1.77		2.24		2.58
26			1.78		3.16		1.84		2.32		2.92		2.98		4.06
29			1.33		2.30		1.56		1.93		1.93		2.35		2.63
44			1.66		2.19		1.33		1.82		1.86		2.27		2.80
45			1.37		1.92		1.18		1.37		1.73		1.73		2.46
46			1.71		2.42		1.59		2.07		2.18		2.30		2.78
47			1.66		2.24		1.58		1.91		1.99		2.32		2.82
48			1.65		2.76		1.53		2.30		2.41		2.49		3.25
49															
Rate of Descent	1.0		1.9		5.1		3.6		3.4		2.9		5.5		8.0
Hull Angle	4.5°		6.5°		6.0°		5.0°		7.0°		8.0°		9.0°		9.5°
I.A.S.	103		95		97		102		89		89		89		88
Water Speed	101 K		101 K		105 K		109K		99 K		96 K		96 K		97 K

Table 3 b.

Maximum Stress — G.W. = 71,000

Flight No. 31 - 5 Nov. '54

Pickup No.	Ldg 1	Landing No. 2		Landing No. 3		Landing No. 4		Landing No. 5		Landing No. 6		Landing No. 7		Landing No. 8	
		Ten.	Comp.	Ten.	Comp.	Ten.	Comp.	Ten.	Comp.	Ten.	Comp.	Ten.	Comp.	Ten.	Comp.
27															
28															
30		1054	2258	1054	5719	1204	2559	1656	3612	3010	4666	1806	8428	2258	7826
31		936	936	2028	624	936	936	1560	1248	2184	936	2652	780	3120	1248
32		228	152	607	152	911	228	304	152	456	152	607	304	759	228
33			120	602						421	120	722	361	361	
34		1590	954	2862	795	1590	954	1749	1272	1908	1272	4452	1272	4293	1272
35		516		1032					688	688	516	1204	344	1376	576
36		319	319	399	319	479	319	319	479	479	479	479	798	878	638
37				137						892		206		137	
38		266	133	2660		1397	200	1131	266	1131	133	532	266	665	
39			126	440	502	251	251	377	377	502	126	126	377	440	251
40		131	262	131	262	197	131	262	590	131	786	197	131	197	328
41															
42		209	209		973	139			626	139	834	139	904	139	1043
43		142	354	142	1274	212	212	142	1133	354	920	354	1204		2124

Table 3 c.

Maximum Pressures

G.W. = 71,000

Flight No. 31 - 5 Nov. '54

Pickup No.	Ldg. 1		Ldg. 2		Ldg. 3		Ldg. 4		Ldg. 5		Ldg. 6		Ldg. 7		Ldg. 8
1															
2															
3															
4															
5															
6															
7															
8															
9											34.5				7.3
10			30.7		29.8		15.8		18.4		50.4		39.4		55.2
11															
12											4.4				
13															
14															
15															
16															
17															
18			90.1		25.7		25.0		28.8		65.1		33.3		16.7
19			46.0		60.6		13.8		11.7		17.6		29.3		15.1
20			51.2		51.9		29.2		39.8		28.4		40.6		32.5

Table 4 a.

Maximum Load Factors

Flight No. 26 - 29 Sept. '54

G.W. = 64,000
C.G. = 26% MAC

	Pickup No.	Ldg 1		Ldg 2		Ldg 3		Ldg 4		Ldg 5					
	21	1.72		1.24		1.64		1.32		1.64					
C.G.	22	2.10		1.53		2.10		1.78		1.97					
	23	1.67		1.02		1.52				1.43					
	24	1.97		1.41		2.10				1.71					
	25	1.96		1.37		1.87				1.79					
	26	3.19		1.69		2.90				2.15					
L.H.E.	29	2.2		1.45		2.3				1.95					
	44	2.01		1.31		2.01		1.39		1.78					
	45	1.53				1.49		1.35		1.53					
	46	2.13		1.23		2.24		1.23		1.85					
	47	1.87		1.24		1.99		1.16		1.65					
	48	2.24		1.36		2.38		1.25		1.93					
L.H.E. (Sanborn)	49	2.13		1.48		1.99				1.82					
1 sec/ touch	Rate of Descent	2.0		4.0		3.4		4.1		4.5					
	Hull Angle	8°		6°		6°		7°		6°					
	I.A.S.	77 K		88 K		81 K		81 K							

Table 4 b.

Maximum Stress

Flight No. 26 - 29 Sept. '54

G.W. = 64,000
C.G. = 26% MAC

Cable No.	Landing No. 1		Landing No. 2		Landing No. 3		Landing No. 4		Landing No. 5	
	Ten.	Comp.	Ten.	Comp.	Ten.	Comp.	Ten.	Comp.	Ten.	Comp.
27										
28										
30	1440	5760	720	2304	1872	6624	504	2304	1152	4608
31	2140	153	765		1990	918			1680	765
32	520	149	223		520	74.3			446	74.3
33	902		291		640		175		757	
34	2010	930	620		2640	1550			1550	1080
35	850	340	170		850	510			680	170
36	306	306	76.6		536	230			230	306
37										
38	2315	129	1157		772		1157	193	1543	322
39	1030		485		939	242	545		545	242
40		1431		602		1506		377	151	1092
41	1600	200	1000	300	1450	400	800	450	1000	400
42		1105		390		1040				1040
43		1160		580		1668				1015

Table 4 c.

Maximum Pressures

Flight No. 26 - 29 Sept. '54

G.W. = 64,000
C.G. = 26 % MAC

Pickup No.	Ldg 1		Ldg 2		Ldg 3		Ldg 4		Ldg 5						
1															
2															
3															
4															
5					5.3		9.1								
6															
7															
8															
9	35.4						20.2								
10	41.3		44.2		48.7		36.3		61.1						
11							7.3								
12															
13	33.9				23.6		8.4								
14							13.1								
15															
16															
17					39.1		42.0		30.5						
18															
19	42.7		35.5		45.5		14.4		34.3						
20	54.4		34.7		46.5		22.4		35.0						

Table 5 a.

Maximum Load Factors

Flight No. 27 - 8 Oct. '54

G.W. = 64,000
C.G. = 26% MAC

	Pickup No.	Ldg 1		Ldg 2		Ldg 3		Ldg 4		Ldg 5		Ldg 6			
	21			1.50		1.33		2.16		4.16		1.58			
C.G.	22			1.44		1.44		1.44		2.52					
	23			1.45		1.55		1.40		1.79		1.50			
	24			1.26		1.32		1.60		2.32					
	25			1.30		1.39		1.56		2.46					
	26			1.84		1.72		1.75		3.29					
L.H.E	29			1.37		1.33		1.57		2.49					
	44	1.57		1.50		1.41		1.65		2.63					
	45	1.56		1.56		1.65		1.46		2.11					
	46	1.47		1.70		1.35		1.47		1.76					
	47	1.41		1.65		1.33		1.49		1.39					
	48	1.60		1.60		1.60		1.83		2.66					
L.H.E (San-born)	49														
	Rate of Descent	3.1		1.7		3.0				5.1					
	Hull Angle	5.0°		4.0°		4.5°				4.5°					
	I.A.S.	95		89		89		90		83					
	Water Speed	94		90		84		85		90				Knots	

Table 5 b.

Maximum Stress

Flight No. 27 - 8 Oct. '54

G.W. = 64,000
C.G. = 26% MAC

Pickup No.	Landing No. 1		Landing No. 2		Landing No. 3		Landing No. 4		Landing No. 5		Landing No. 6				
	Ten.	Comp.	Ten.	Comp.	Ten.	Comp.	Ten.	Comp.	Ten.	Comp.	Ten.	Comp.			
27	2380	492													
28															
30				1806		1660	1050	3010	1660	7370					
31				474	1106		1422		2528	948					
32			306		306	153	383		919						
33	120	240			120		420		900						
34			640	800	800		1120		3040	960					
35			680		680		850		1360	340					
36				159	159		239		636	477					
37															
38	396	132	198		264	132	1452	330	3168	528					
39	374	187	125	187	250	312	250	187	250	749					
40			459	524		459		1048	262	1510					
41	1573														
42				277		415		554		1246					
43	141	212		282	141	423	141	564		1128					

Table 5 c.

Maximum Pressures

Flight No. 27 - 8 Oct. '54

G.W. = 64,000
C.G. = 26% MAC

Pickup No.	Ldg 1		Ldg 2		Ldg 3		Ldg 4		Ldg 5						
1															
2															
3															
4															
5															
6															
7															
8															
9							33.0		40.3						
10			16.0		24.7		17.0		21.1						
11									12.5						
12															
13							18.1		13.0						
14							6.0		19.7						
15															
16															
17			15.8		14.5										
18			20.4		14.2		40.8		34.0						
19			21.2		4.2		9.6		11.6						
20			18.8		28.6		15.1		31.9						

Table 6 a.

Maximum Load Factors

Flight No. 29 - 27 Oct. '54

G.W. = 64,000
C.G. = 26 % MAC

	Pickup No.	Ldg 1		Ldg 2		Ldg 3		Ldg 4		Ldg 5		Ldg 6		Ldg 7	
	21	1.91		1.91		2.83		7.15		2.00		2.00		3.24	
C.G.	22	1.62		1.40		1.89		3.85		1.45		1.62		2.38	
	23	1.30		1.25		2.68		3.38						2.09	
	24	1.32		1.27		2.11		3.76						2.48	
	25	1.43		1.26		2.29		4.35						2.29	
	26	1.72		1.84		3.28		8.56						3.88	
L.H.E	29	1.65		1.37		1.93		4.25						2.58	
	44														
	45														
	46														
	47														
	48														
L.H.E (Sand)	49														
	Rate of Descent	4.5		4.5		7.7		13.3		2.2				11.1	
	Hull Angle	2.0°		2.0°		6.0°		4.5°		5.0°		2.5°		3.5°	
	I.A.S.	91		97		86		79		92		95		91	Knots
	Water Speed	99		110		98		93		103		109		100	Knots

Table 6 b.

Maximum Stress

Flight No. 29 - 27 Oct. '54

G.W. = 64,000
C.G. = 26% MAC

Pickup No.	Landing No. 1		Landing No. 2		Landing No. 3		Landing No. 4		Landing No. 5		Landing No. 6		Landing No. 7	
	Ten	Comp.	Ten.	Comp.	Ten.	Comp.	Ten.	Comp.	Ten.	Comp.	Ten.	Comp.	Ten.	Comp.
27														
28														
30														
31	1264	474	474	474	2212	632	6004						2844	948
32	228		304		607	76	1746	152					759	152
33														
34	800	320	640	160	2240	960	7360	1920					2560	1280
35					692	519	10034	865					865	519
36					239	477	1272	1034					636	318
37							277	138					138	138
38														
39														
40														
41														
42														
43														

Table 6 c.

Maximum Pressures

Flight No. 29 - 27 Oct. '54

G.W. = 64,000
C.G. = 26% MAC

Pickup No.	Ldg 1		Ldg 2		Ldg 3		Ldg 4		Ldg 5		Ldg 6		Ldg 7		
1															
2															
3															
4					.7		40.5						32.9		
5							33.1								
6															
7							5.1								
8															
9	36.5				.8										
10	39.0		35.5		61.5		57.1						16.3		
11					.8		1.5								
12					10.5		82.6						12.9		
13	15.9												15.1		
14	3.6				2.0		8.9						3.6		
15							30.3								
16							11.0								
17															
18	20.1		23.3												
19	16.7		15.1		30.5		42.6						21.7		
20	40.3		41.3		44.5		20.7								

Table 7 a.

Maximum Load Factors

Flight No. 28 - 21 Oct. '54

G.W. = 64,000
C.G. = 26% MAC

	Pickup No.	Ldg 1													
	21	2.16													
C.G.	22	1.81													
	23	1.50													
	24	1.53													
	25	1.52													
	26.	2.20													
L.H.E	29	1.70													
	44	1.74													
	45	1.74													
	46	1.95													
	47	1.90													
	48	2.30													
L.H.E (Sand)	49														
	Rate of Descent	4.5													
	Hull Angle	3.5													
	I.A.S.	92													
	Water Speed	96													

Table 7 b.

Maximum Stress

Flight No. 28 - 21 Oct. '54

G.W. = 64,000
C.G. = 26% MAC

	Landing No. 1														
Pickup No.	Ten.	Comp.													
27															
28															
30		4050													
31															
32	546														
33	482														
34	1600														
35	692														
36	239														
37	208														
38	1463	200													
39	376	313													
40		1080													
41															
42		545													
43		423													

Table 7 c.

Maximum Pressures

Flight No. 28 - 21 Oct. '54

G.W. = 64,000
C.G. = 26% MAC

Pickup No.	Ldg 1														
1															
2															
3															
4															
5															
6															
7															
8															
9	28.4														
10	39.7														
11															
12															
13	25.0														
14	4.6														
15															
16															
17															
18	37.4														
19	15.9														
20	34.3														

TABLE 8

Weight Distribution

Wing Station	64,000 lb	72,000 lb	55,000 lb
57	5372	5372	5372
140	13,040	13,040	13,040
233	1544	1544	1544
353	1372	1372	1372
489	1806	1806	1806
623	610	610	610
Hull Station			
25	1406	1406	1406
125	3242	4242	2042
261	11,621	12,221	9882
433	7708	11,043	5087
568	6000	8020	3950
760	4146	4146	2896
892	2229	2229	2229
923	2433	2433	2433
1025	1331	1331	1331

TABLE 9

Weight and Stiffness Properties

MASS NO.	PANEL B.L.	PANEL H.S.	WT (lb)	ELASTIC AXIS H.S.	ELASTIC AXIS W.L.	CG LOCATION H.S.	CG LOCATION B.L.	CG LOCATION W.L.	I_{PEA} ($lb\text{-}in^2$)	I_{REA} ($lb\text{-}in^2$)	S_P (lb-in)	S_R (lb-in)	STIFFNESS EIx10-9 ($lb\text{-}in^2$)	STIFFNESS GIx10-9 ($lb\text{-}in^2$)
1_S	223 to 178	---	73	936.8	--	943.3	208	--	29,514	---	474.5	--		
2_S	178 to 118	---	96.7	932.9	--	936.8	148	--	51,223	---	377.1	--	.2888	.2360
3_S	118 to 58	---	163.32	929.1	--	931.0	88	--	107,040	---	317.9	--	1.4175	.6620
4_S	58 to 0	---	217.98	925.3	--	934.5	29	--	191,666	---	2014.	--	3.8850	1.3557
1_H		1112.2 to 967.5	1331	--	--	1025.1	--	--	15,494,983.6	---	135,362.7	--	3.6175	1.6870
2_H		967.5 to 812.5	2229	--	--	891.9	--	--	24,865,203.	---	0	--	138.60	21.00
3_H		812.5 to 657.5	4146	--	--	759.9	--	--	0	---	0	--	224.49	36.05
4_H		657.5 to 502.5	3199	--	--	567.8	--	--	0	---	0	--	333.51	73.92
5_H		502.5 to 347.5	7708	--	--	432.8	--	--	167,801,320.	---	906,672.	--	467.58	127.27
													655.42	164.36

TABLE 9

Weight and Stiffness Properties (Continued)

MASS NO.	PANEL B.L.	PANEL H.S.	WT (LB)	ELASTIC AXIS H.S.	ELASTIC AXIS W.L.	CG LOCATION H.S.	CG LOCATION B.L.	CG LOCATION W.L.	I_{PEA} (lb-in^2)	I_{REA} (lb-in^2)	S_P (lb-in)	S_R (lb-in)	STIFFNESS EIx10-9 (lb-in^2)	STIFFNESS GIx10-9 (lb-in^2)
6_H	--	347.5 to 192.5	9332	--	--	261.0	--	--	0	--	0	--		
													449.04	114.75
7_H	--	192.5 to 37.5	3242	--	--	125.3	--	--	0	--	0	--		
													215.83	61.90
8_H	--	37.5 to -117.5	1406	--	--	25.1	--	--	0	--	0	--		
1_W	708 to 567	---	305.	425.6	--	421.7	622.6	197.8	299,234.	--	-1189.50	--		
													1.295	1.550
2_W	567 to 411	---	903.	427.7	228.98	421.0	488.7	171.1	3,033,734.	6,131,818.	-6050.10	0		
													5.460	10.750
3_W	411 to 292	---	685.7	429.9	--	439.1	353.4	192.4	1,466,166.	--	6308.44	--		
													18.655	23.283
4_W	292 to 173.5	---	772.5	431.9	--	451.8	233.3	190.8	1,786,305	--	15,372.75	--		
													47.845	17.350
5_W	173.5 to 87	---	5378.9	441.7	--	342.8	139.7	174.1	72,204,584.	--	-531,973.21	--		
													71.400	44.433
6_W	87 to 0	---	2686.	432.9	--	456.8	56.8	160.9	5,110,637	--	64,195.40	--		
													86.800	68.650

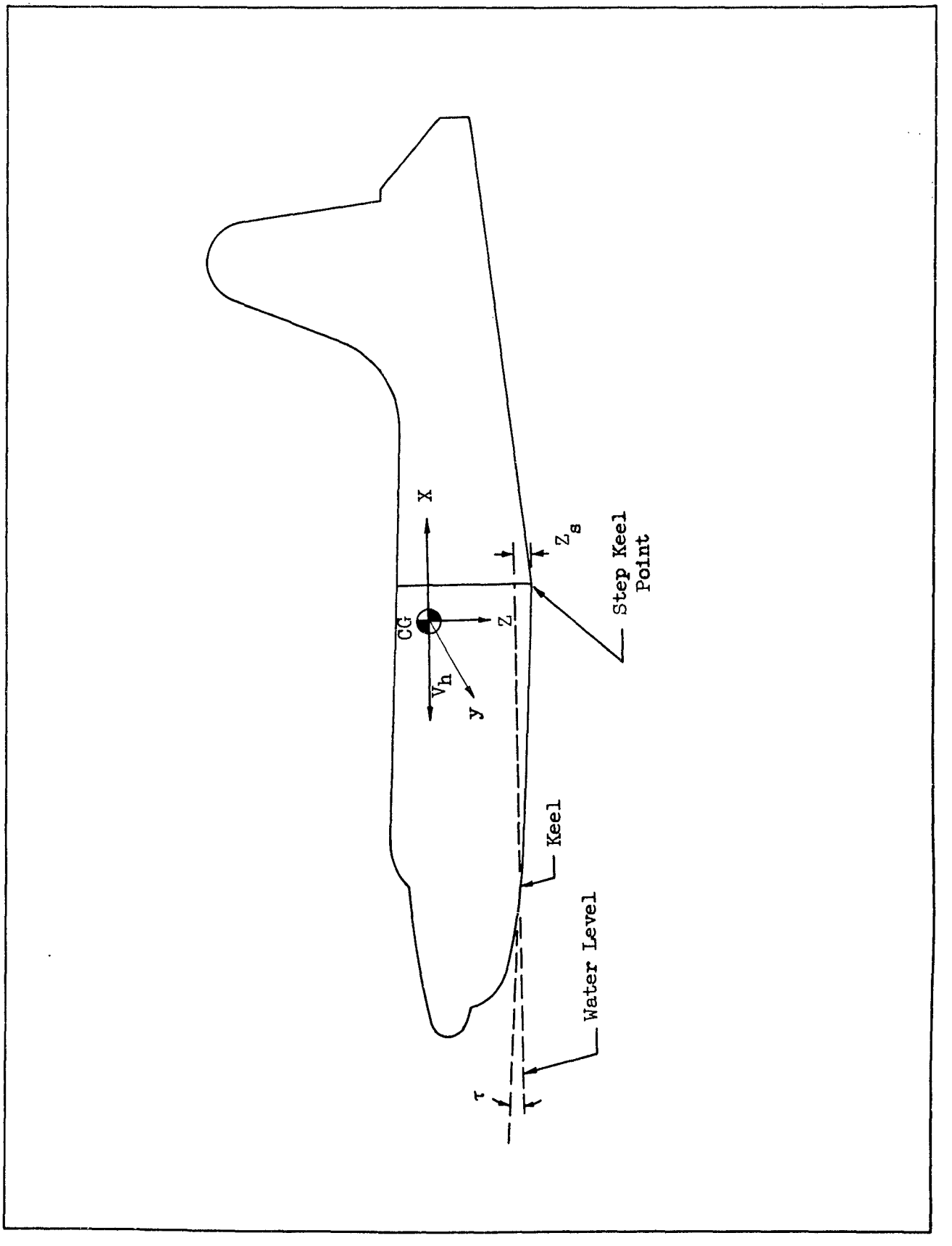

Fig. 1. Airplane Coordinate System

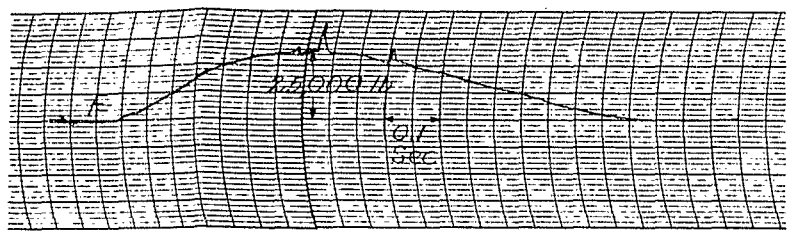

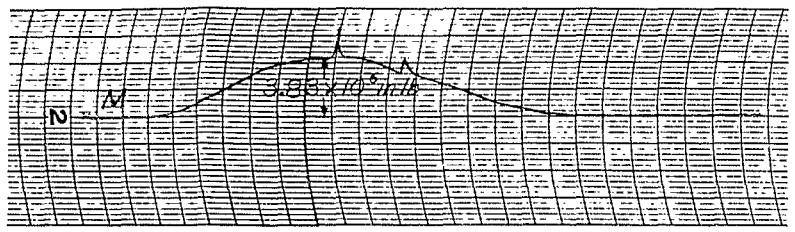

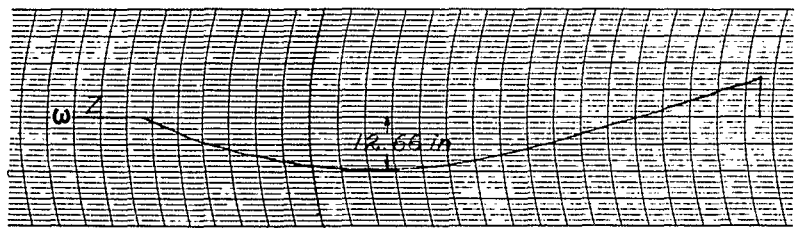

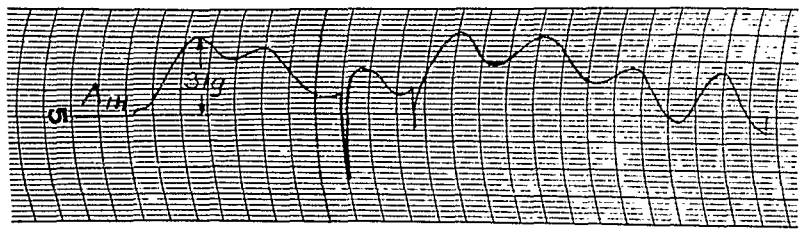

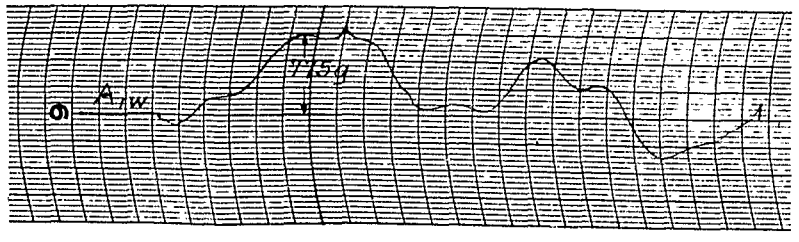

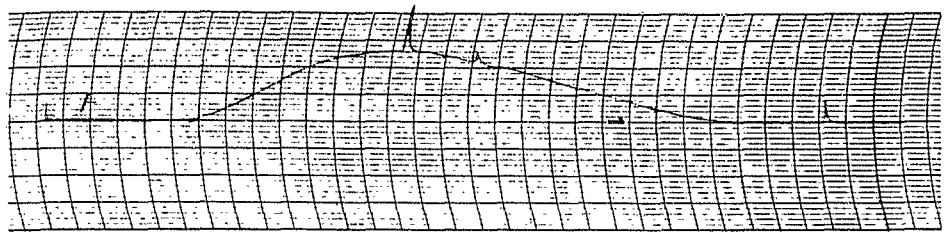

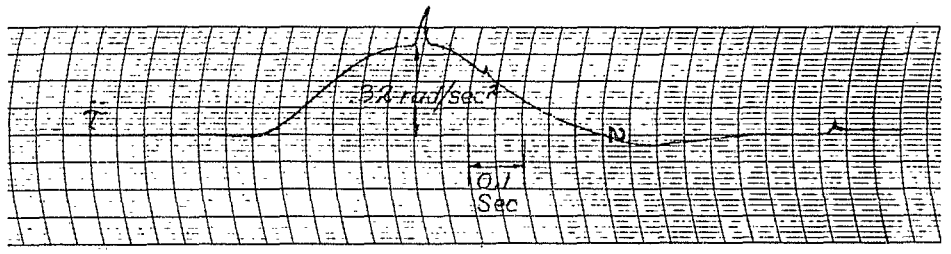

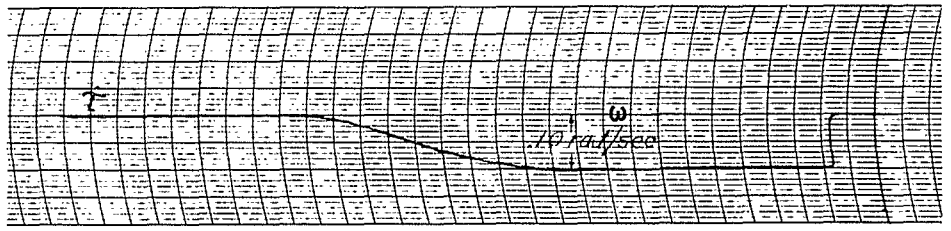

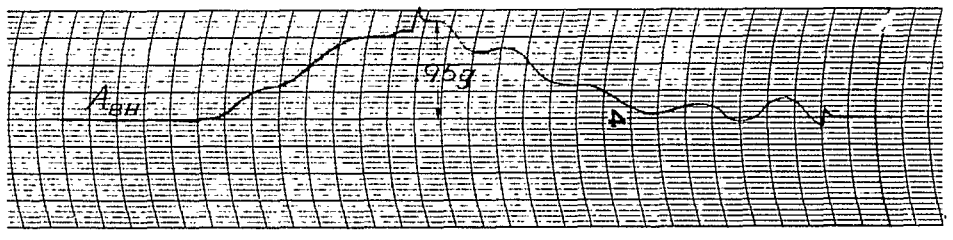

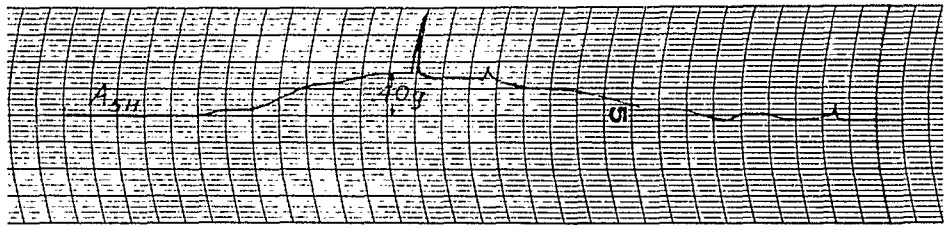

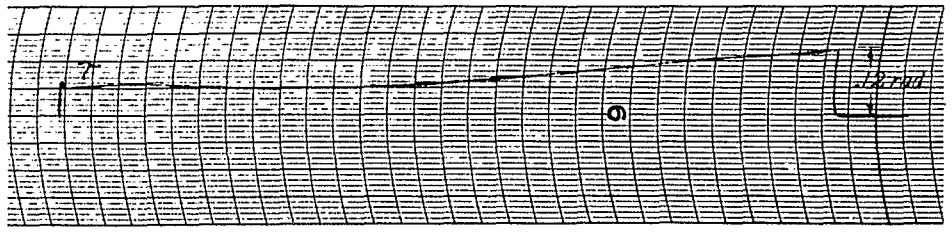

Fig. 2a. REAC Solutions to Impact Problem - Flexible Case

V_x = 185 fps τ_o = 3° $\dot{Z}_o$ = 4 fps

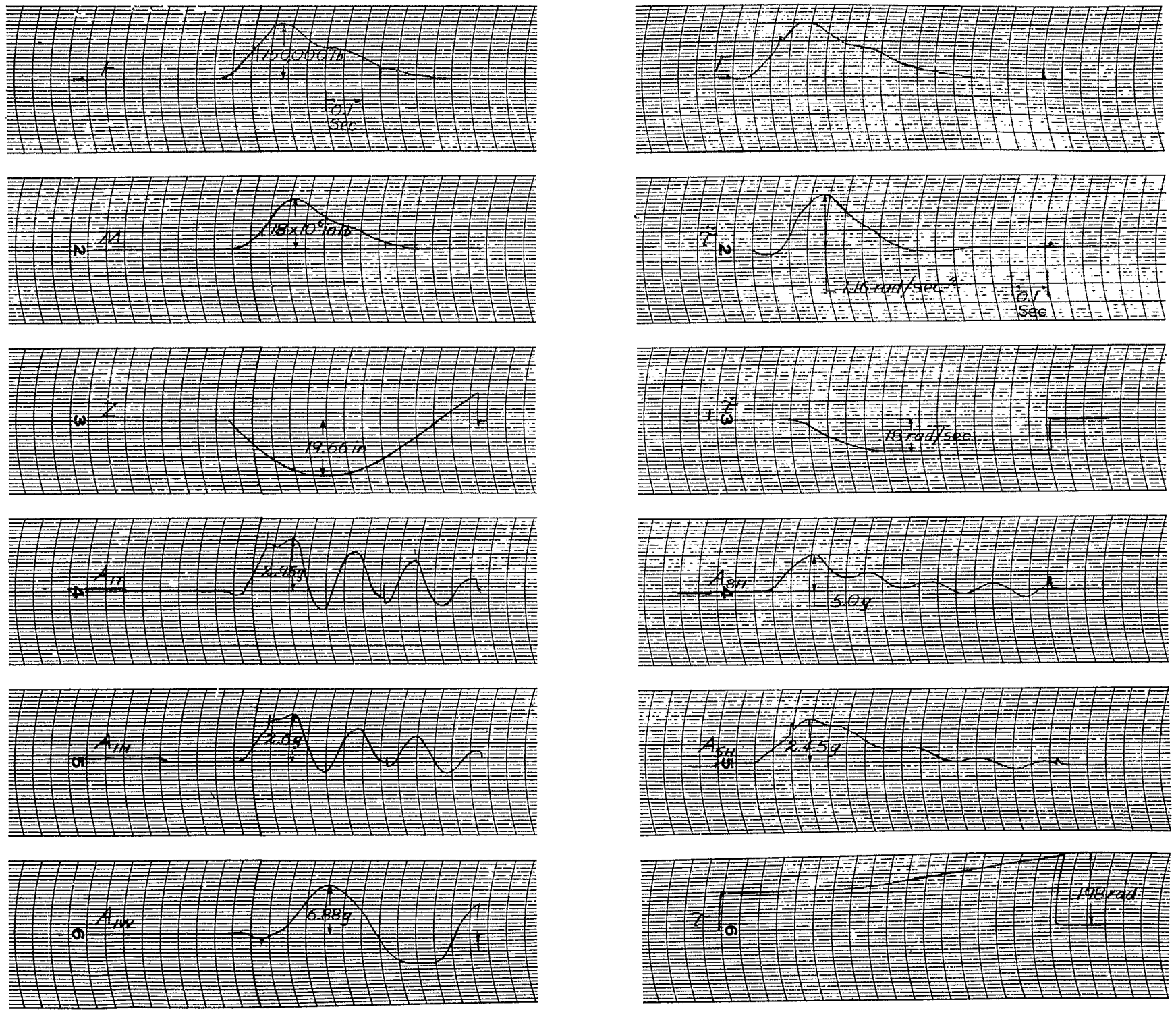

Fig. 2b. REAC Solutions to Impact Problem - Flexible Case

V_x = 185 fps τ_o = 6° $\dot{Z}_o$ = 12 fps

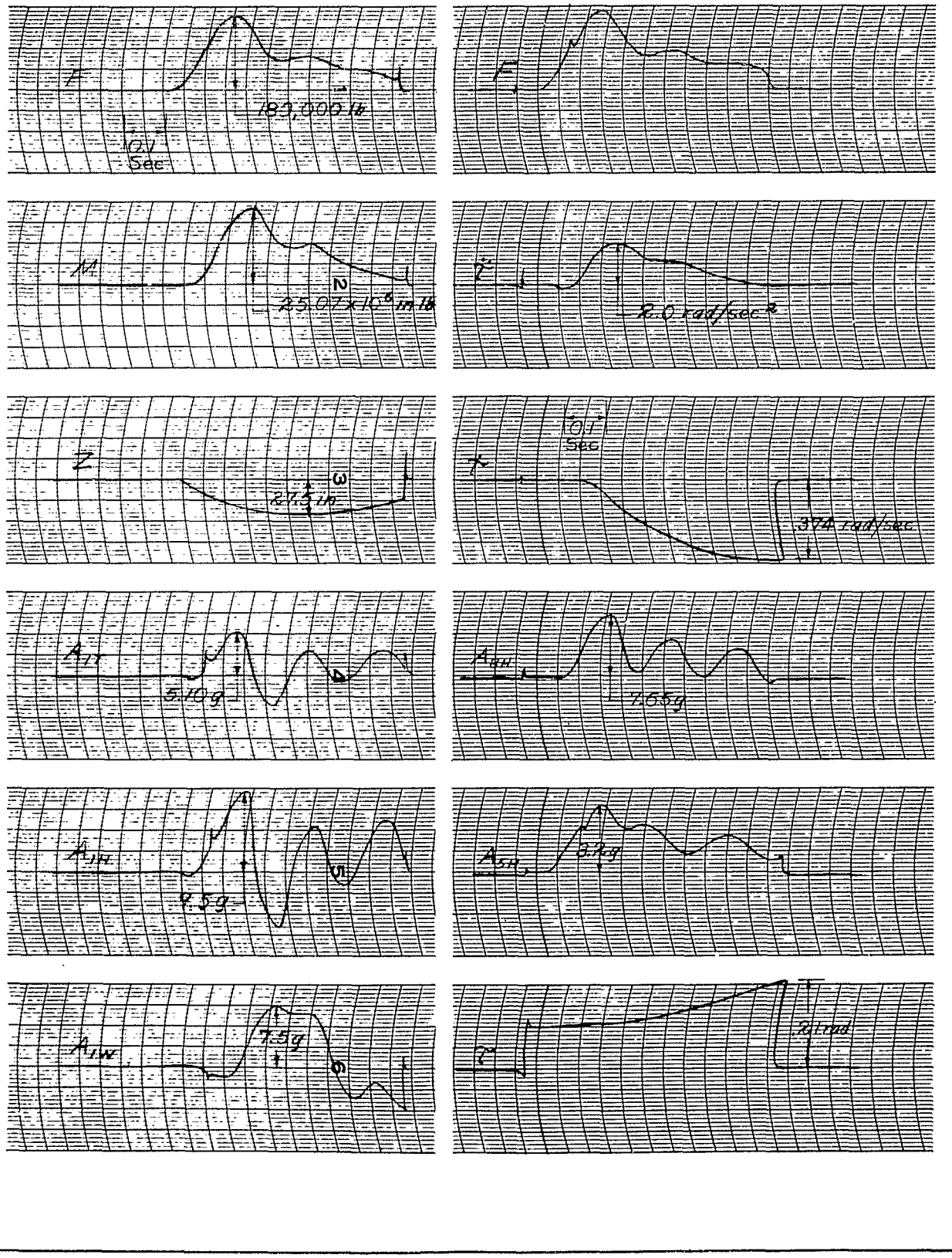

Fig. 2c. REAC Solutions to Impact Problem - Flexible Case

V_x = 160 fps $\quad \tau_o = 6° \quad \dot{Z}_o$ = 12 fps

ER NO. 7515

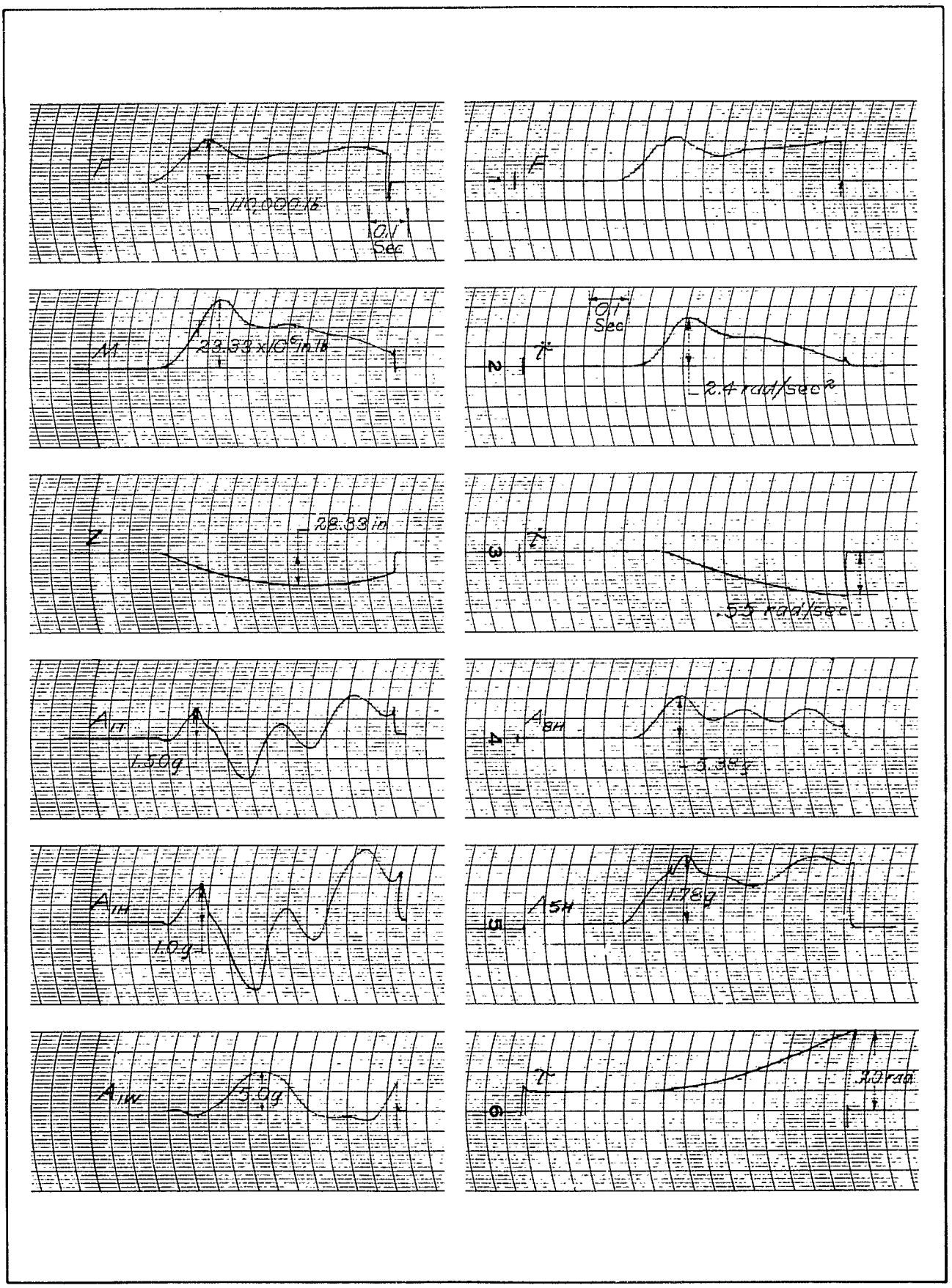

Fig. 2d. REAC Solutions to Impact Problem - Flexible Case

V_x = 185 fps $\quad \tau_o = 3° \quad \overset{o}{Z}_o$ = 12 fps

ER NO. 7515

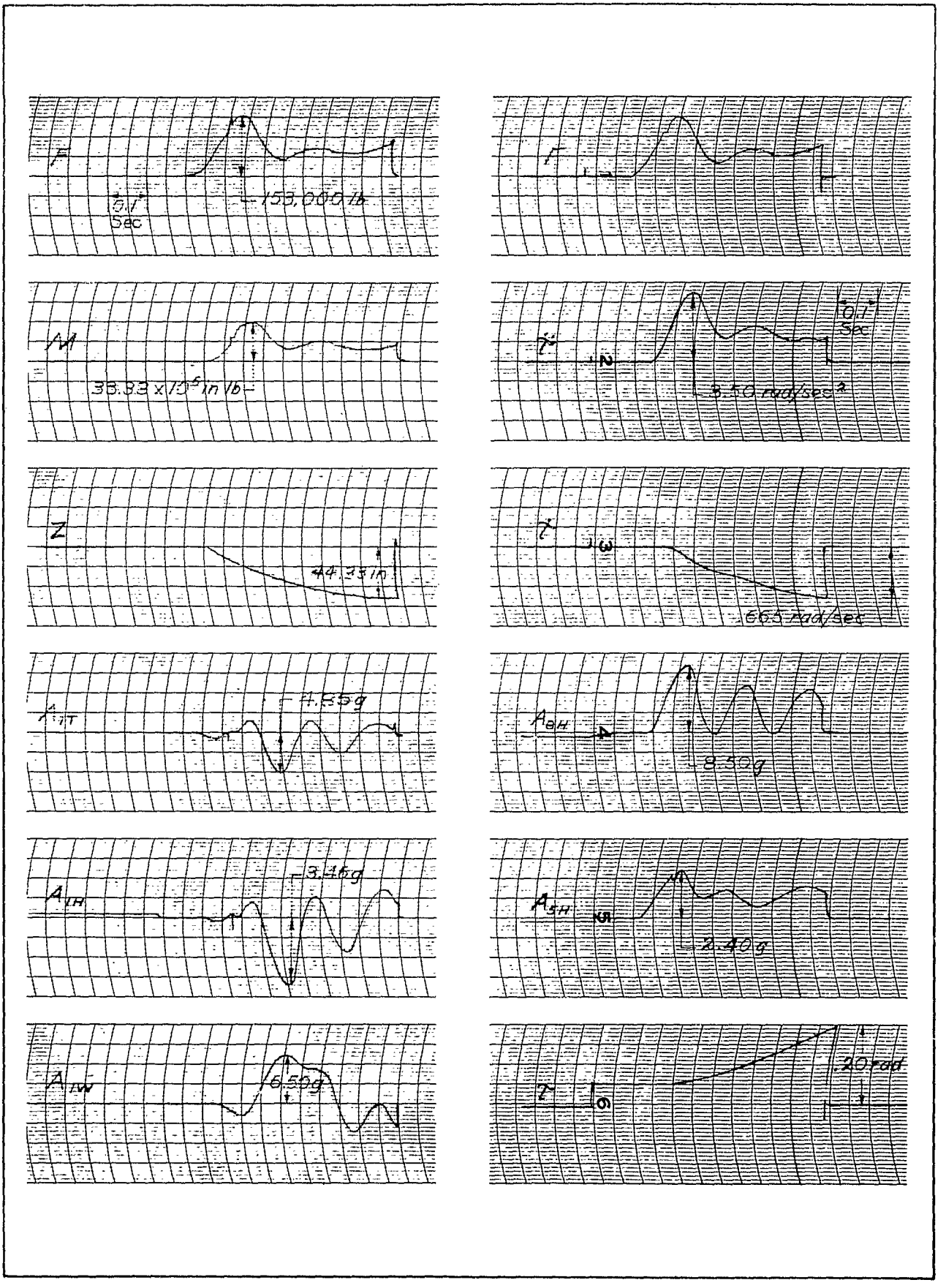

Fig. 2e. REAC Solutions to Impact Problem - Flexible Case

V_x = 160 fps $\quad \tau_o = 3°$ $\quad \dot{Z}_o$ = 16 fps

ER NO. 7515

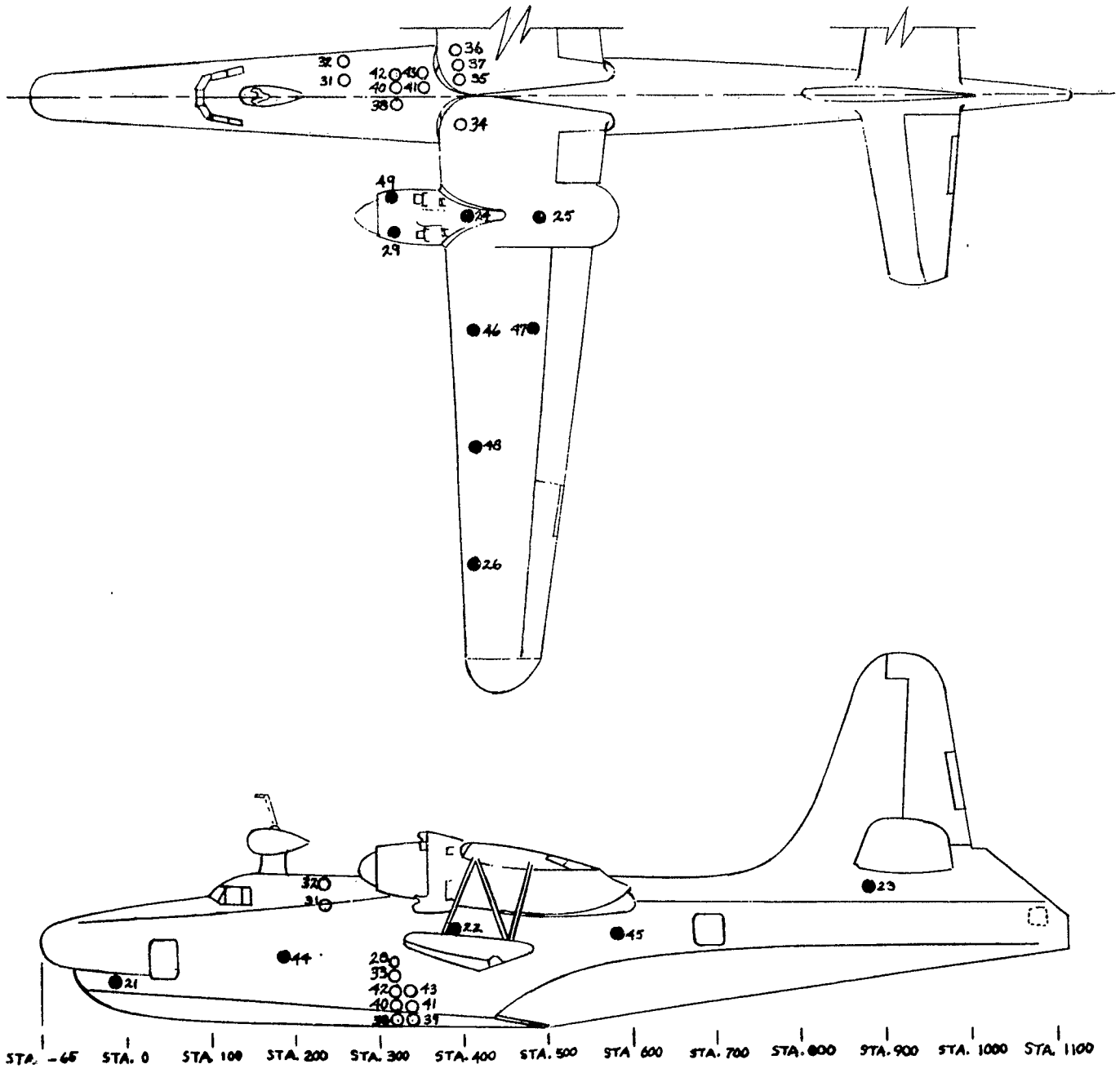

CABLE NO.	ITEM	LOCATION
21	ACCELEROMETER	HULL STA. 18, W.L. 49½ ℄ OF SHIP
22		HULL STA. 396, W.L. 130 ℄ OF SHIP
23		HULL STA. 885, W.L. 160 ℄ OF SHIP
24		L. WING STA. 147.5 - FRONT SPAR
25		L. WING STA. 147.5 - REAR SPAR
26		L. WING STA. 600 - FRONT SPAR
27	STRAIN GAUGE	ENG. MOUNT TUBE - CENTER OF TUBE
28	STRAIN GAUGE	VERTICAL SHEAR - HULL STA. 328 - WEB OF FLOOR FRAME
29	ACCELEROMETER	ENGINE MOUNT, L. H. FWD.
30	STRAIN GAUGE	ENG. MOUNT TUBE - CENTER OF TUBE
31		STA. 236 - CENTER OF LONGERON - R.H. SIDE
32		STA. 236 - WALKWAY STRINGER - R.H. SIDE
33		HULL STA. 328 - ℄ TOP CHORD FLOOR FRAME
34		HULL STA. 386 - CENTER OF LONGERON - L.H. SIDE
35		HULL STA. 386 - WALKWAY STRINGER - R.H. SIDE
36		HULL STA. 386 - OUTB'D FACE OF LONGERON - R.H. SIDE
37		HULL STA. 386 - INB'D FACE OF LONGERON - R.H. SIDE
38		TOP OF KEEL FORMER - STA. 321
39		HULL BOTTOM MIDWAY BETWEEN S-0 & S-1, STA. 338
40		TOP OF S-0 AT ℄ OF VERT. STIFFENER TO STR. ATTACHED AT STA. 328
41		TOP OF S-0 AT ℄ OF VERT. STIFF. BETWEEN STA. 328 & 350
42		TOP OF S-2 AT ℄ OF VERT. STIFF. AT STA. 328
43		TOP OF S-2 AT ℄ OF VERT. STIFF. BETWEEN STA. 328 & 350
44	ACCELEROMETER	℄ HULL STA. 180
45		℄ HULL STA. 574
46		L. WING - STA. 300 - FRONT SPAR
47		L. WING - STA. 300 - REAR SPAR
48		L. WING - STA. 450 - FRONT SPAR
49		ENGINE MOUNT - L.H. FWD.

● ACCELEROMETERS (VERTICAL)
○ STRAIN GAUGES

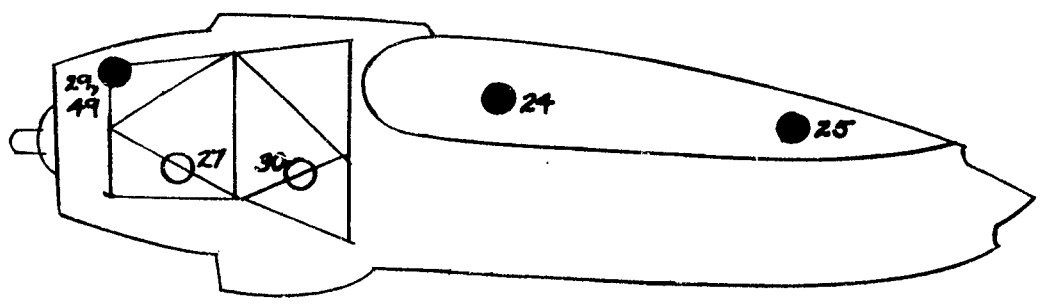

Fig. 3. Location of Instrumentation on Aircraft Structure

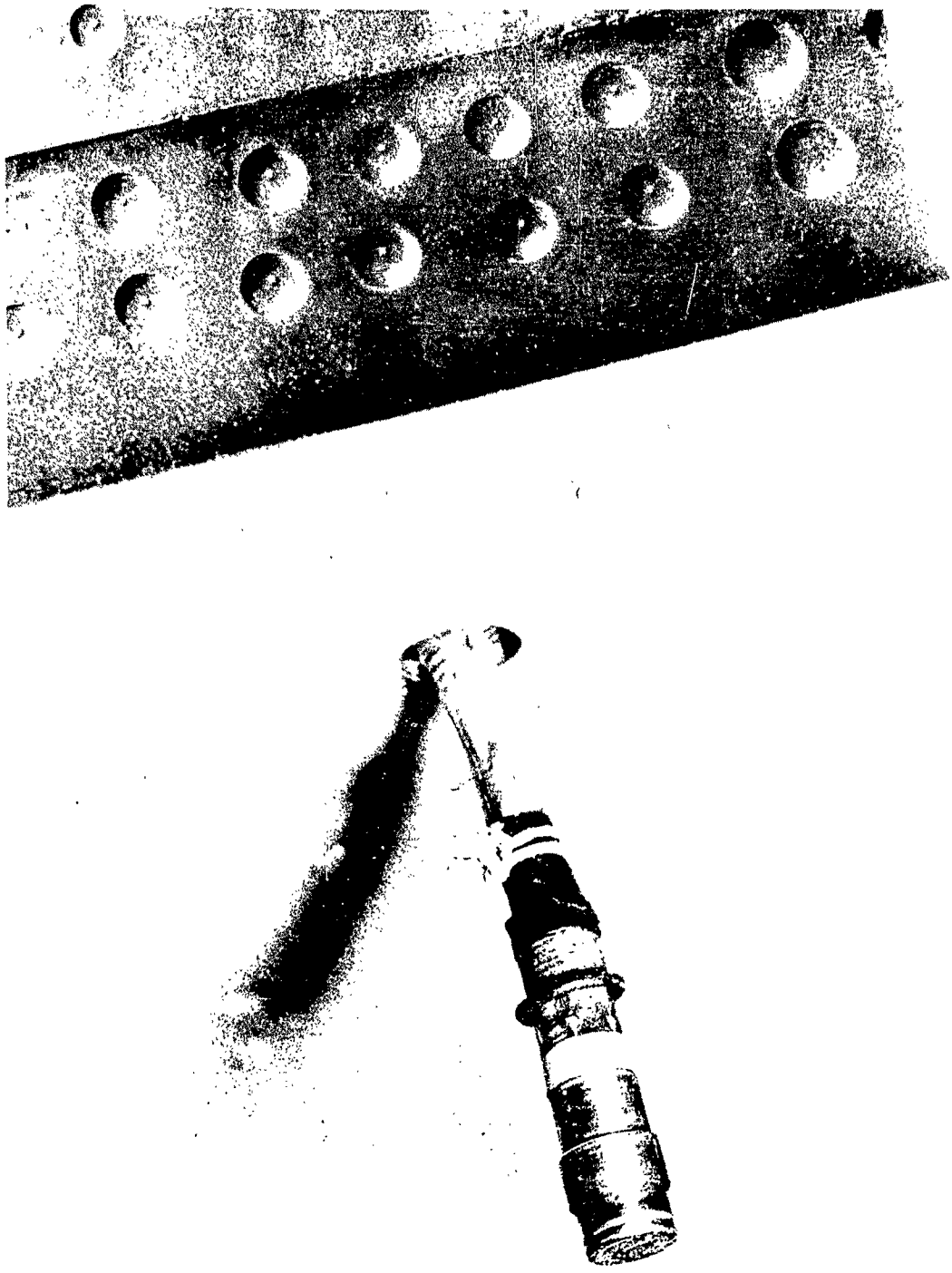

Fig. 4. Pressure Transducer Extending from Hull Bottom

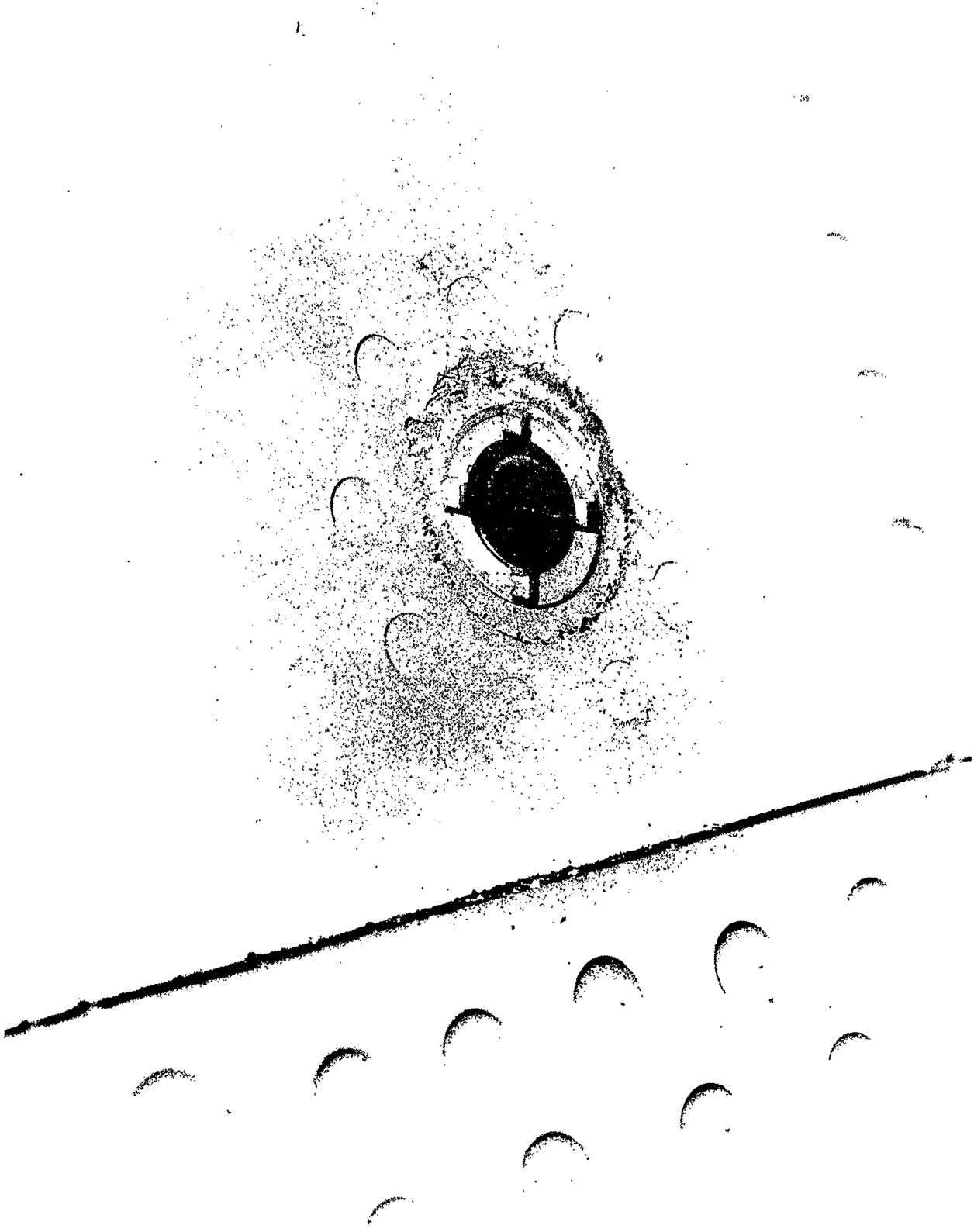

Fig. 5. Pressure Transducer Installed Flush with Hull Bottom

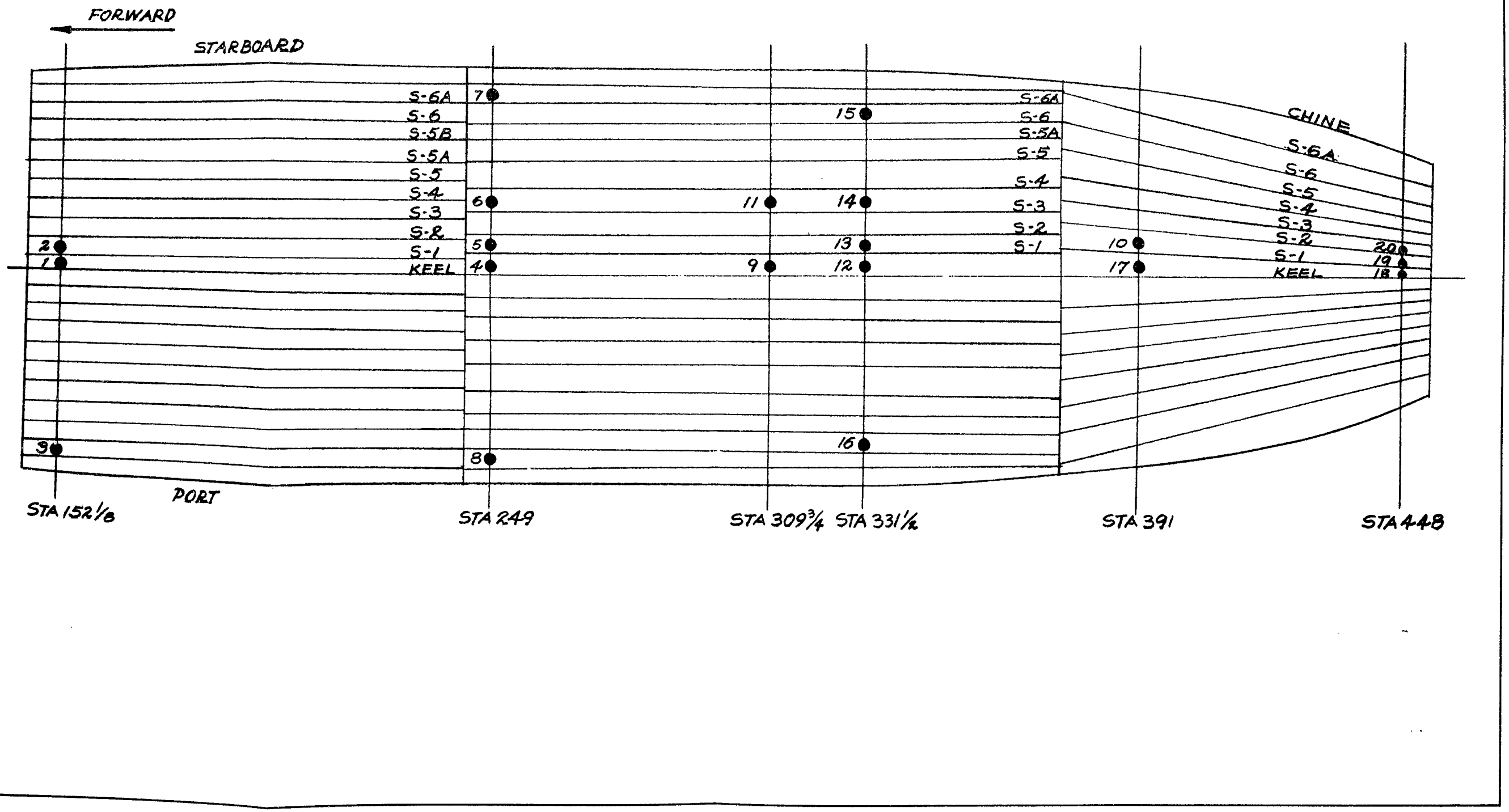

Fig. 6. Hull Bottom Pressure Pickup Locations

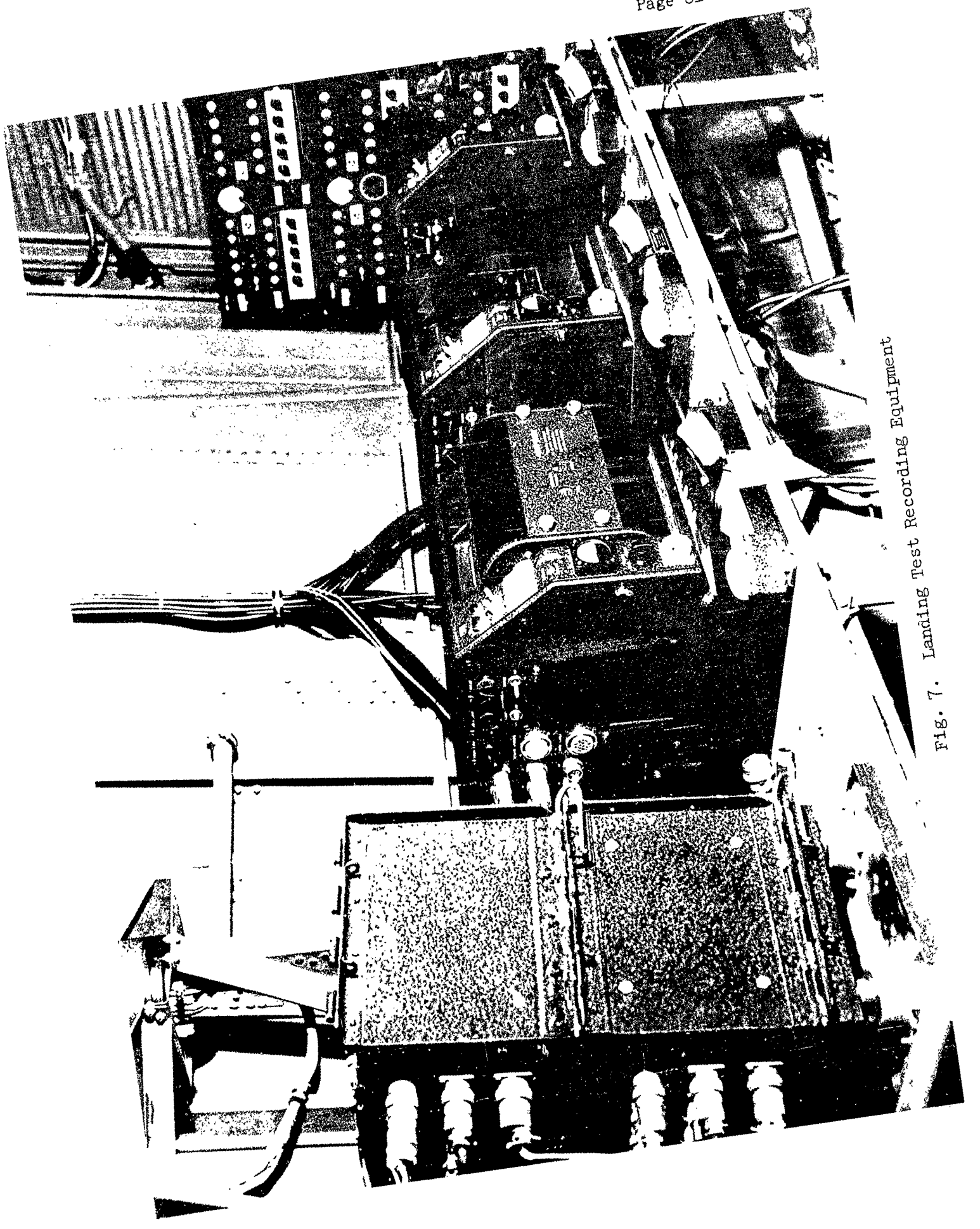

Fig. 7. Landing Test Recording Equipment

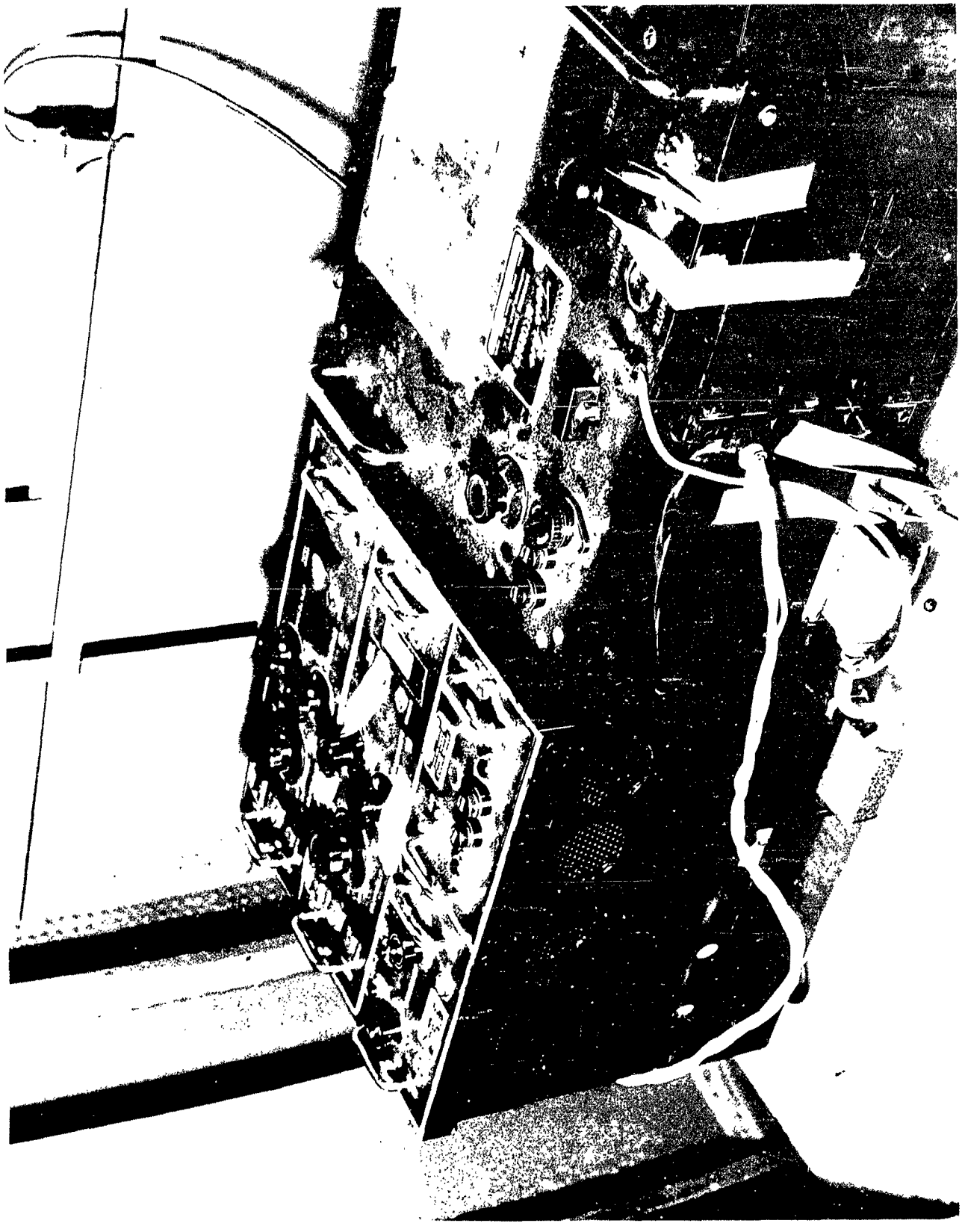

Fig. 8. Sanborn Visual Recorder

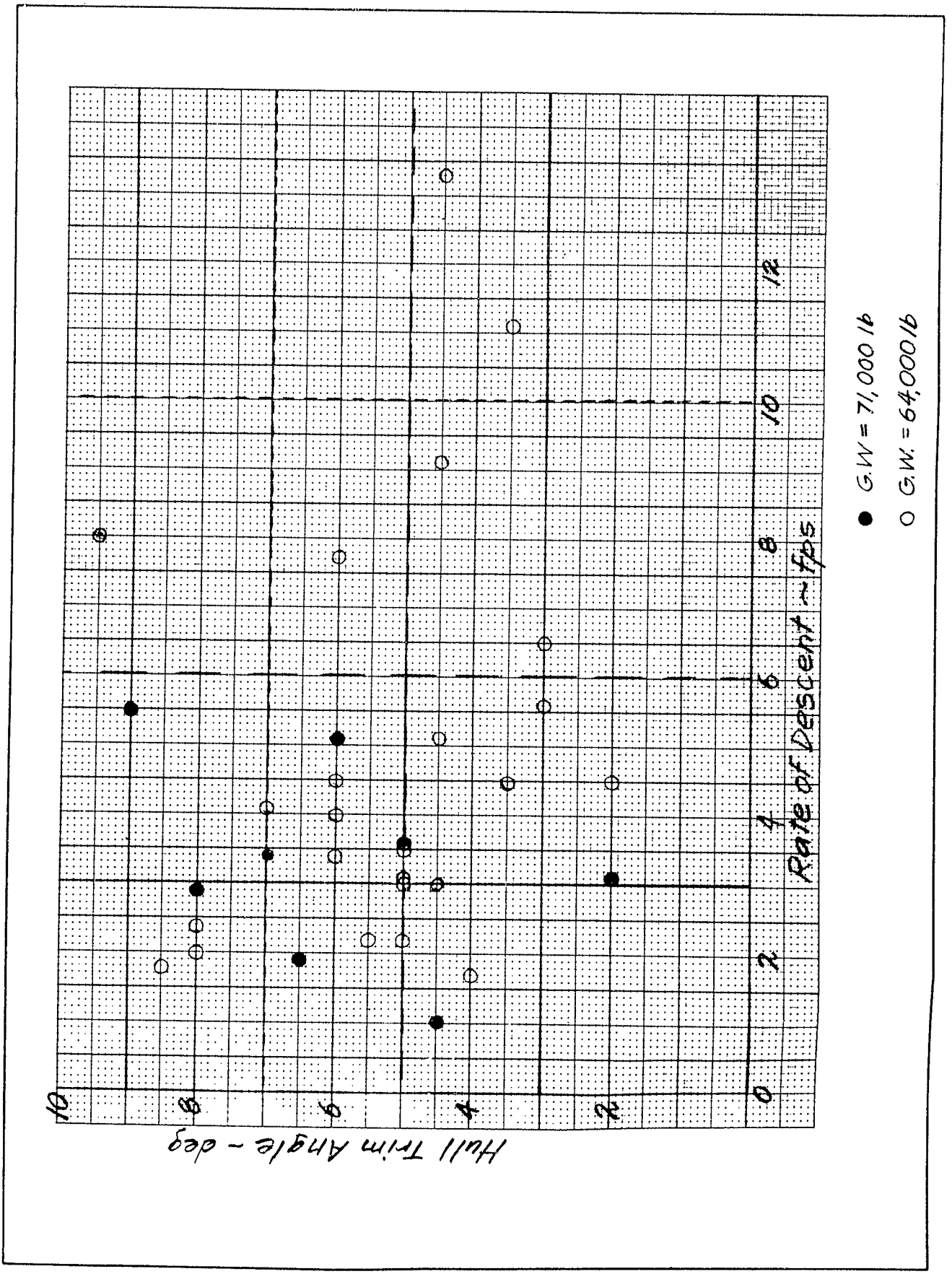

Fig. 9. Hull Trim Angle vs Rate of Descent

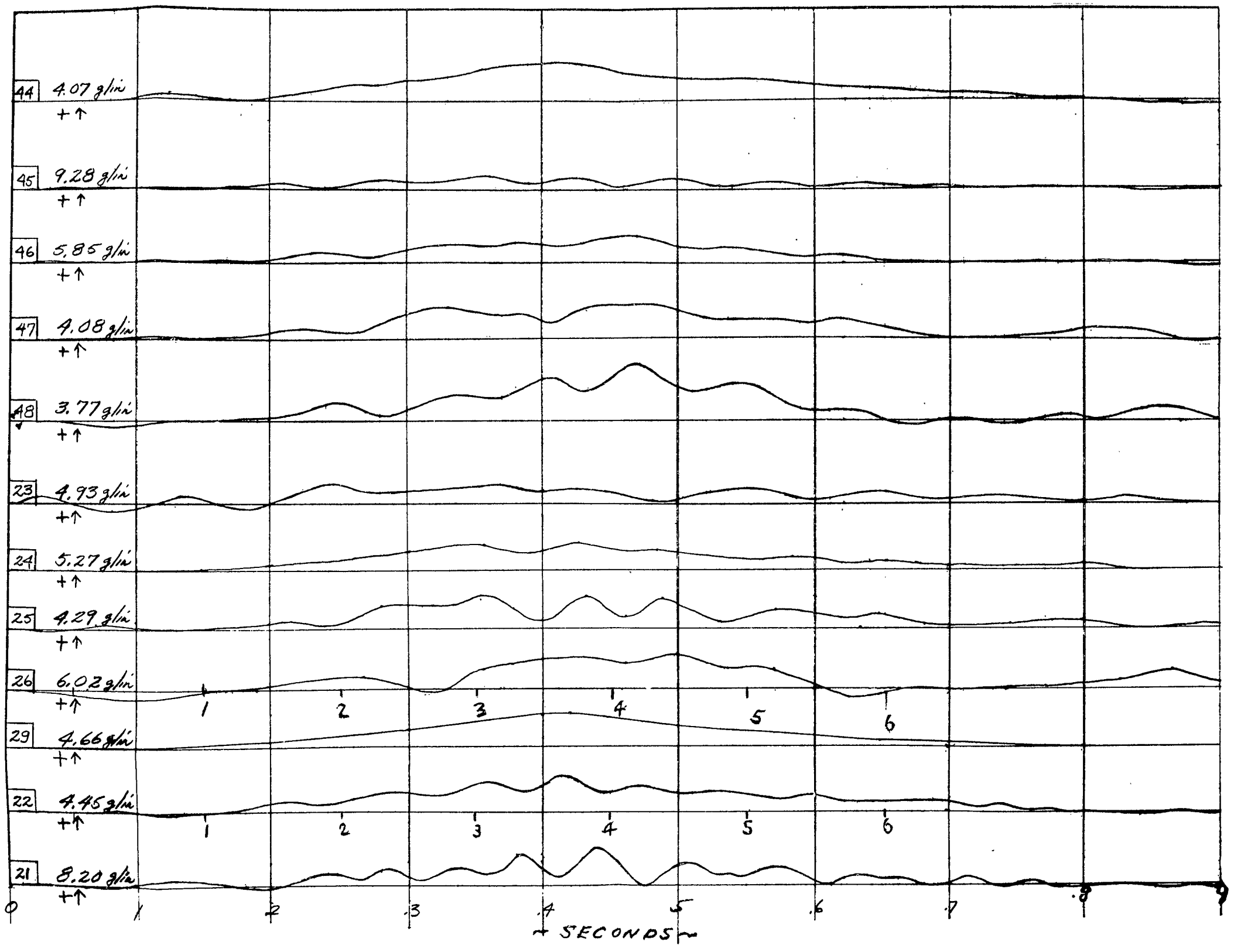

Fig. 10a. Flight 27, Landing 5, 8 October 1954
Accelerations

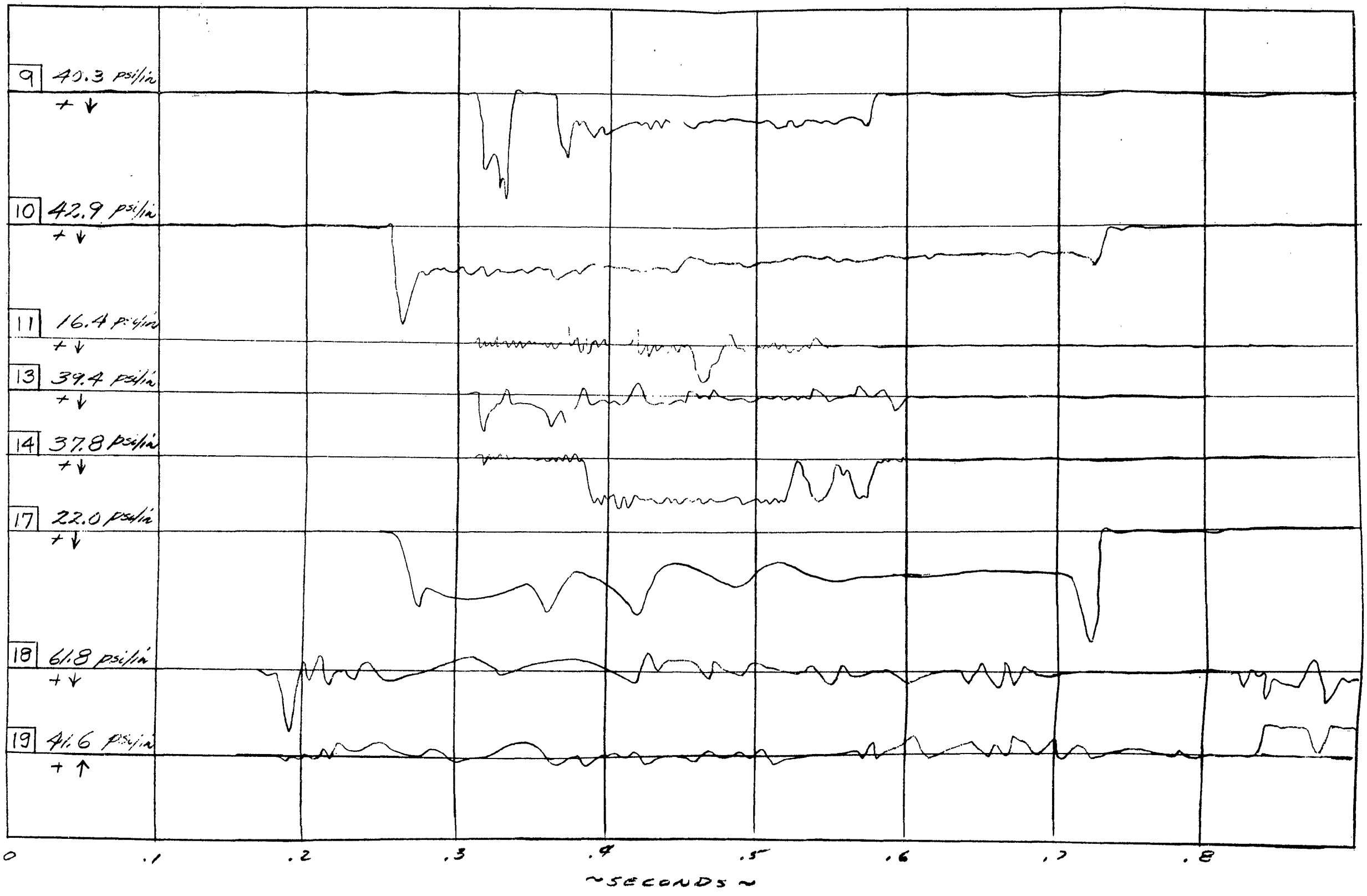

Fig. 10b. Flight 27, Landing 5, 8 October 1954
Pressures

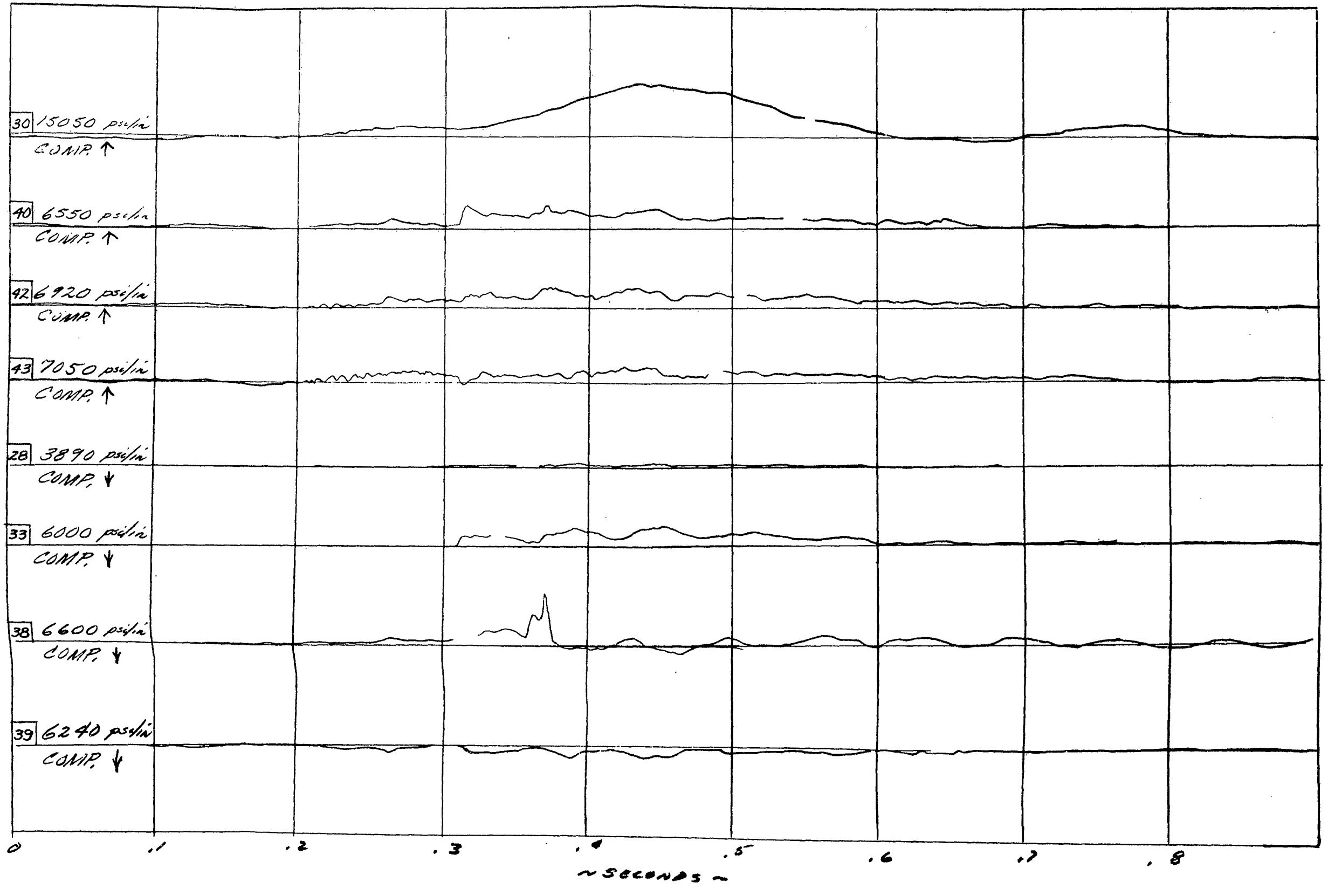

Fig. 10c. Flight 27, Landing 5, 8 October 1954
Strain Gages

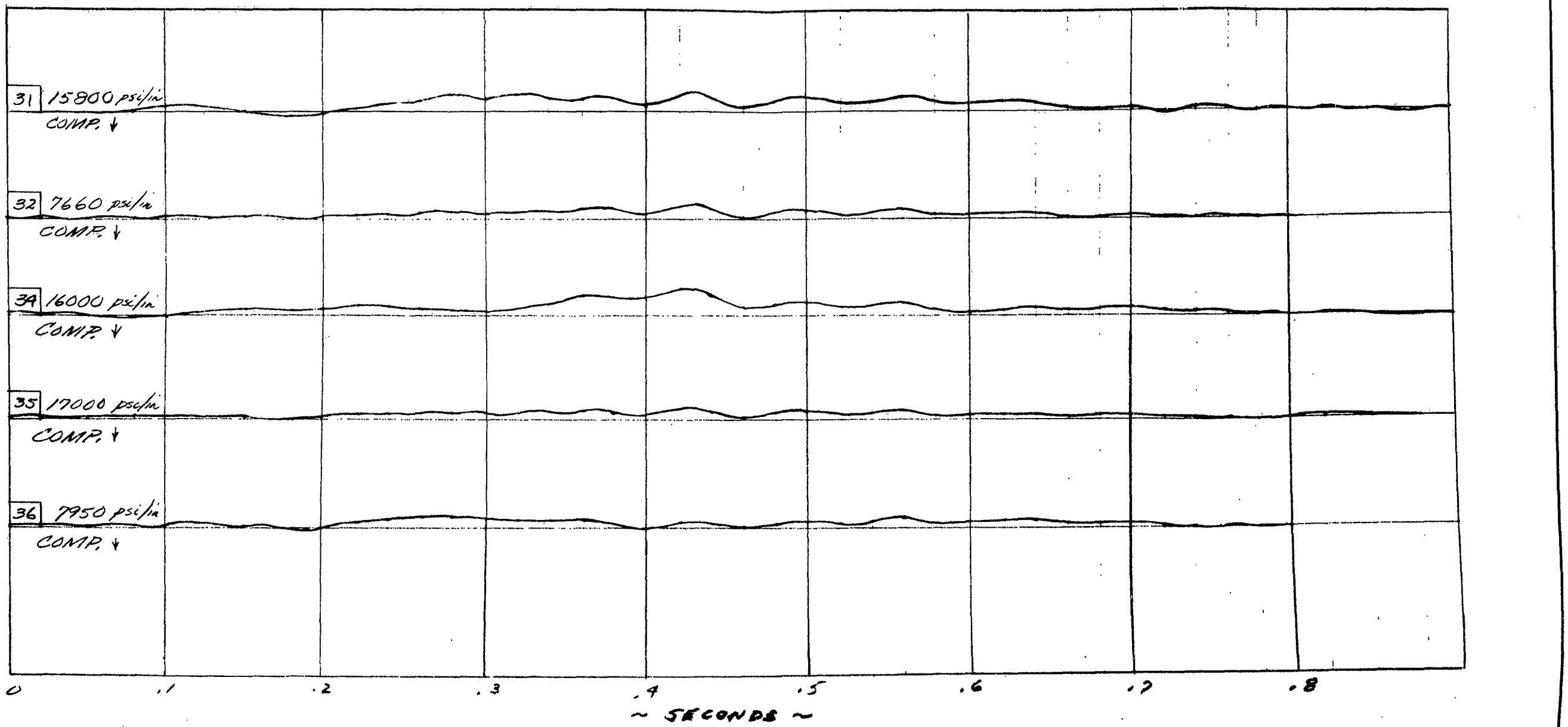

Fig. 10d. Flight 27, Landing 5, 8 October 1954
Strain Gages

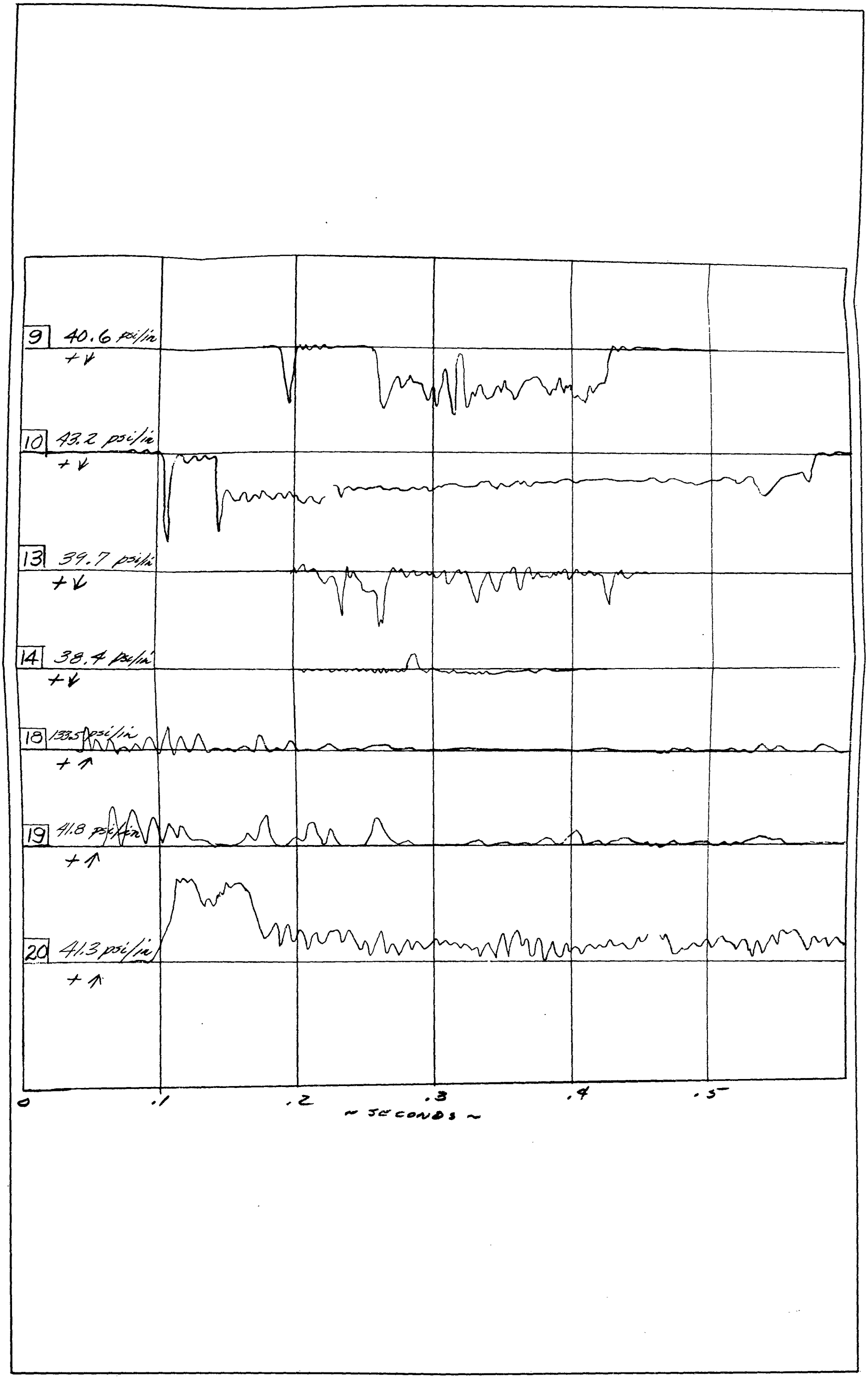

Fig. 11a. Flight 28, Landing 1, 21 October 1954
Pressures

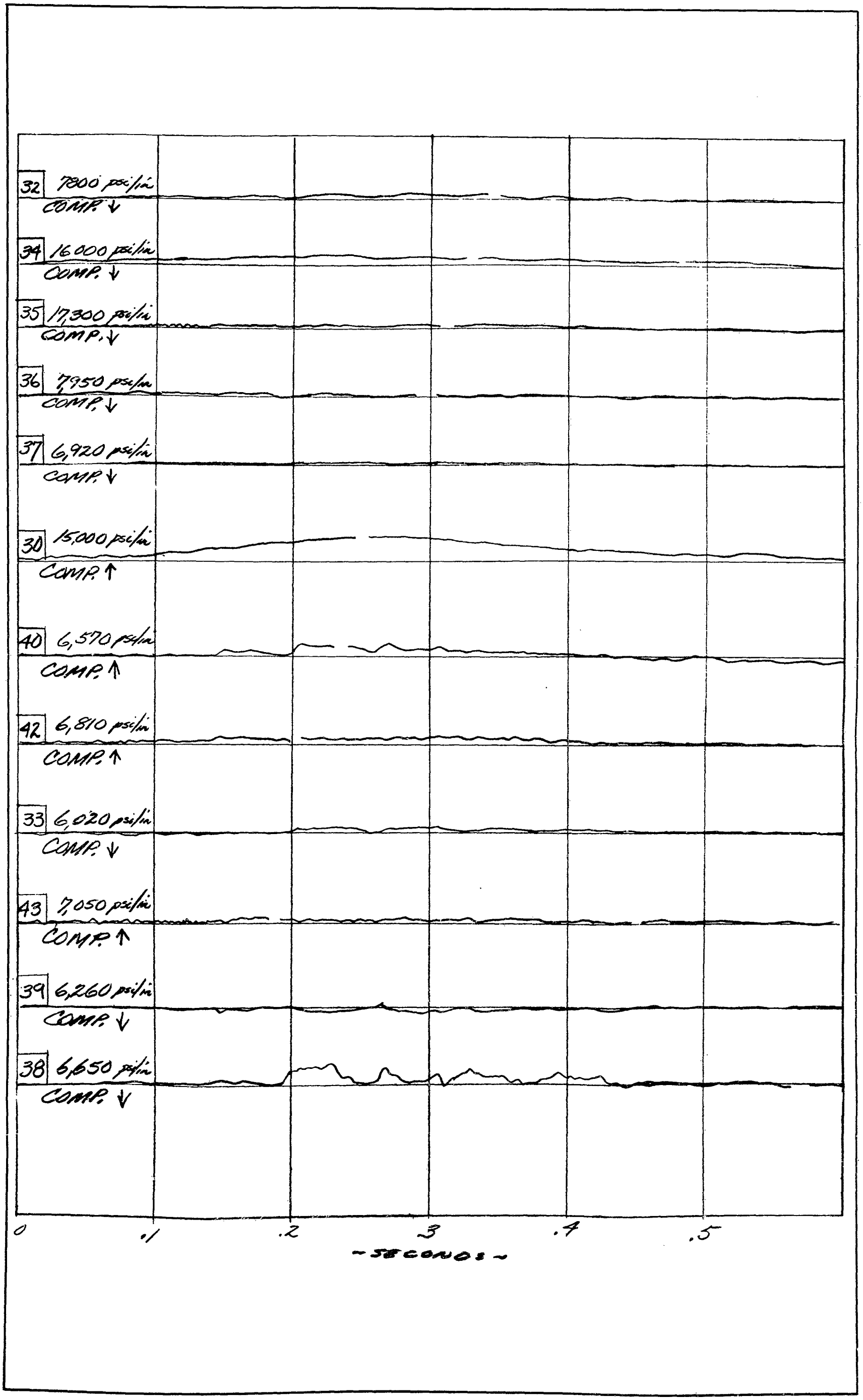

Fig. 11b. Flight 28, Landing 1, 21 October 1954
Strain Gages

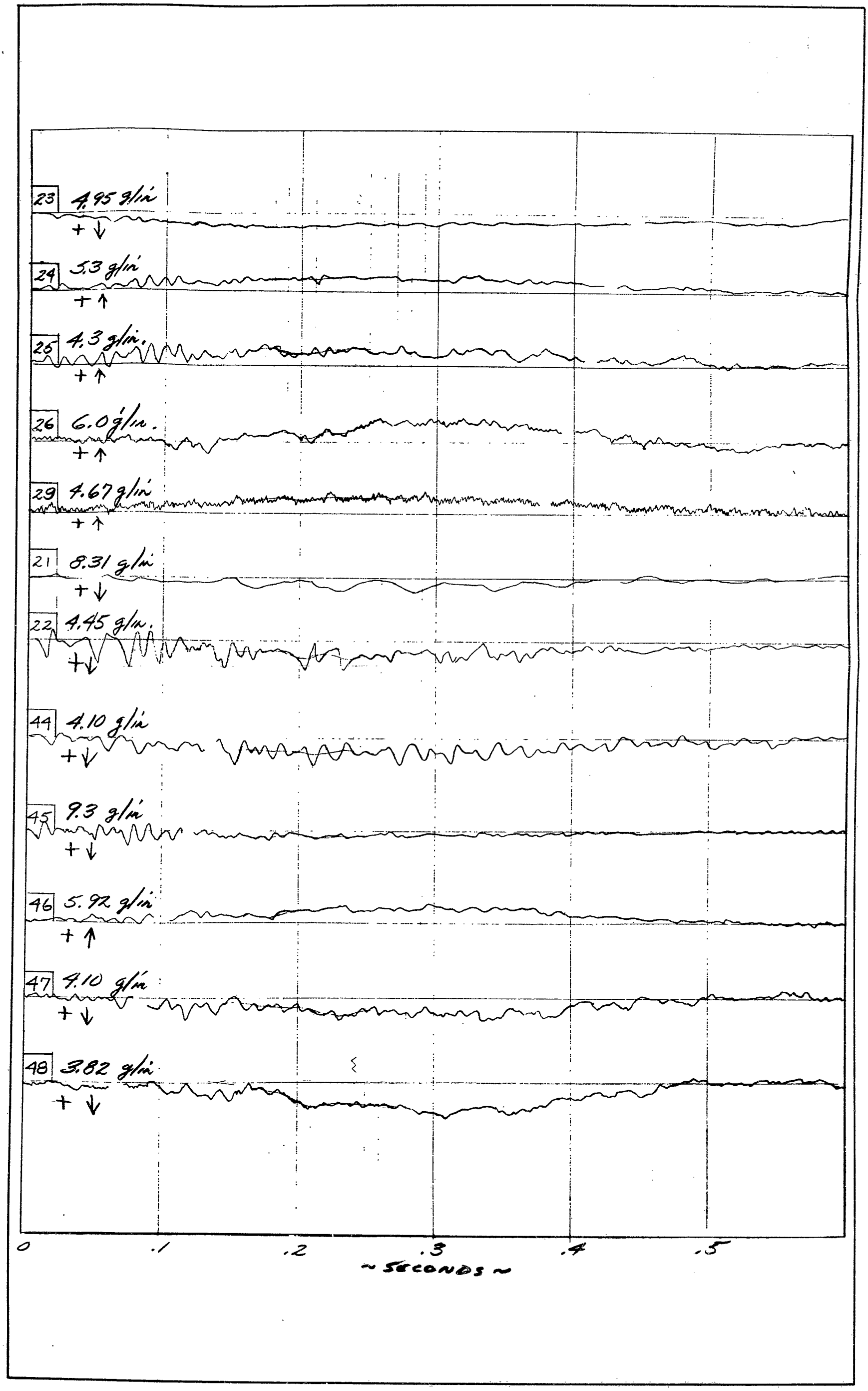

Fig. 11c. Flight 28, Landing 1, 21 October 1954
Accelerations

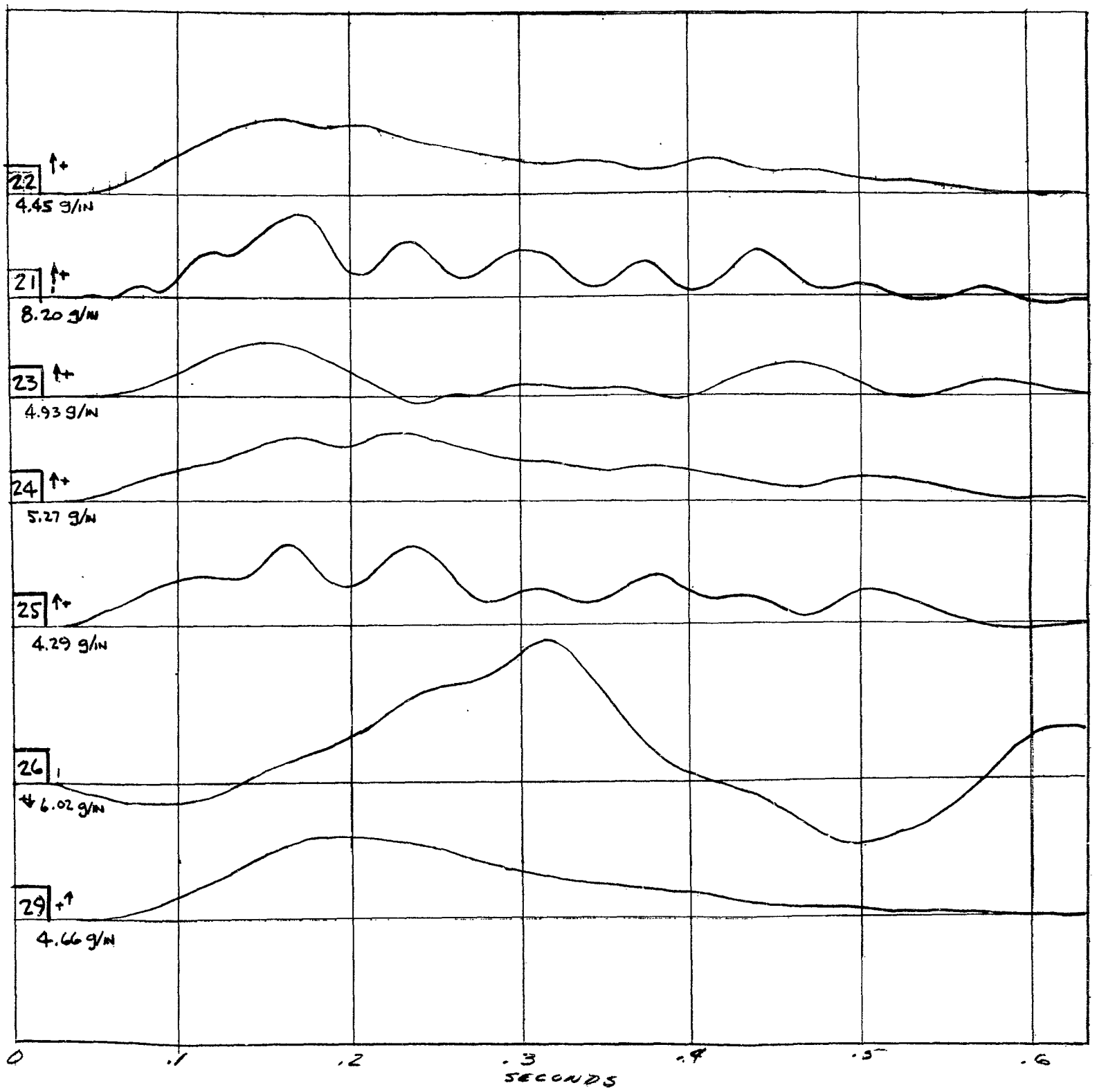

Fig. 12a. Flight 29, Landing 4, 27 October 1954
Accelerations

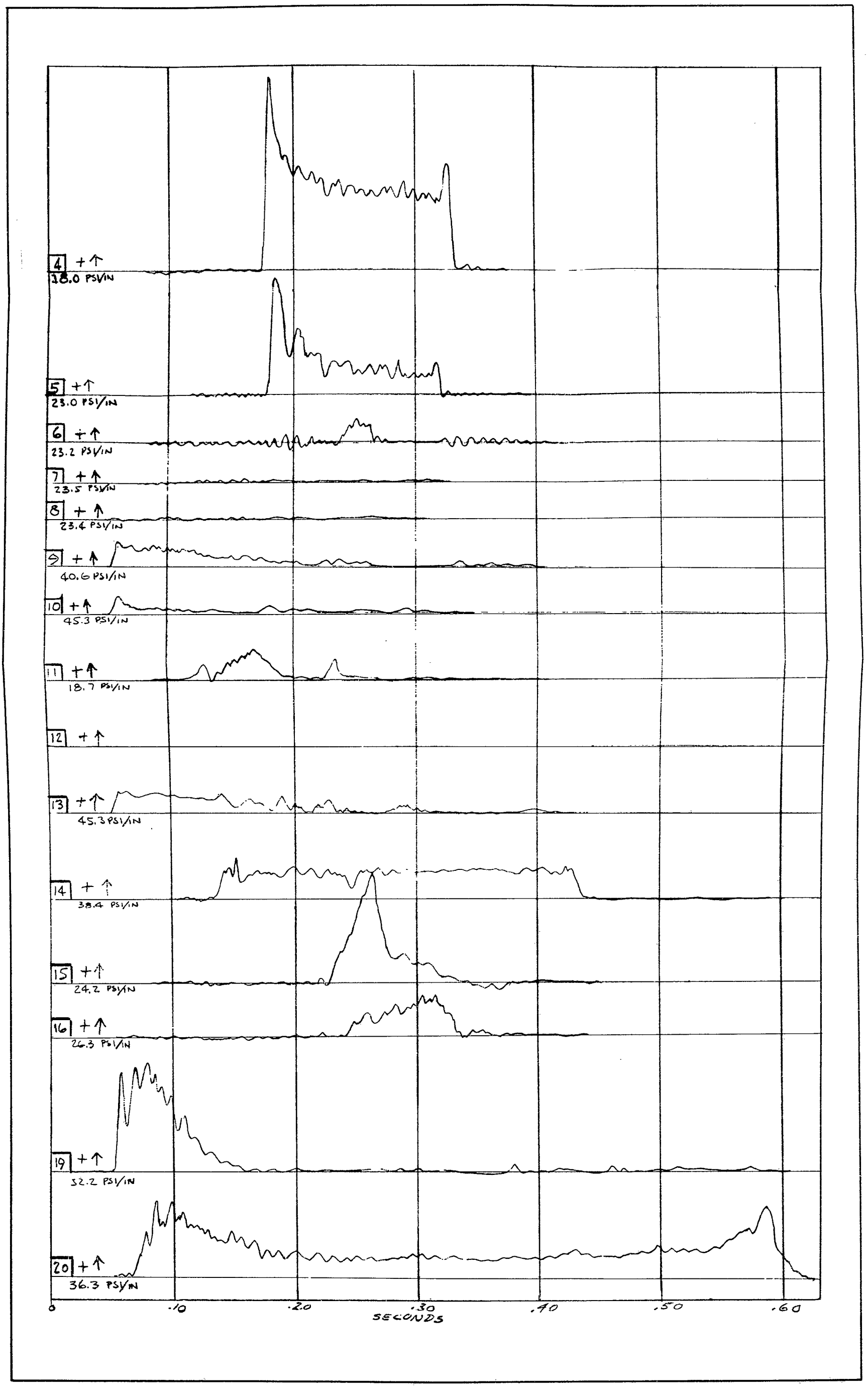

Fig. 12b. Flight 29, Landing 4, 27 October 1954
Pressures

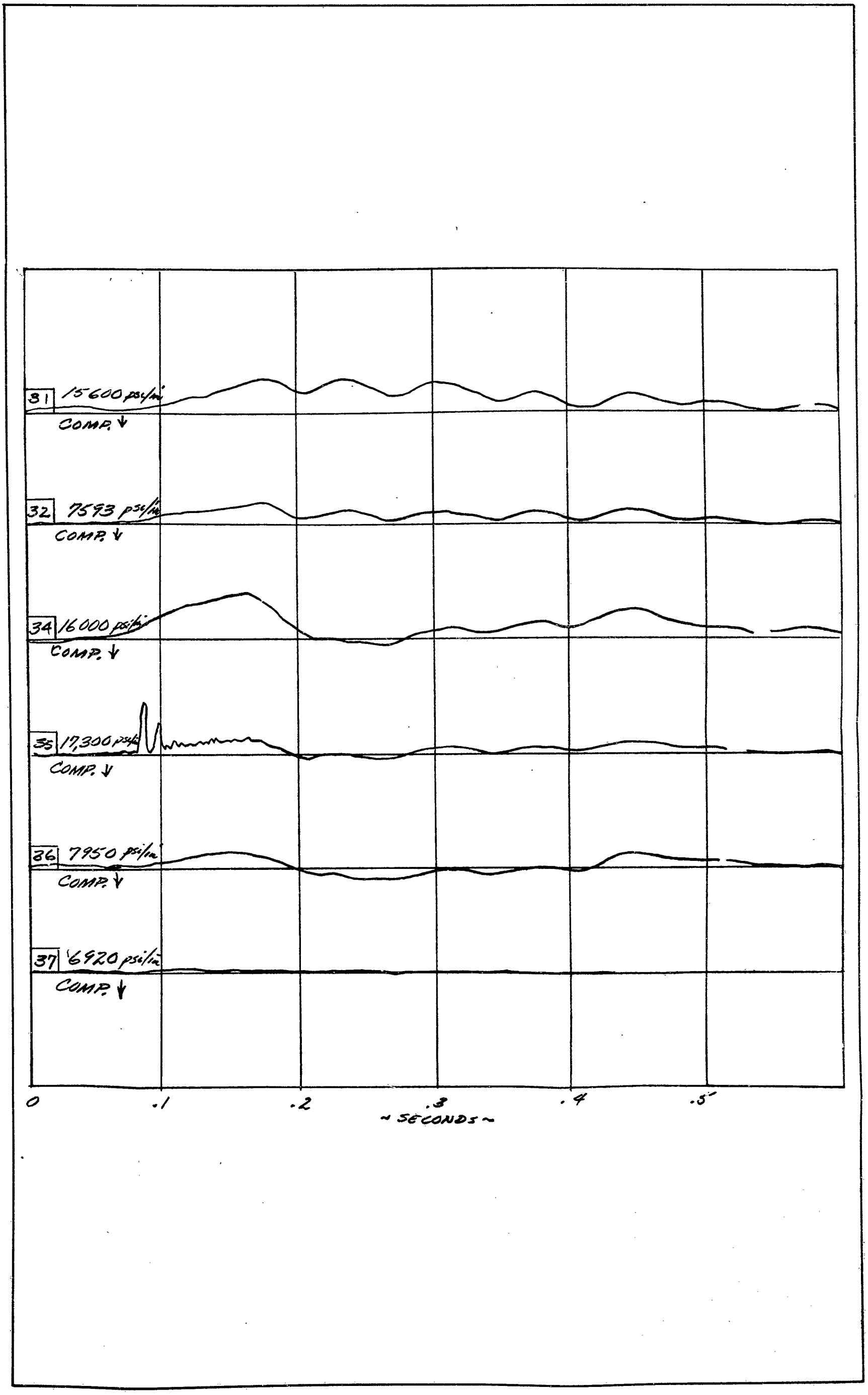

Fig. 12c. Flight 29, Landing 4, 27 October 1954
Strain Gages

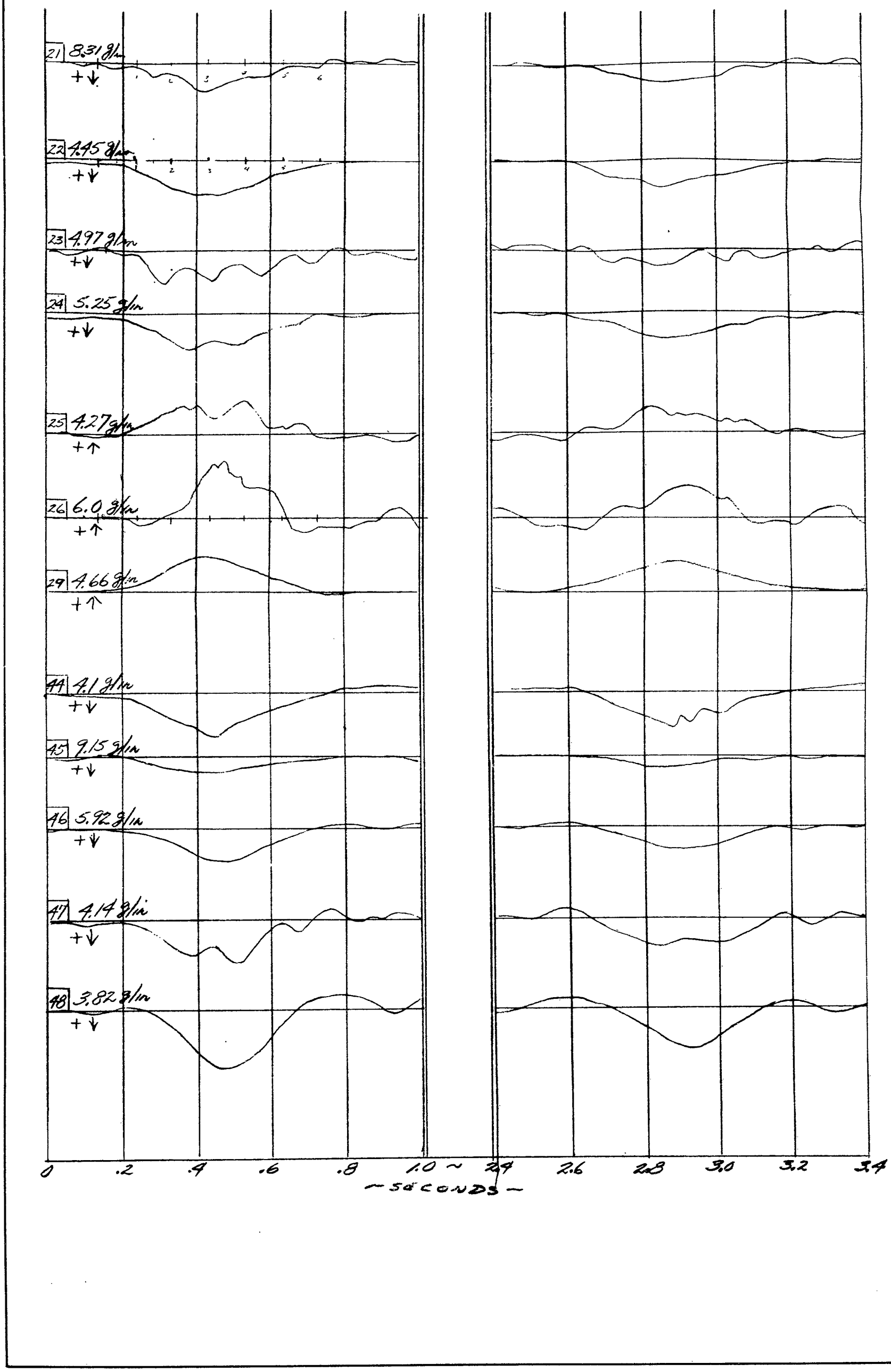

Fig. 13a. Flight 31, Landing 8, 5 November 1954
Accelerations

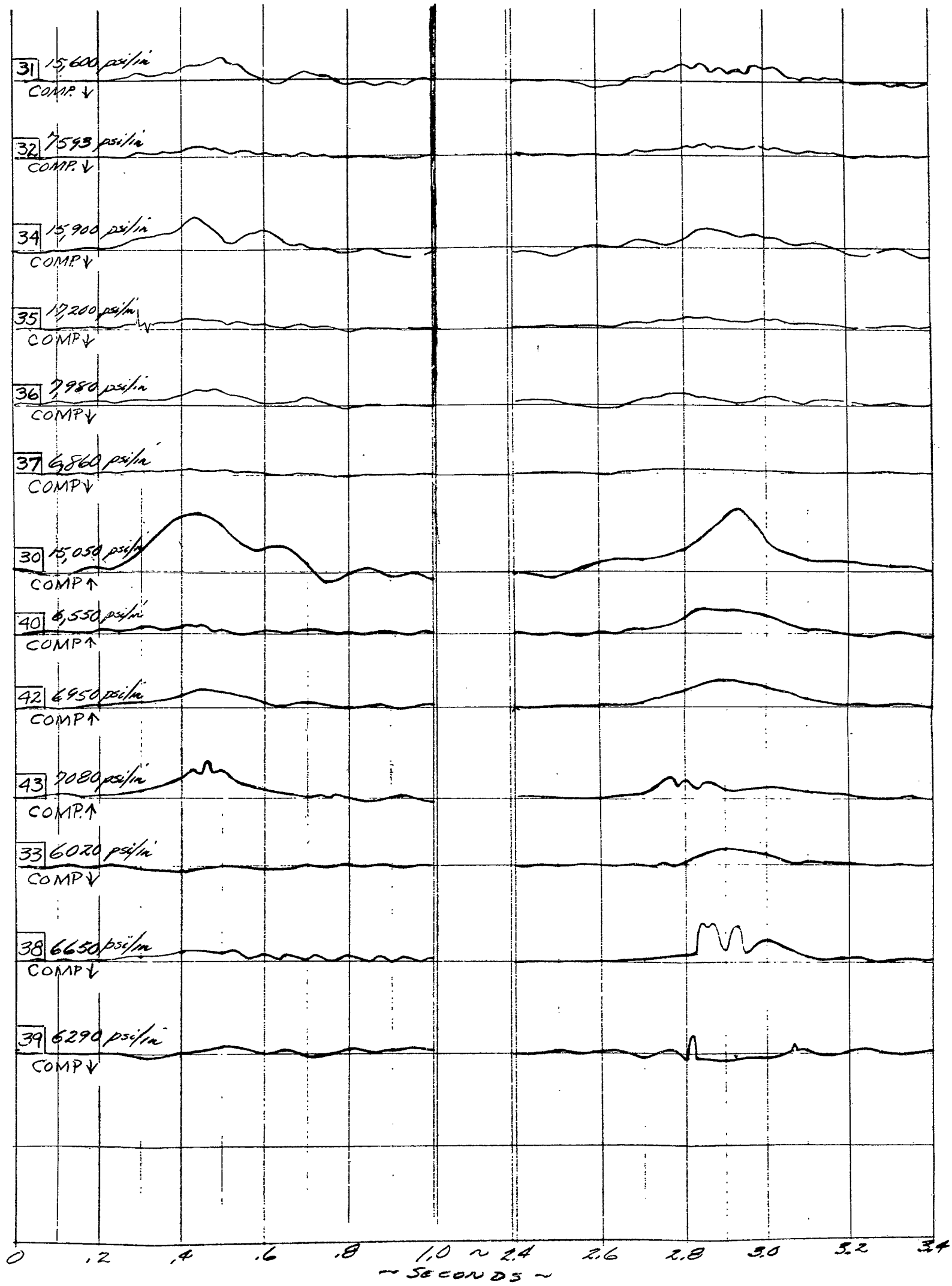

Fig. 13b. Flight 31, Landing 8, 5 November 1954
Strain Gages

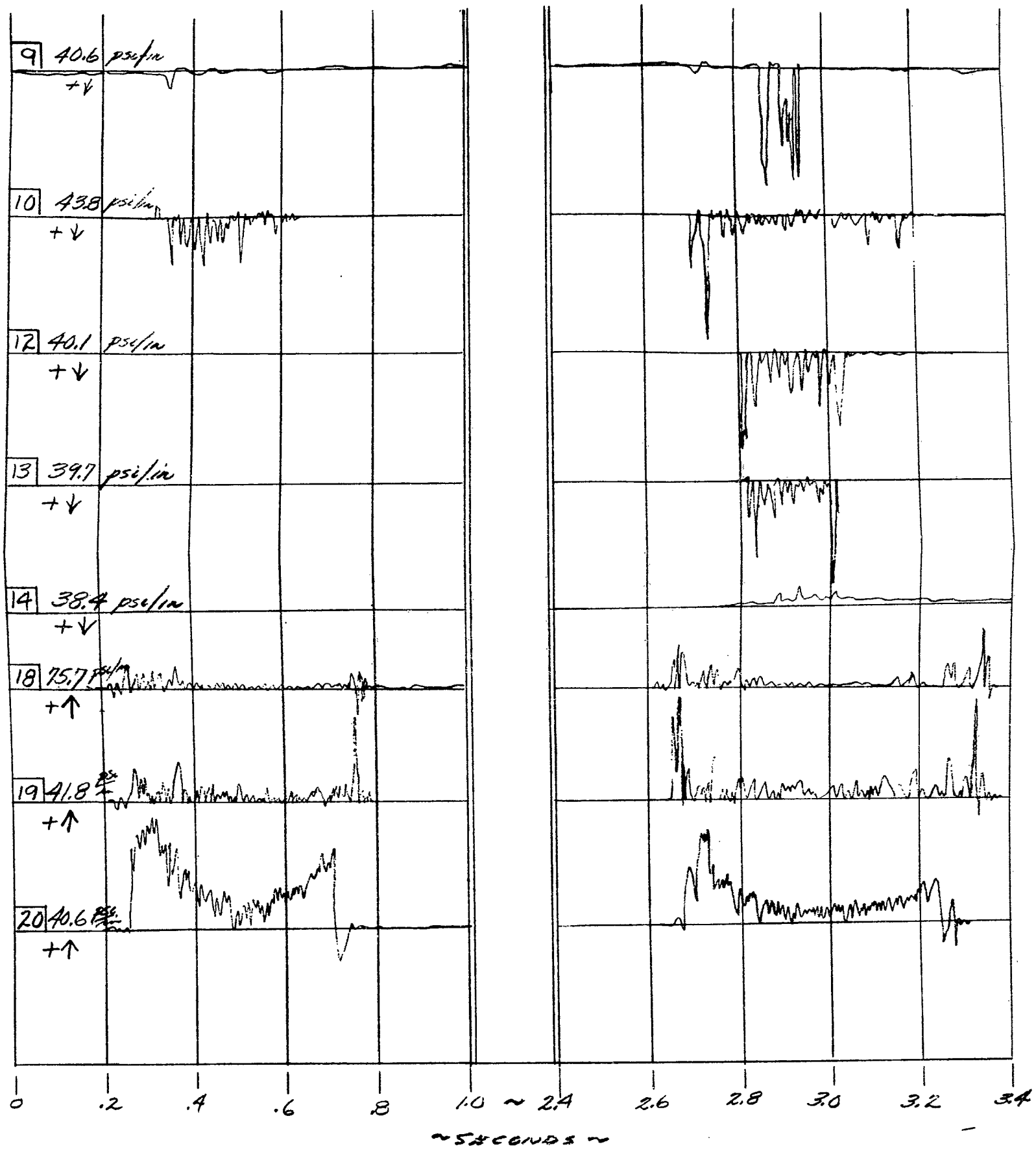

Fig. 13c. Flight 31, Landing 8, 5 November 1954
Pressures

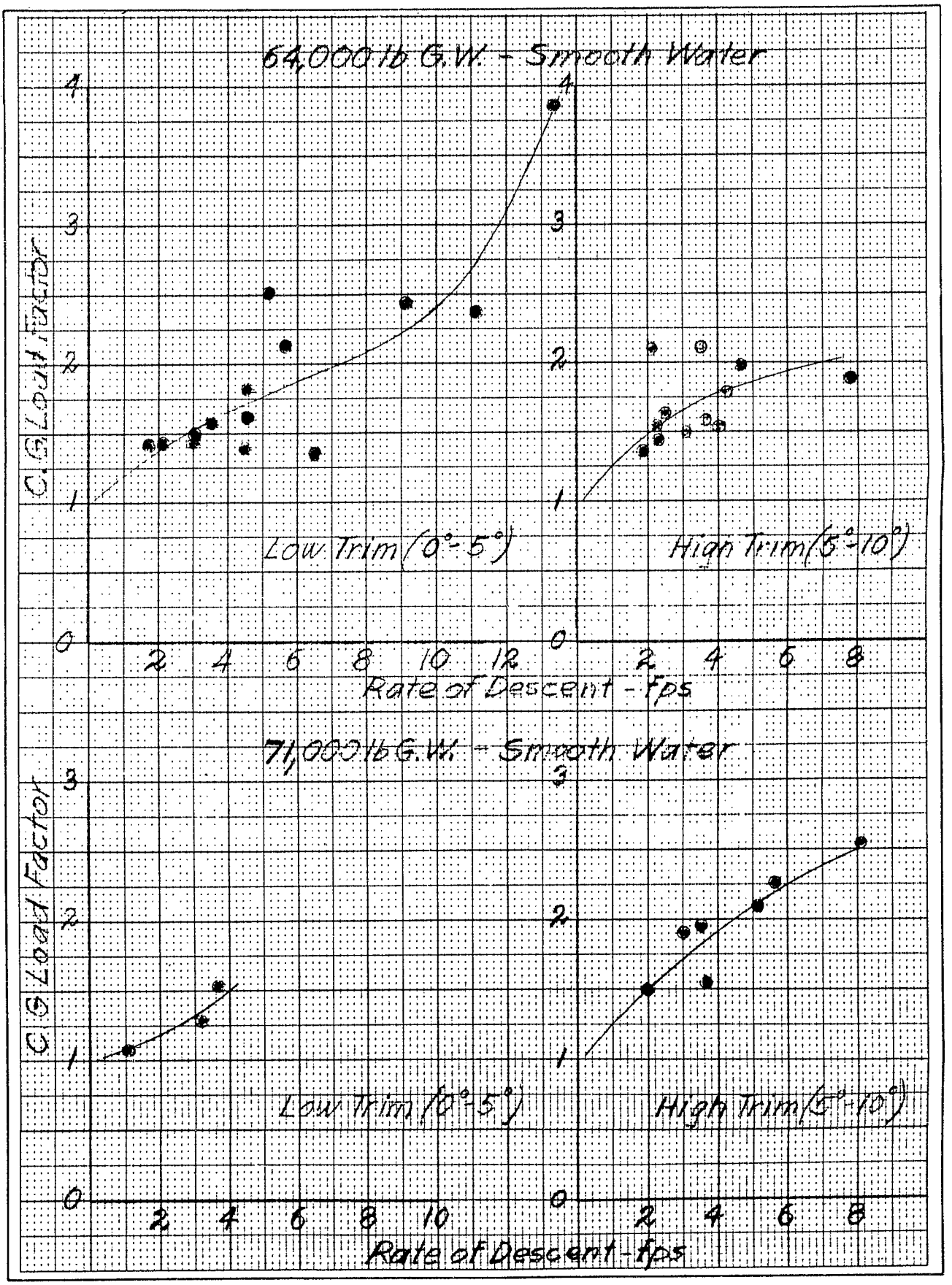

Fig. 14. Rate of Descent vs CG Load Factor

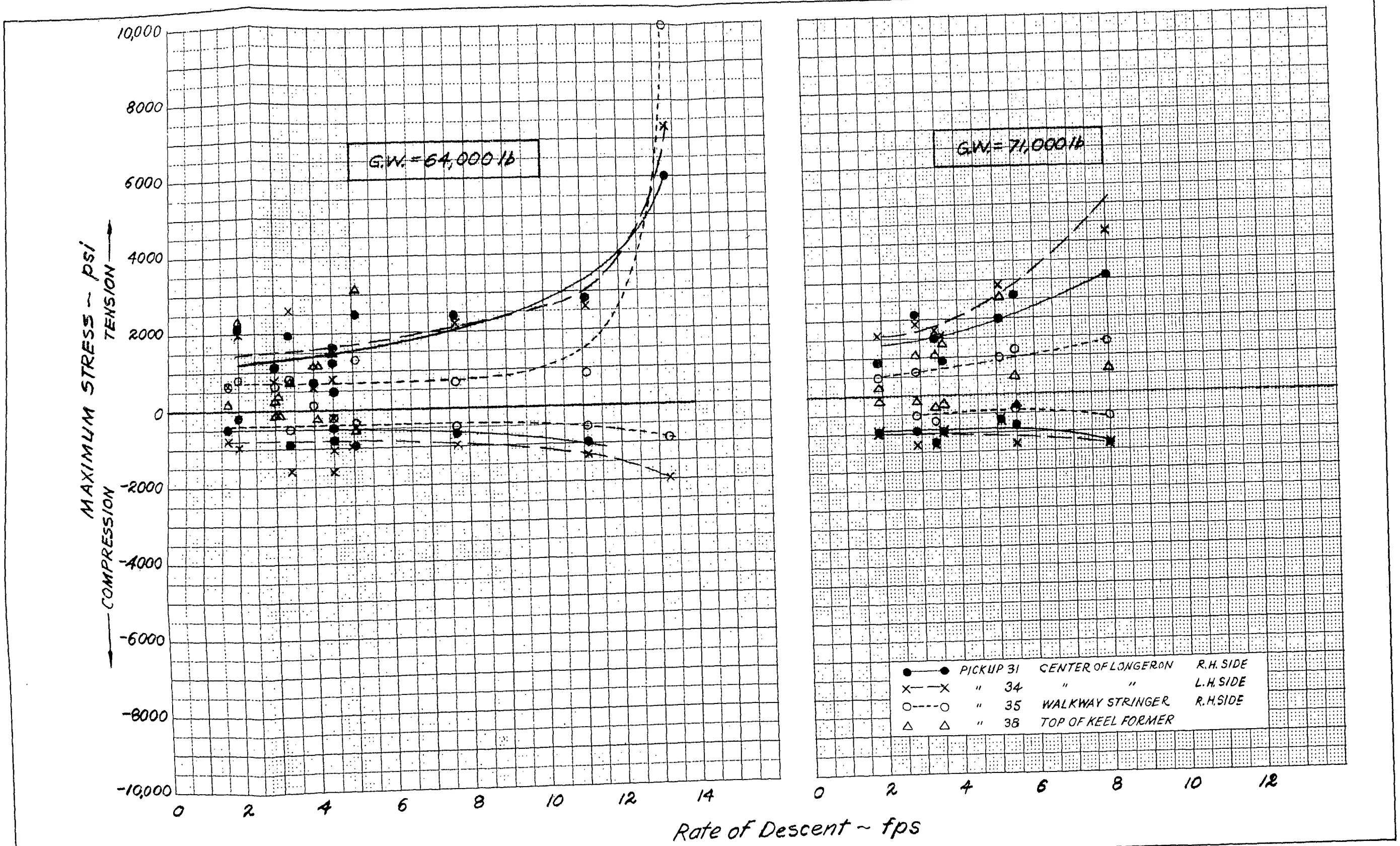

Fig. 15. Maximum Stress vs Rate of Descent

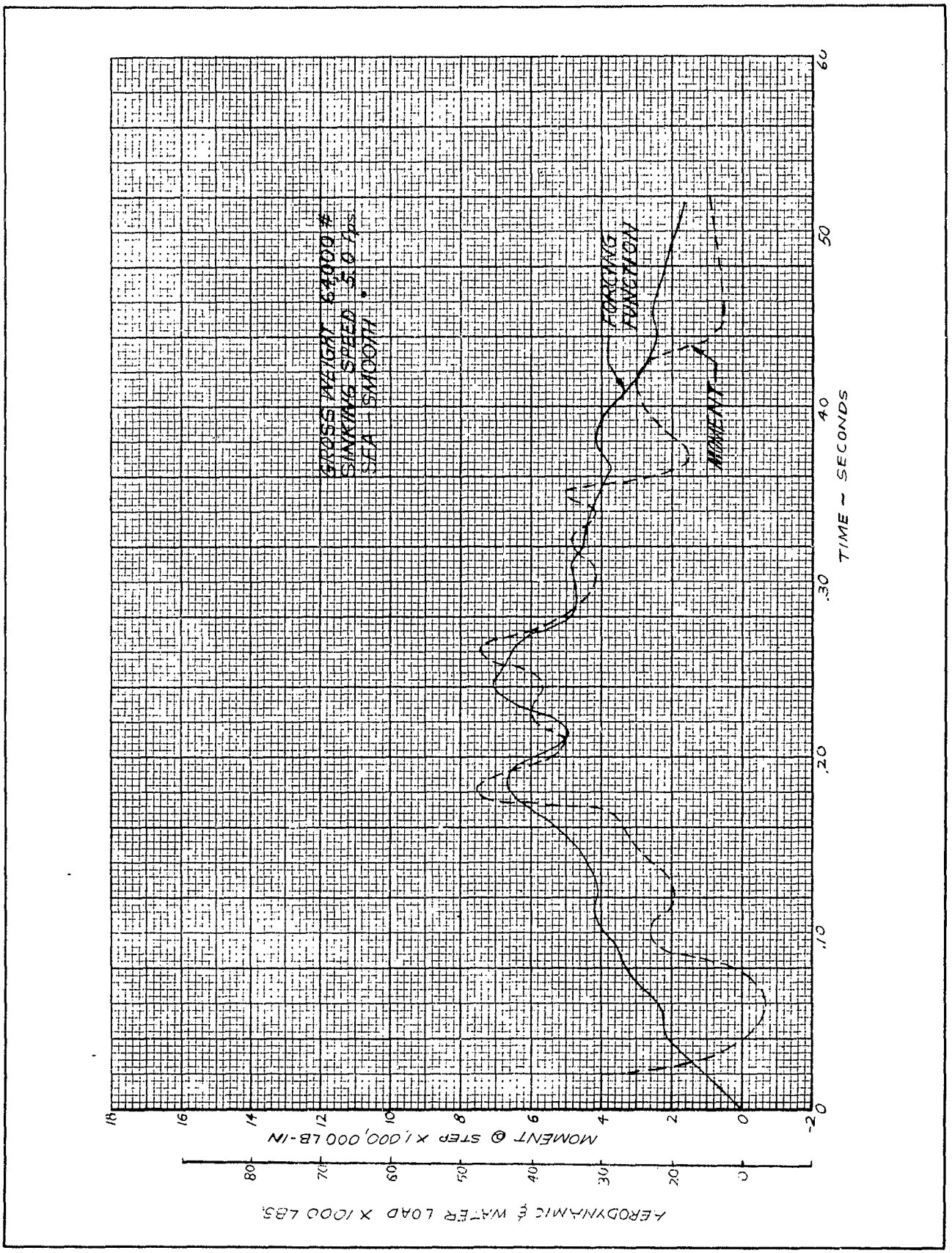

Fig. 16. Forcing Function and Moment Derived from Experimental Data
Flight 27, Landing 5, 8 October 1954

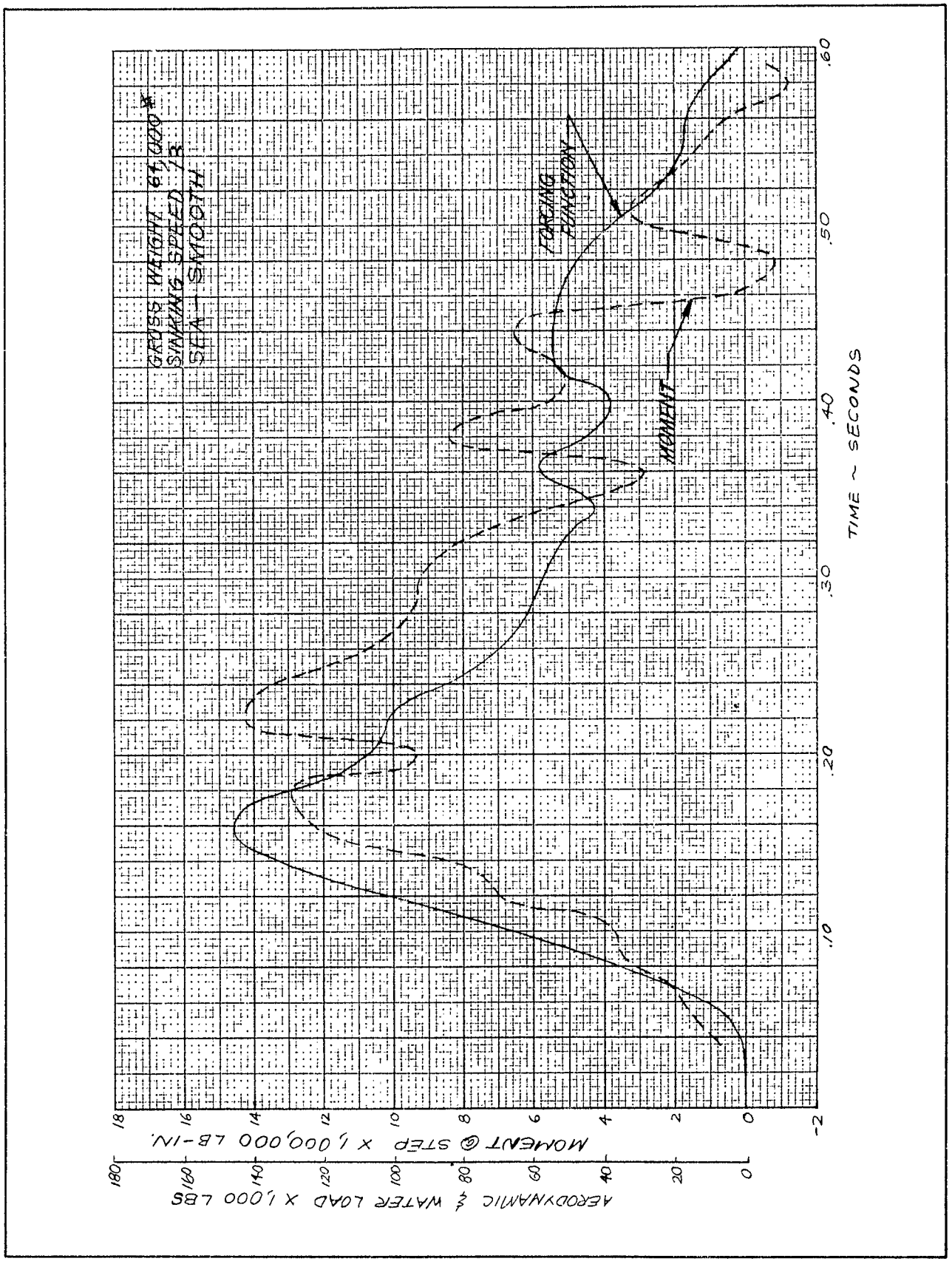

Fig. 17. Forcing Function and Moment Derived from Experimental Data
Flight 29, Landing 4, 27 October 1954

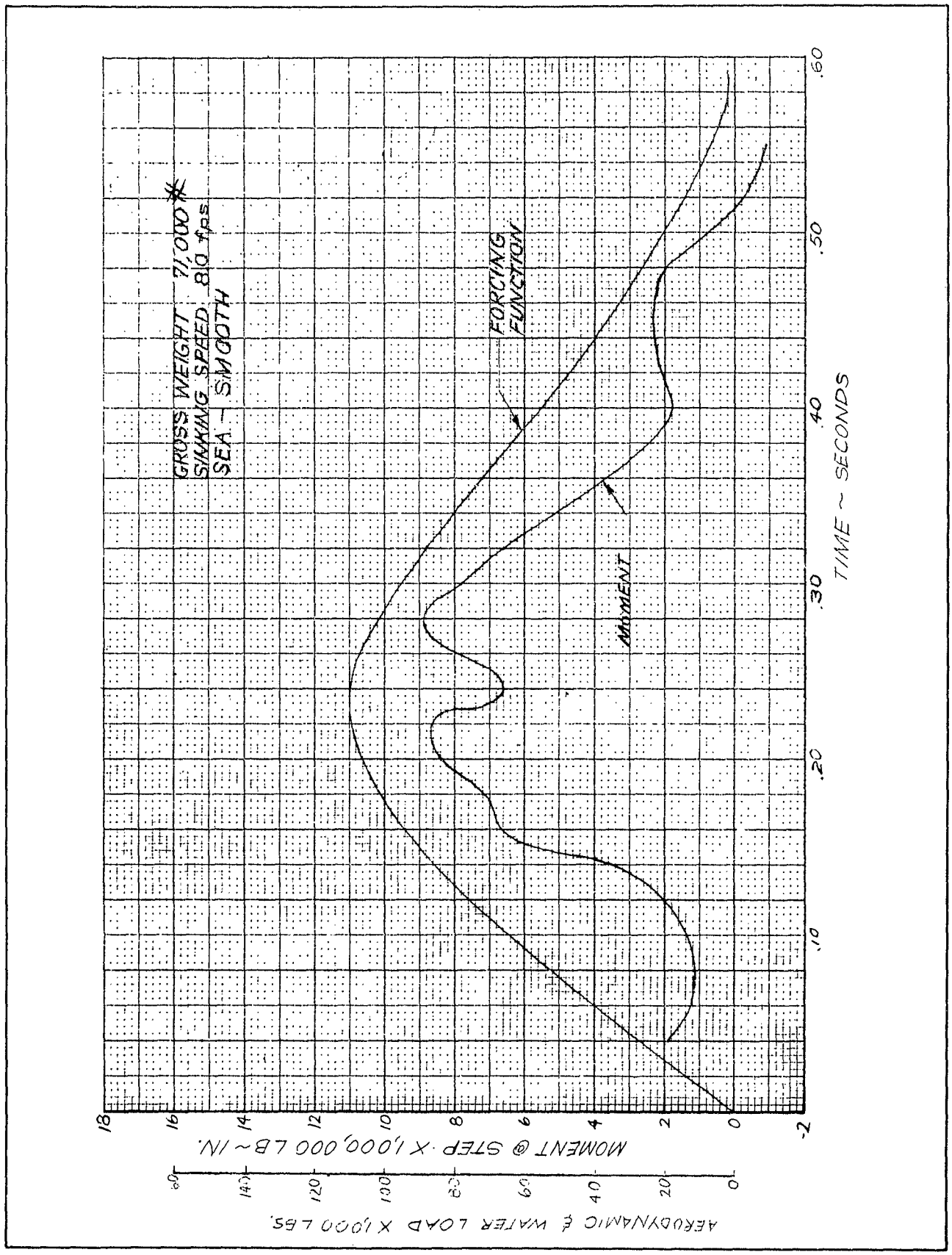

Fig. 18. Forcing Function and Moment Derived from Experimental Data
Flight 31, Landing 8, 5 November 1954

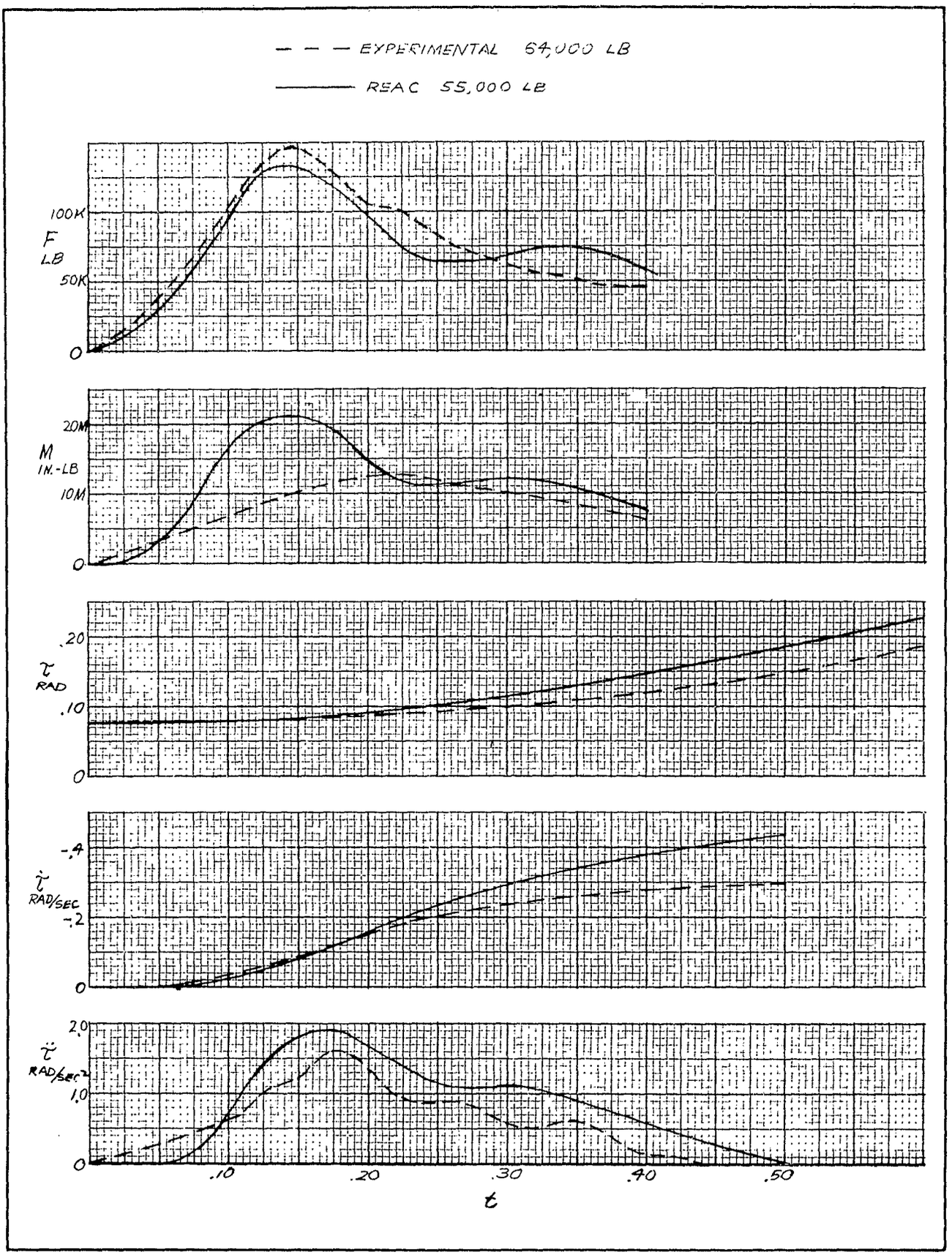

Fig. 19. Experimental vs REAC - Flight 29, Landing 4

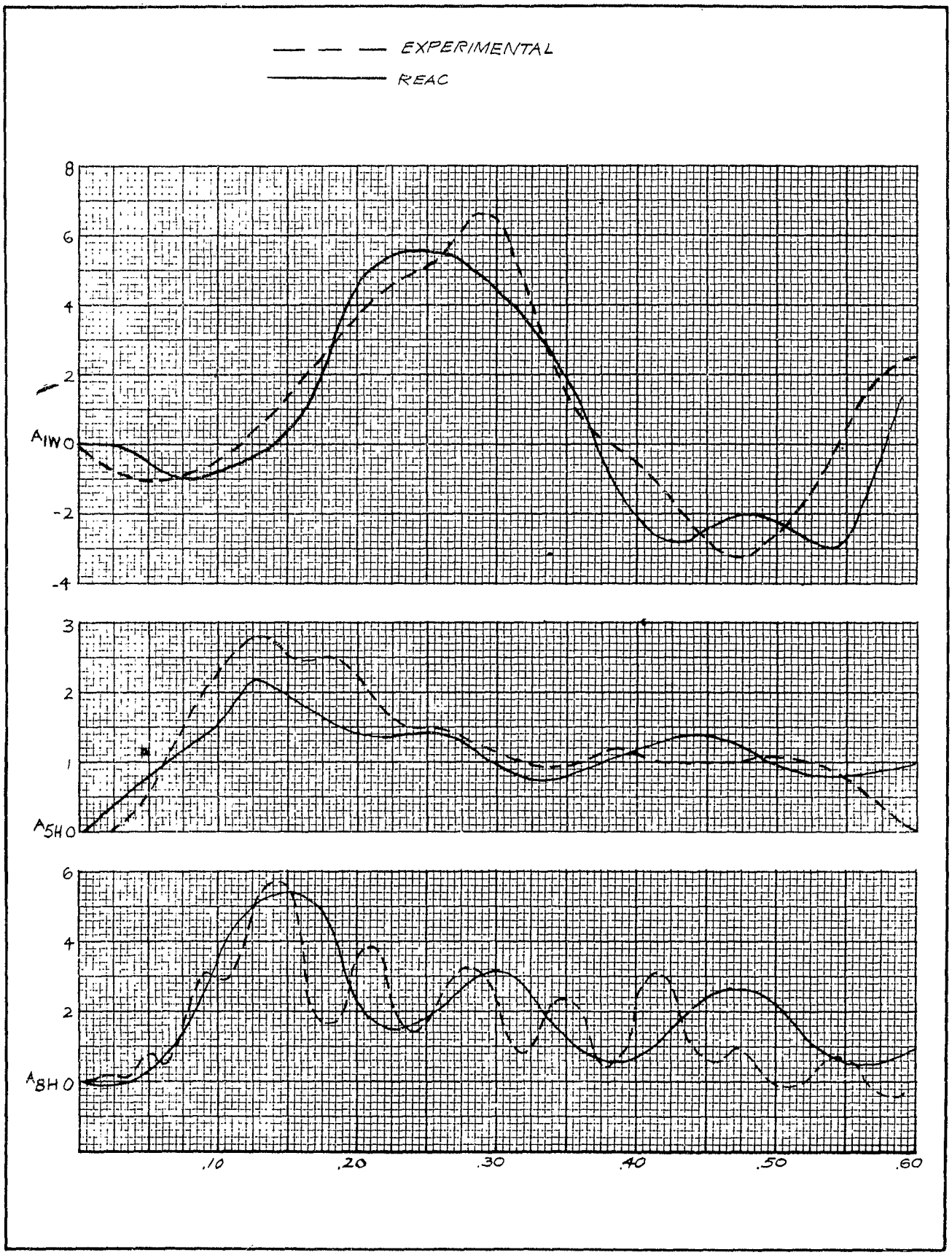

Fig. 20. Experimental vs REAC - Flight 29, Landing 4

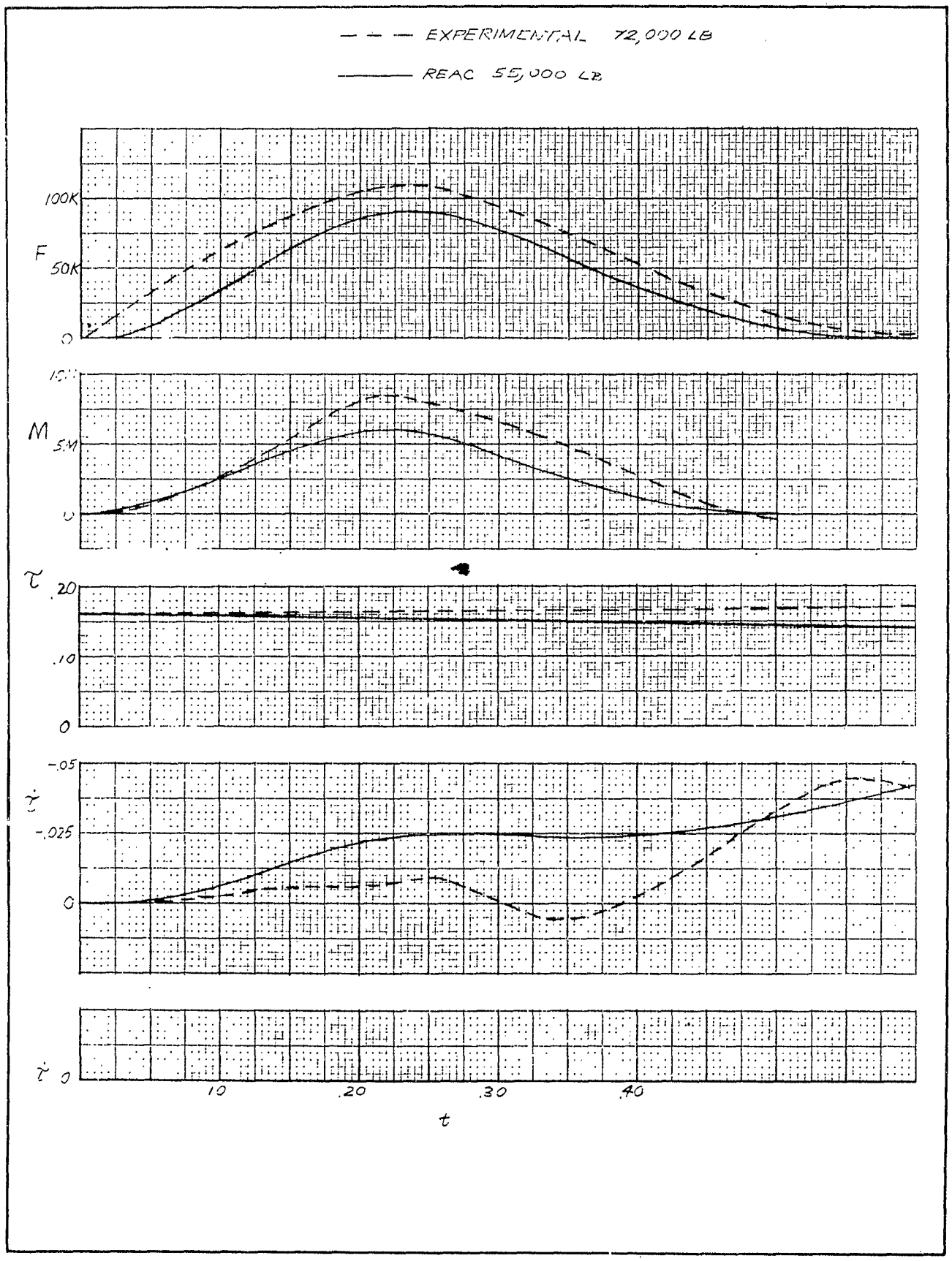

Fig. 21. Experimental vs REAC - Flight 31, Landing 8

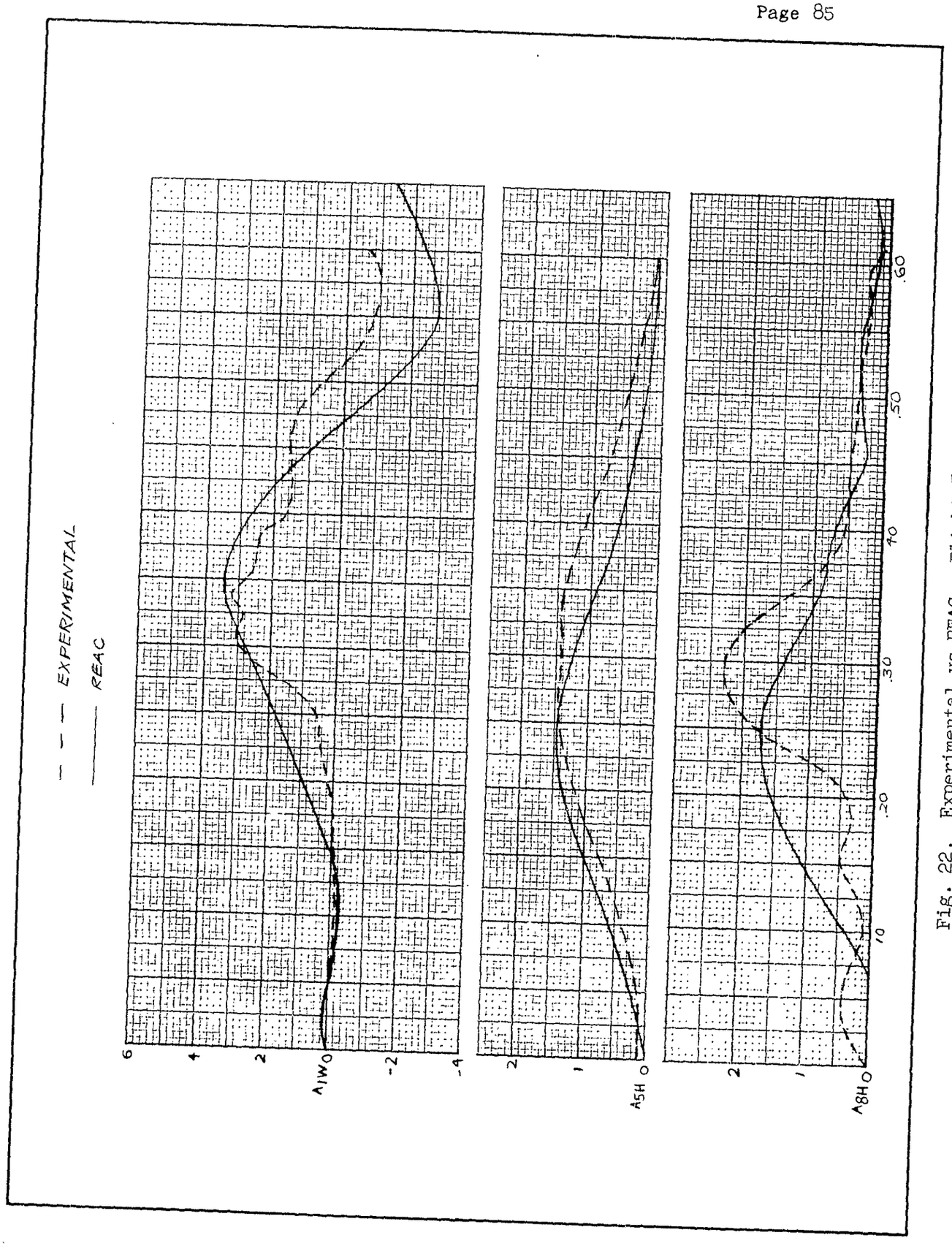

Fig. 22. Experimental vs REAC - Flight 31, Landing 8

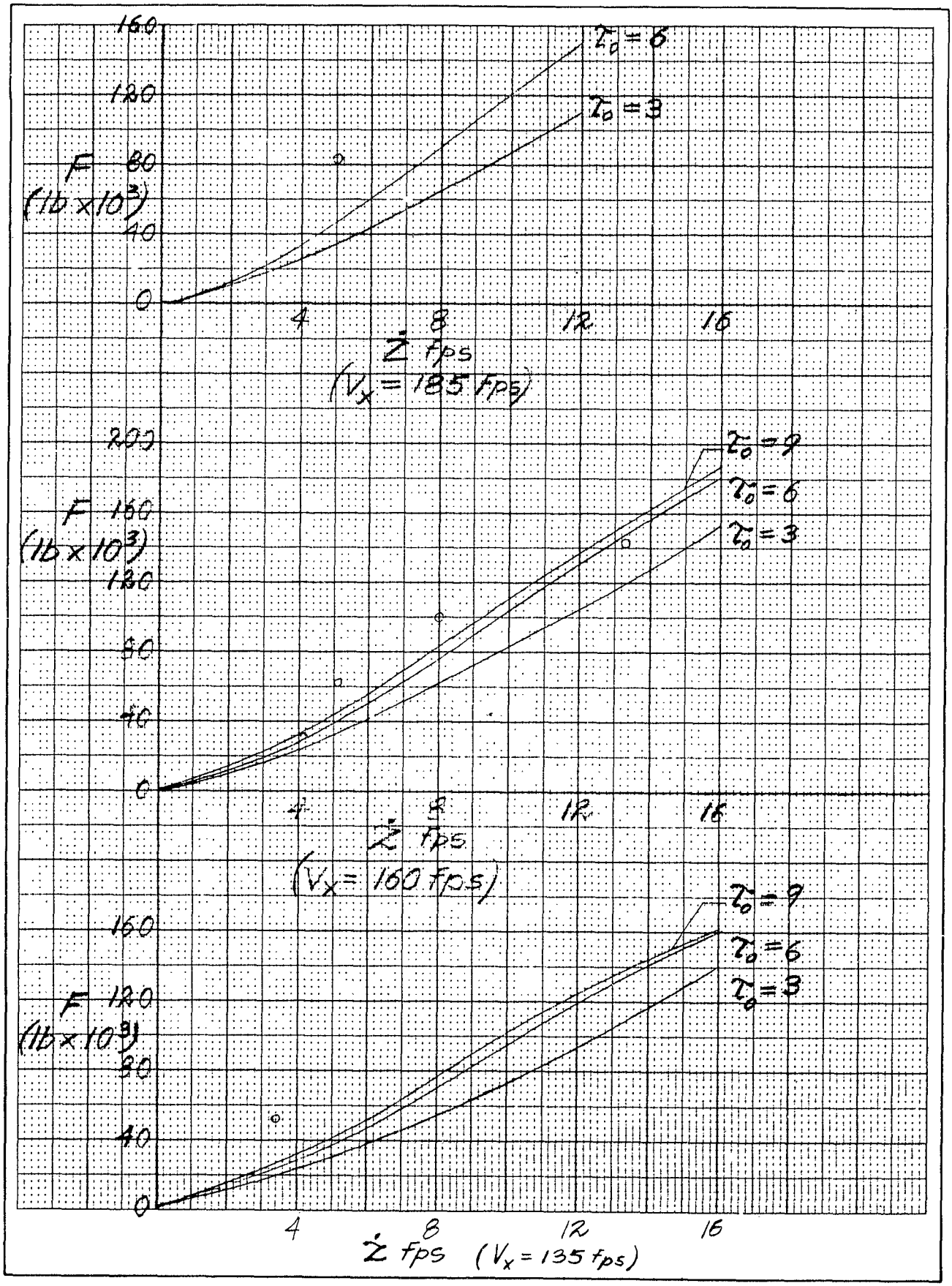

Fig. 23a. Force vs Rate of Descent for Several Landing Speeds and Trim Angles

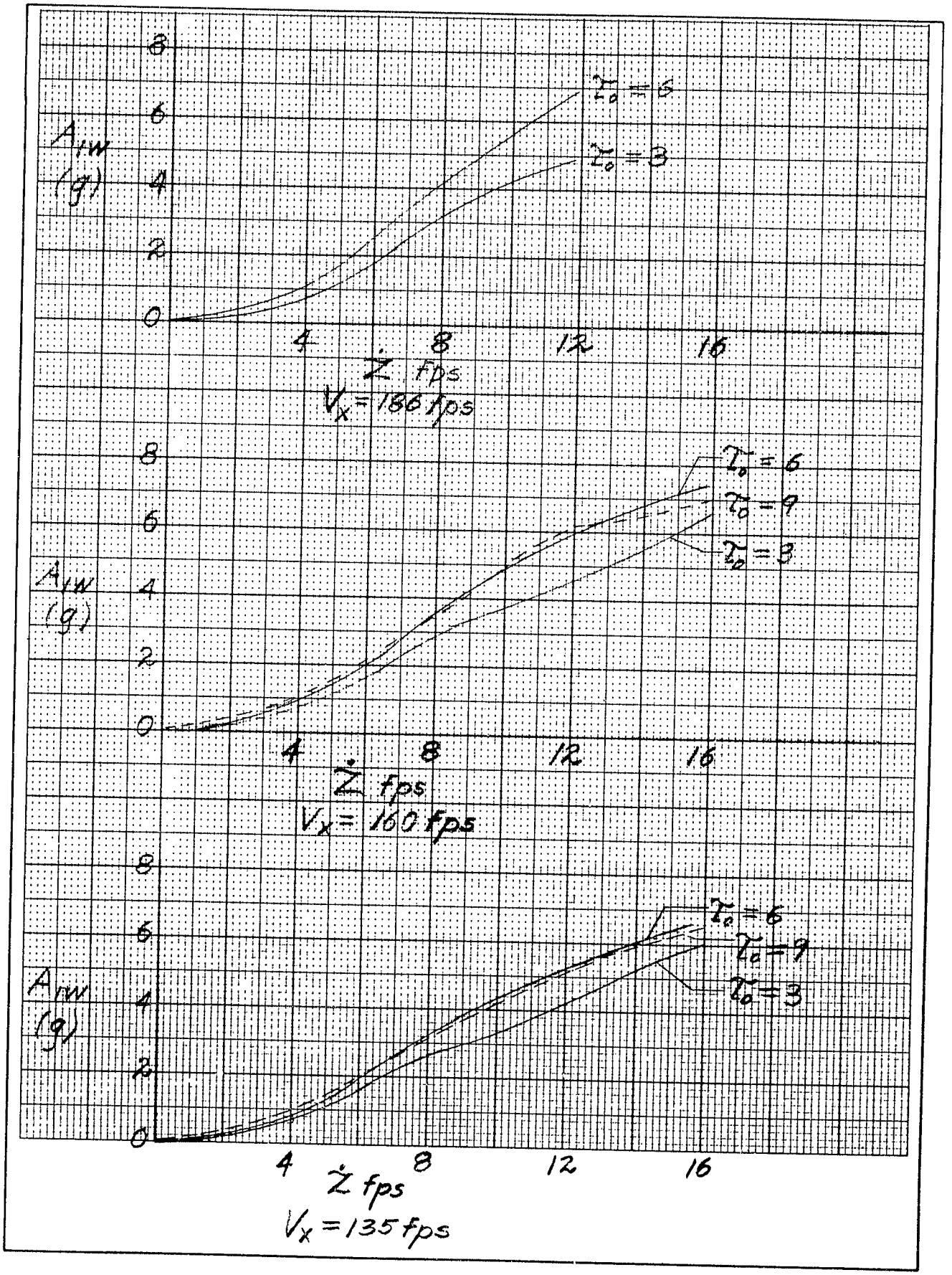

Fig. 23b. Wing Flip Acceleration vs Rate of Descent for Several Landing Speeds and Trim Angles

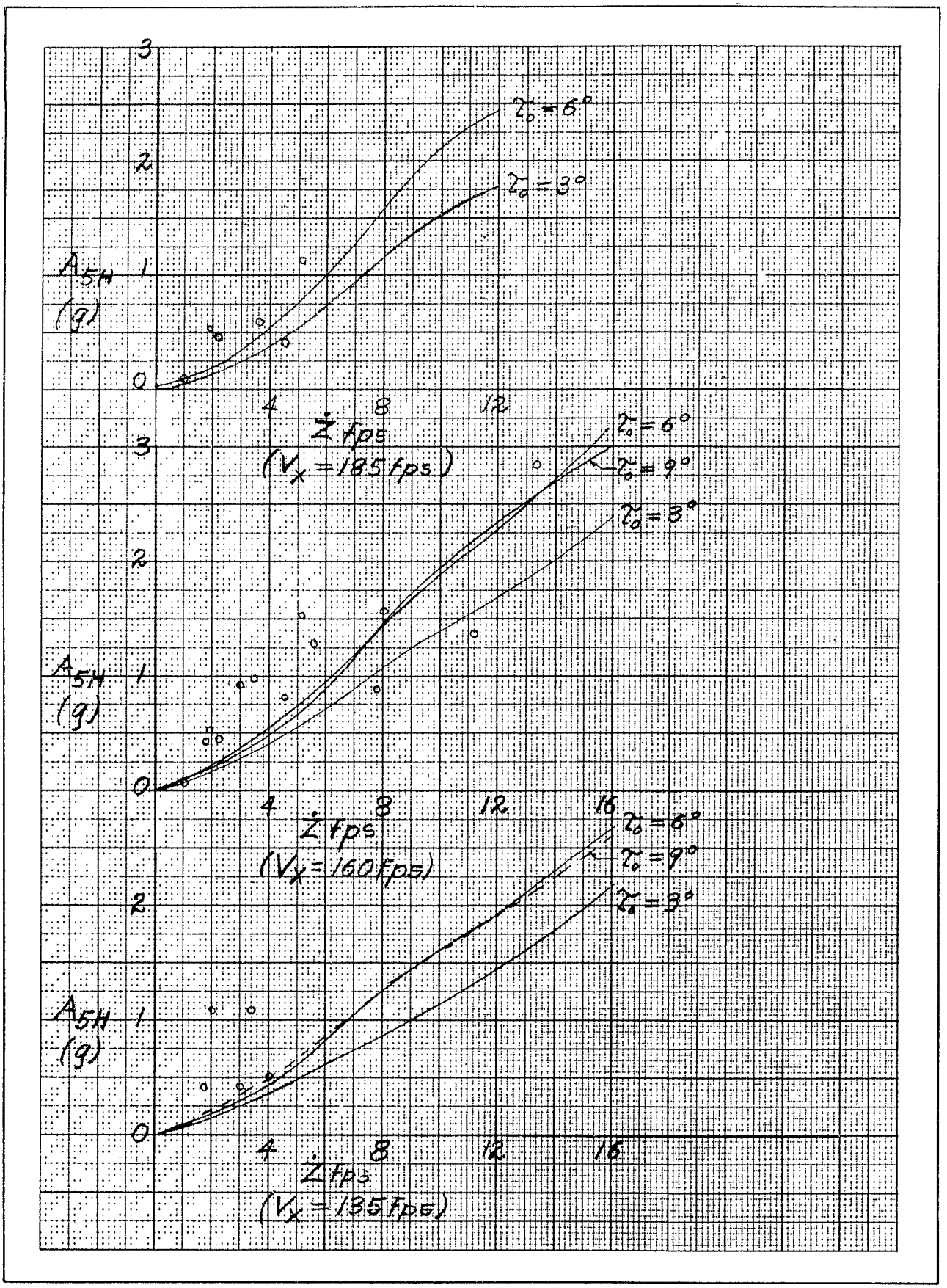

Fig. 23c Airplane Center of Gravity Acceleration vs Rate of Descent for Several Landing Speeds and Trim Angles

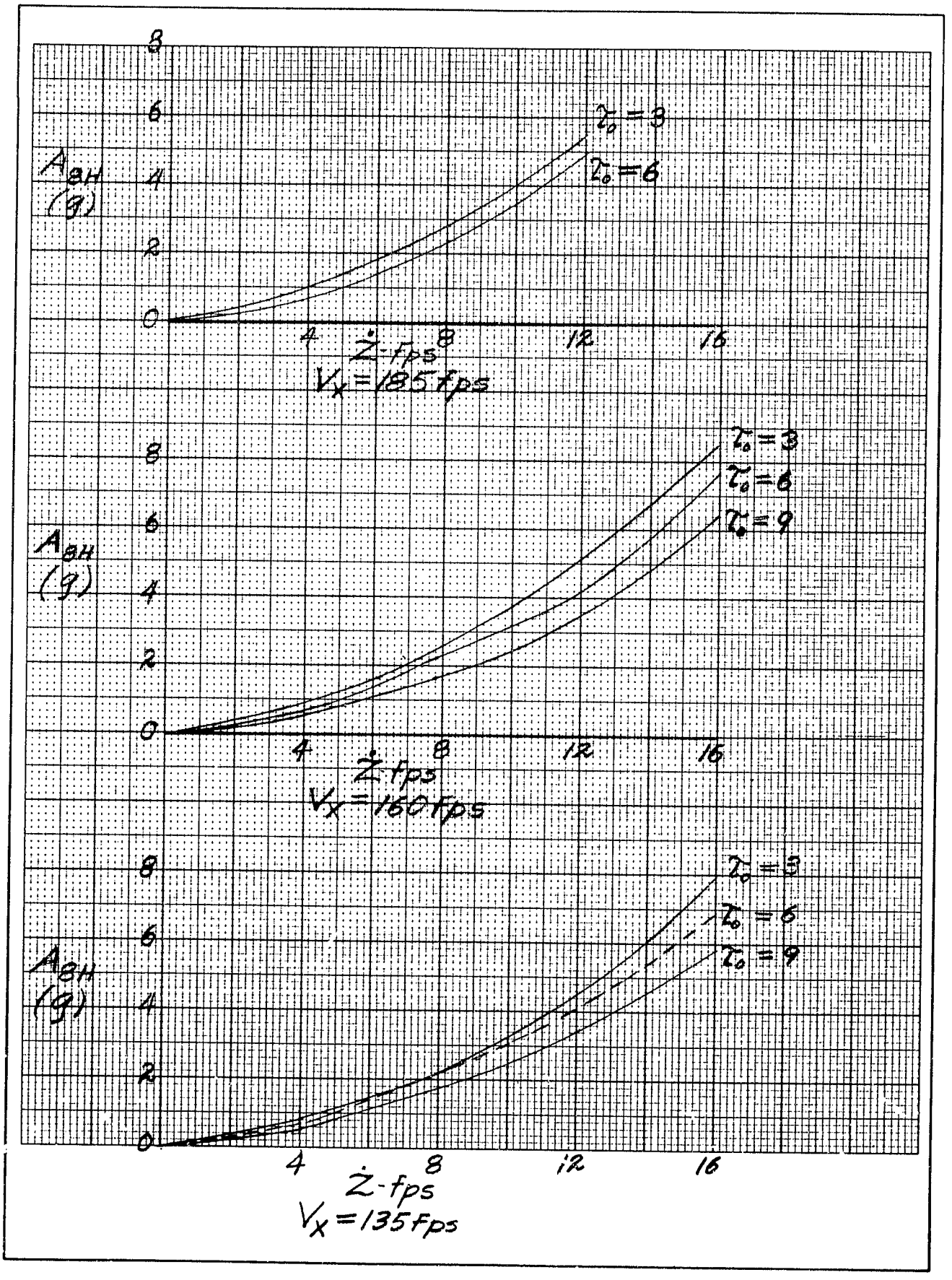

Fig. 23d Bow Acceleration vs Rate of Descent for Several Landing Speeds and Trim Angles.

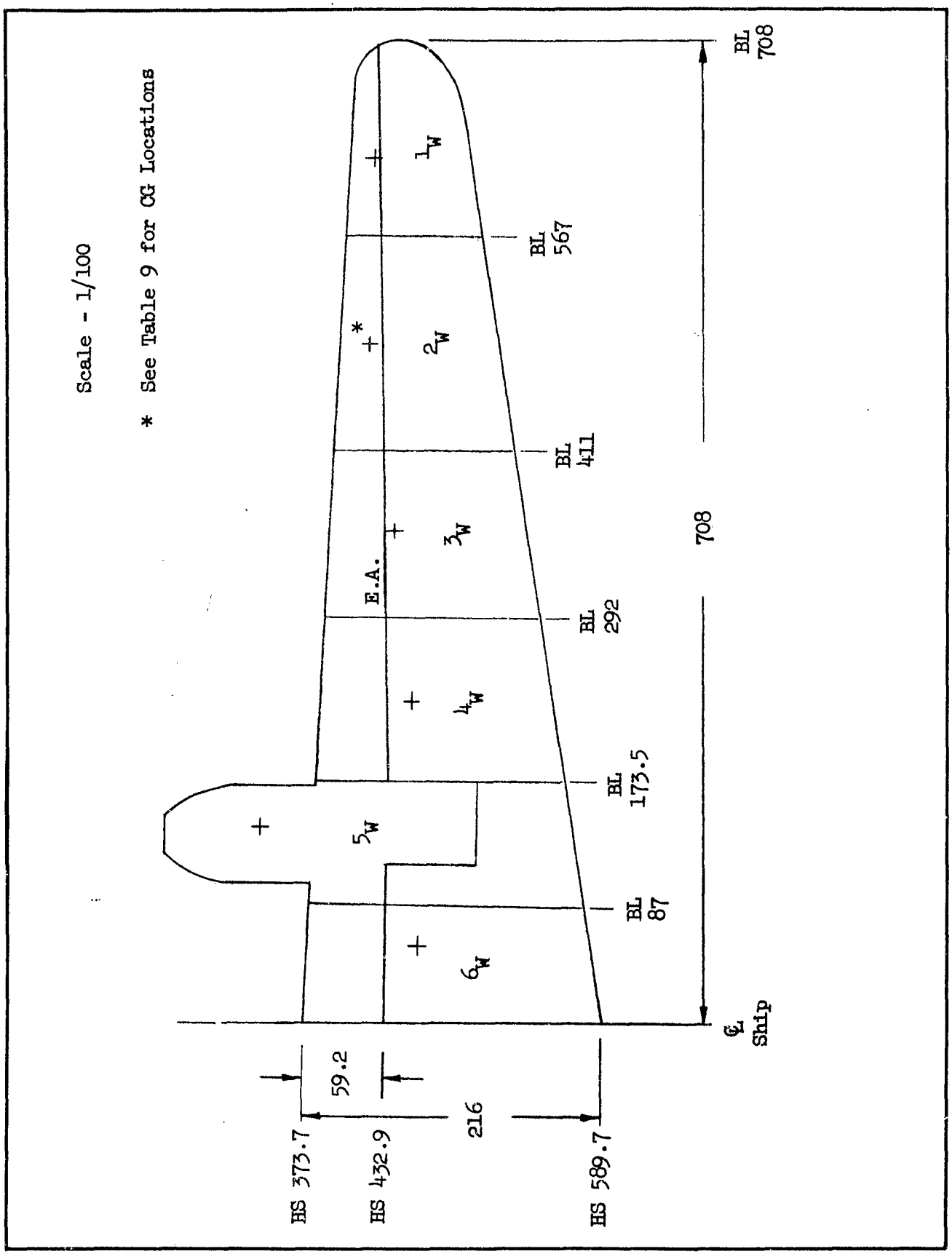

Fig. 24a. Wing Planform

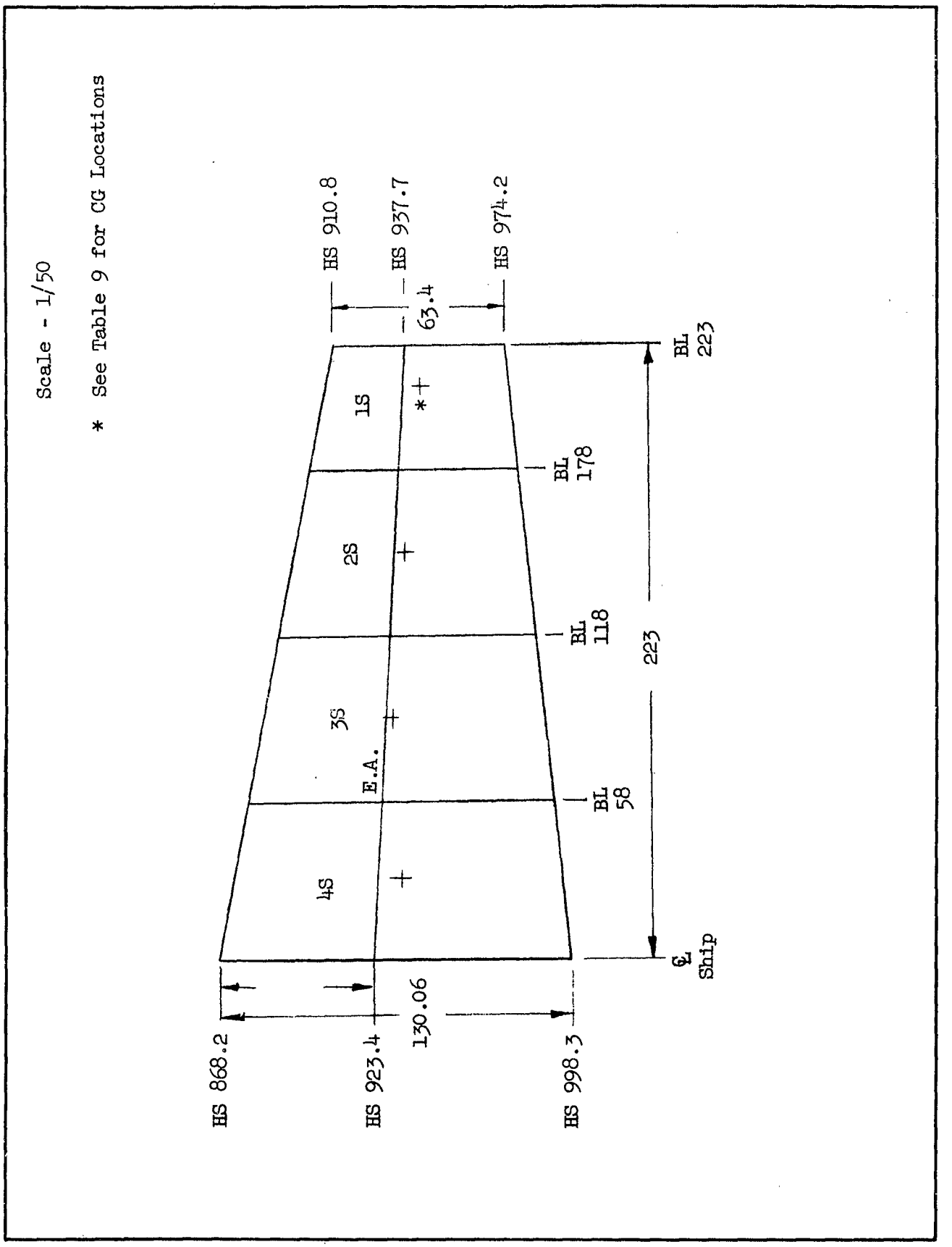

Fig. 24b. Stabilizer Planform

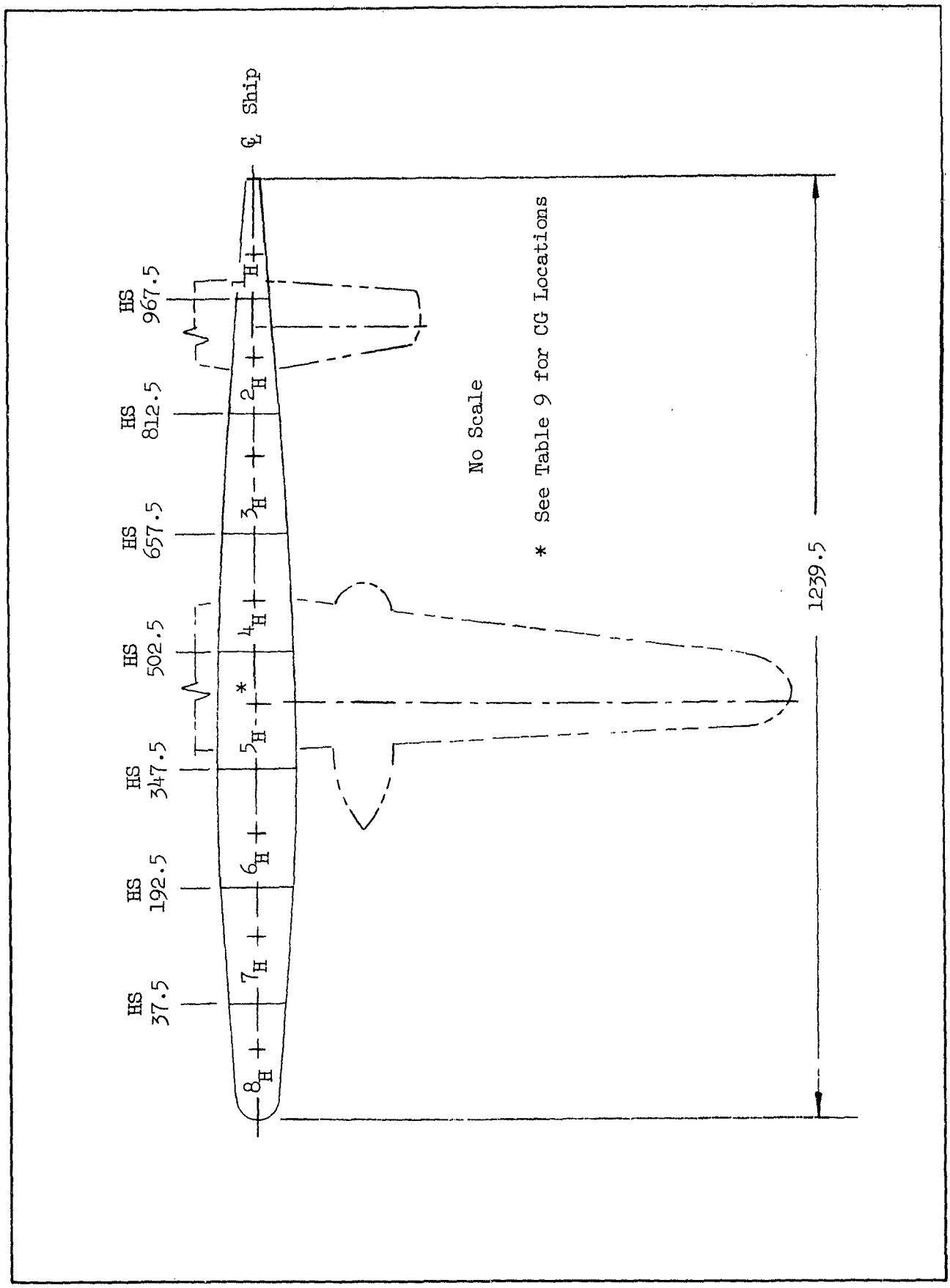

Fig. 24c. Hull Planform

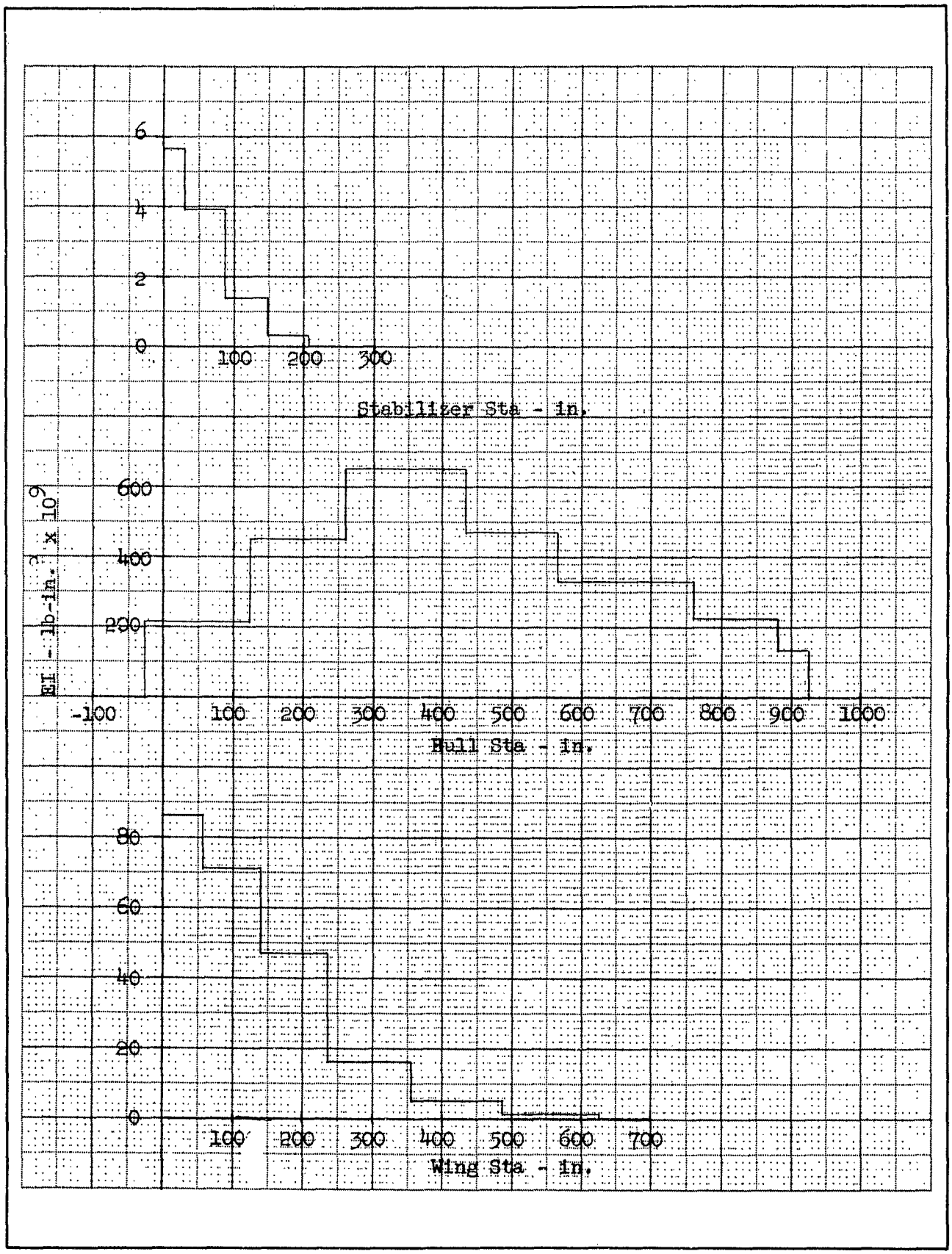

Fig. 25. Average Bending Stiffness Between Mass Stations

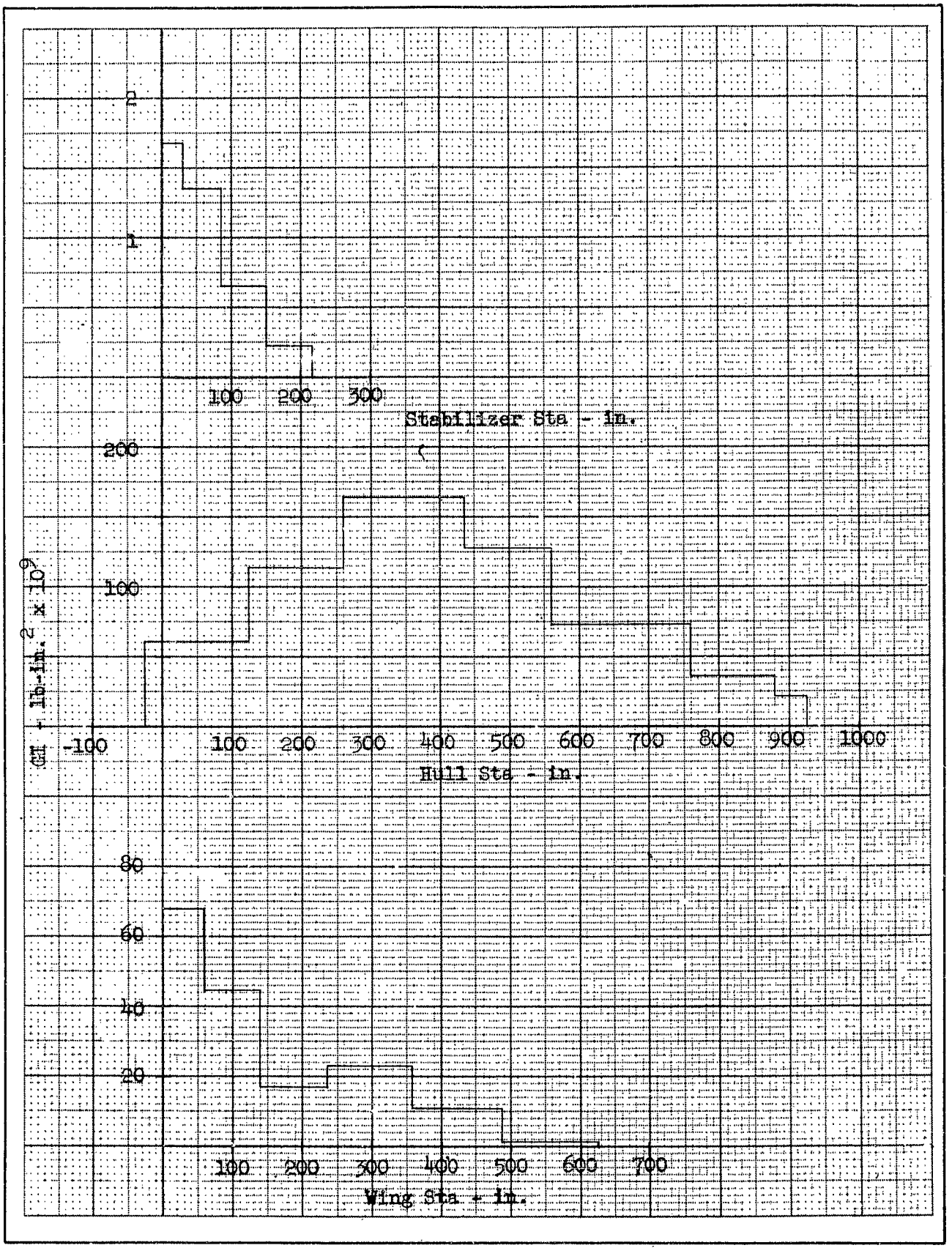

Fig. 26. Average Torsional Stiffness Between Mass Stations

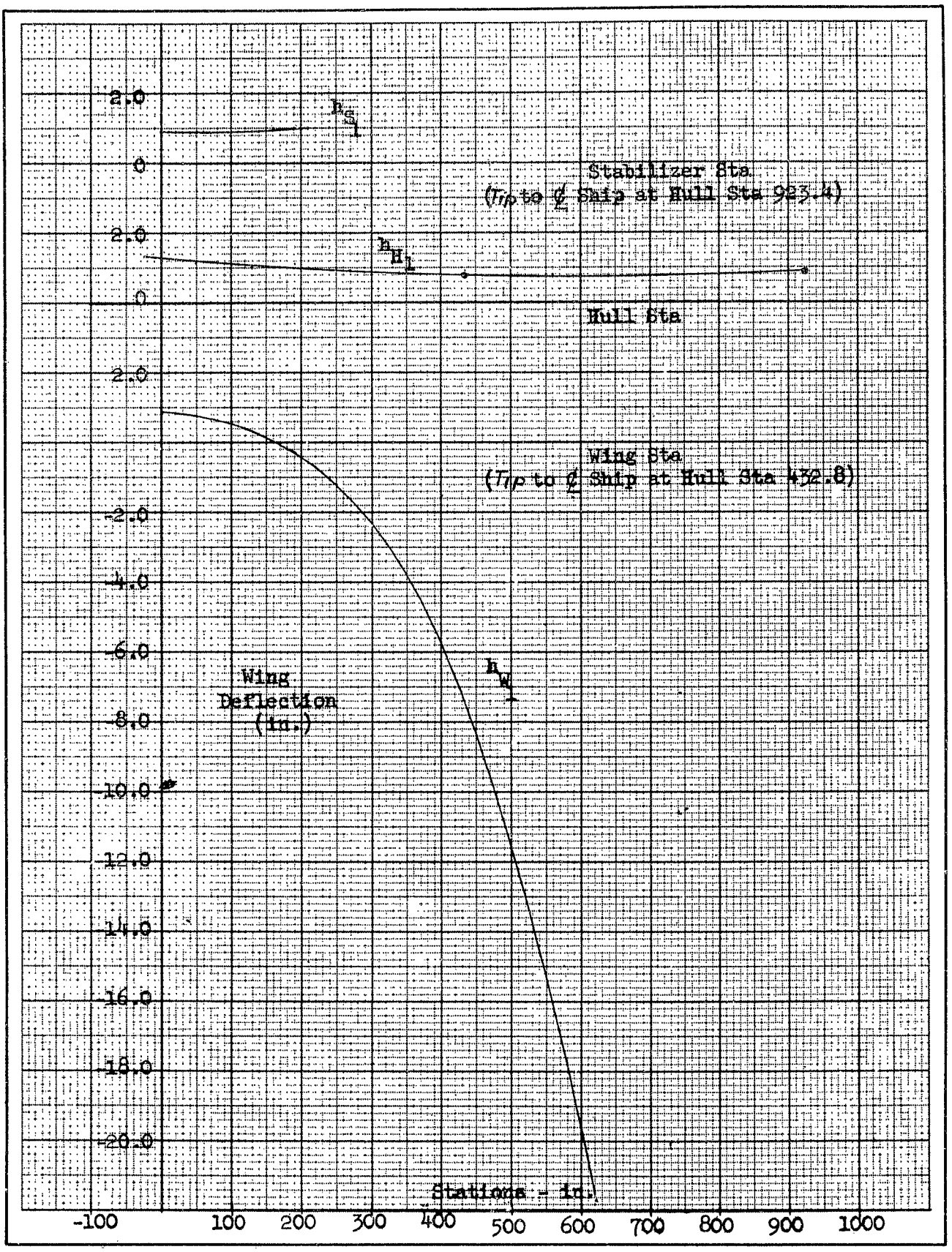

Fig. 27. First Symmetric Airplane Mode

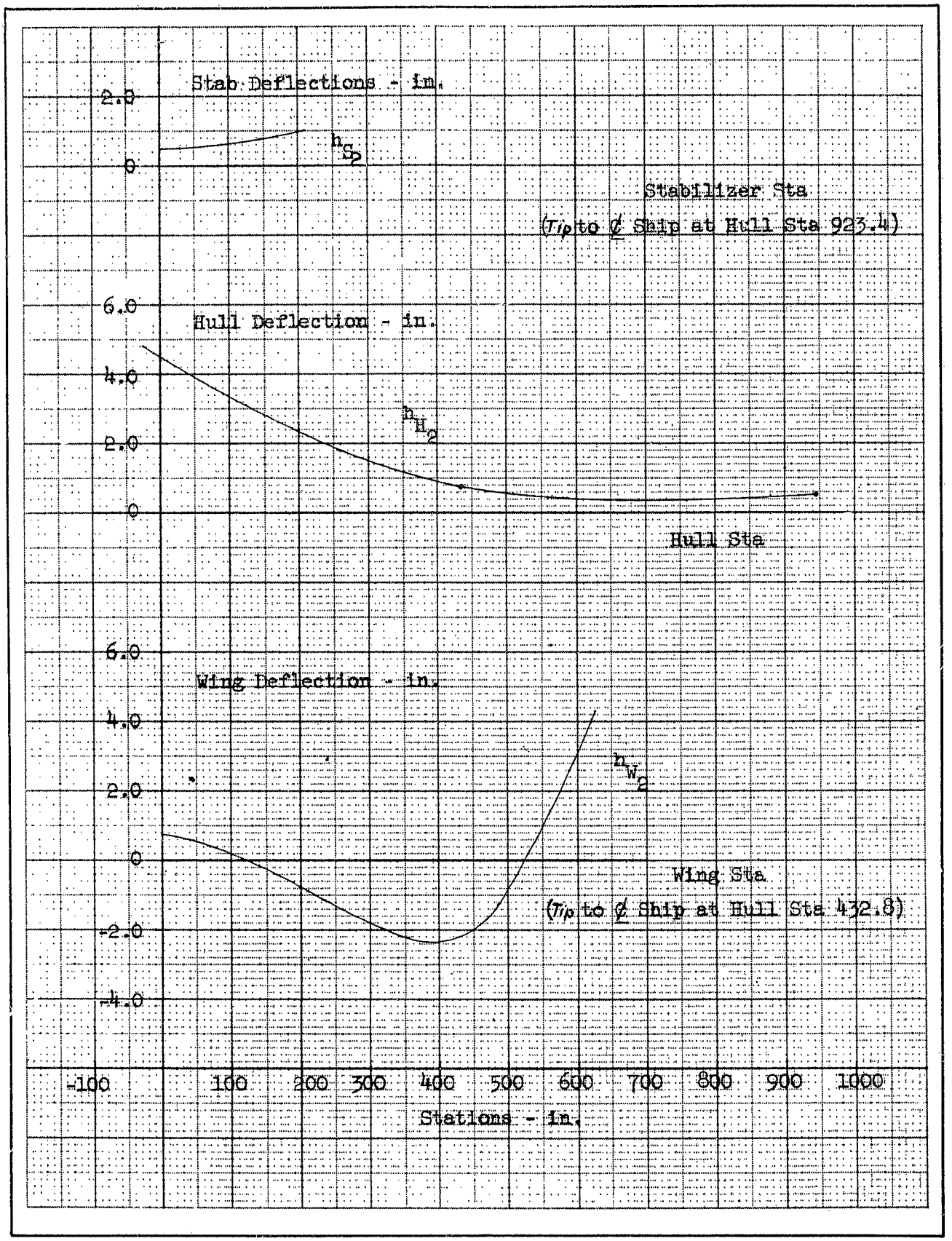

Fig. 28. Second Symmetric Airplane Mode

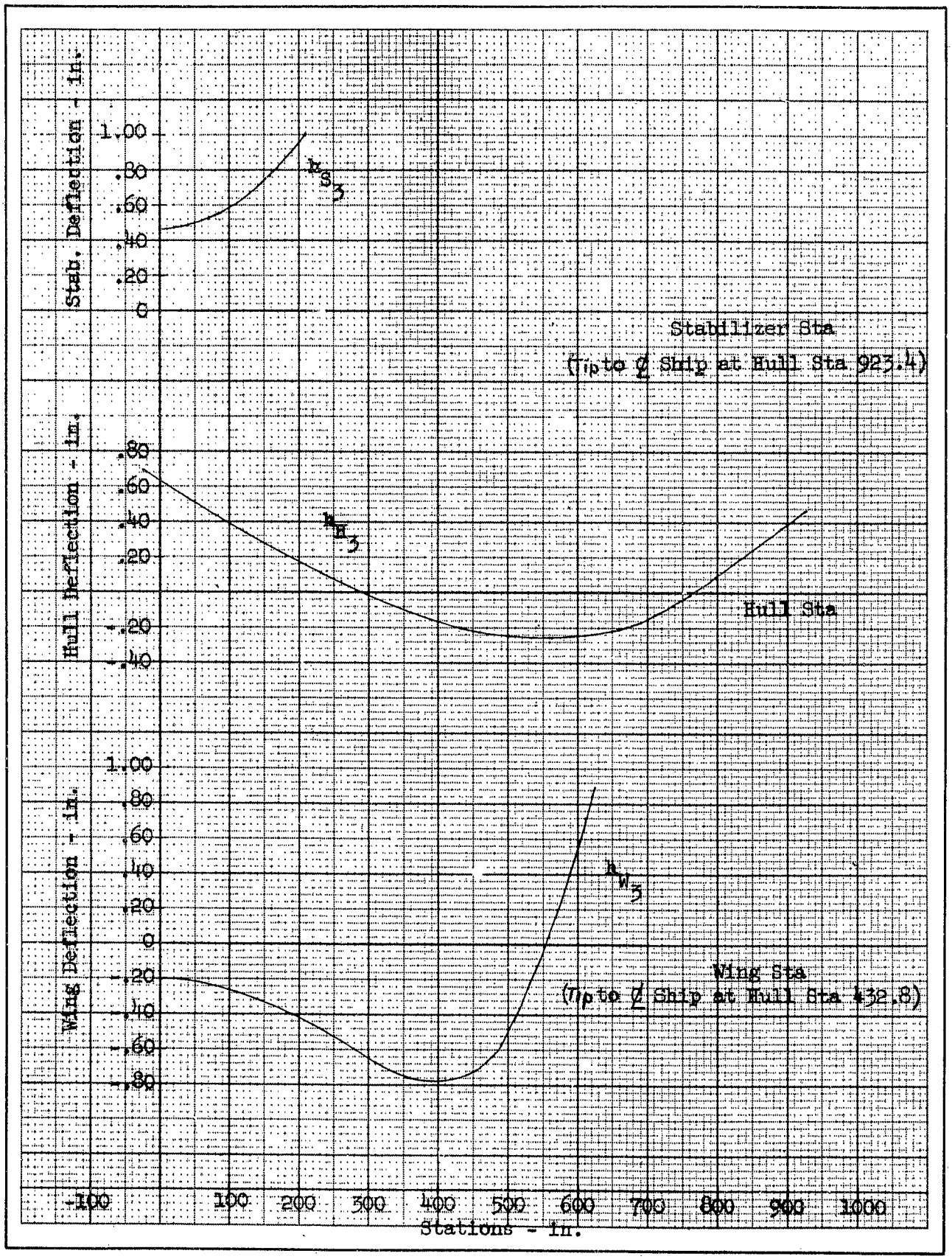

Fig. 29. Third Symmetric Airplane Mode

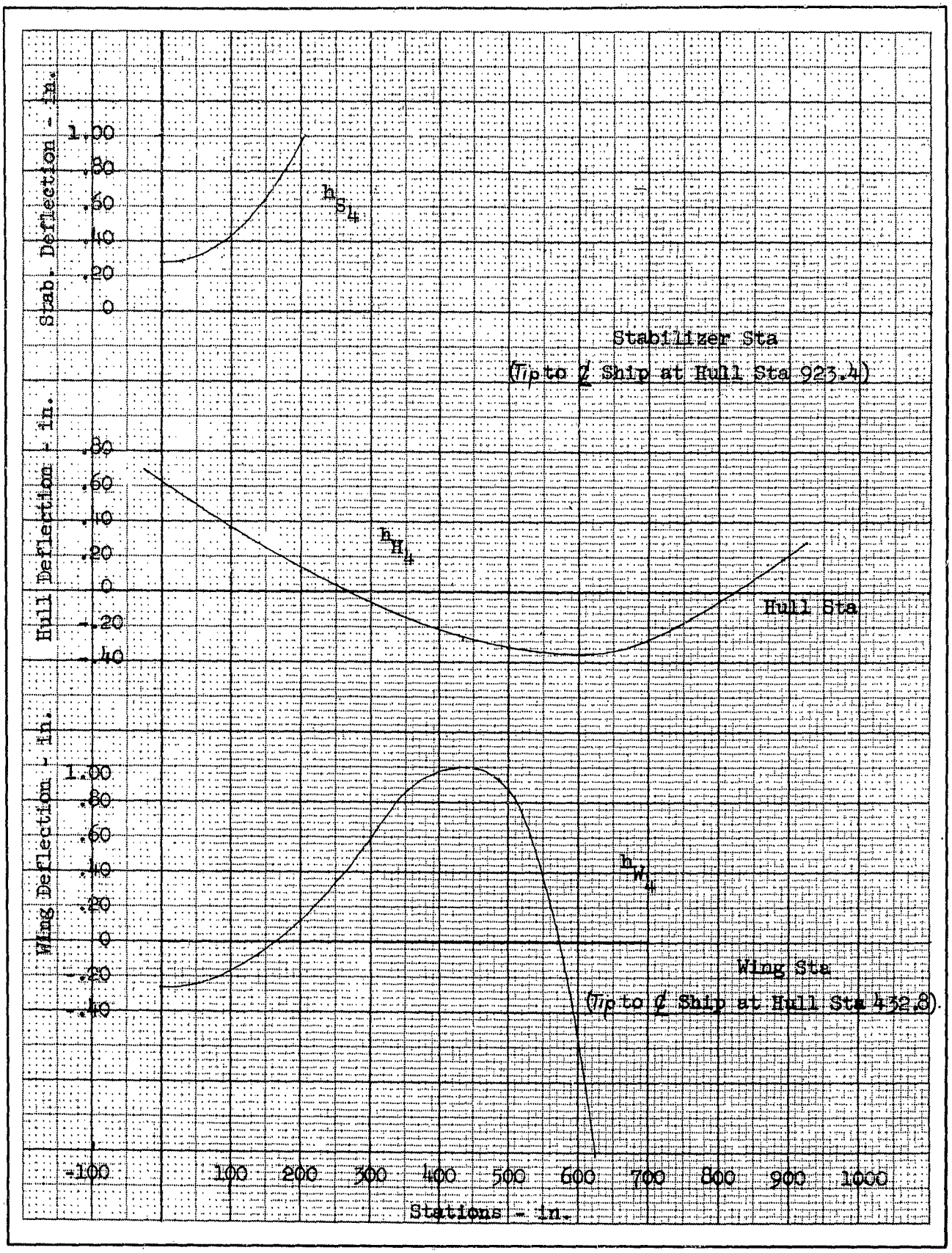

Fig. 30. Fourth Symmetric Airplane Mode